Universidade de São Paulo
Faculdade de Filosofia, Ciências e Letras de Ribeirão Preto

Estudo da conectividade funcional cerebral em regiões com redução da espessura cortical associadas ao envelhecimento sadio

Bruno Hebling Vieira

Dissertação apresentada à Faculdade de Filosofia, Ciências e Letras de Ribeirão Preto da USP, como parte das exigências para obtenção do título de Mestre em Ciências, Área de concentração: Física Aplicada à Medicina e Biologia

Ribeirão Preto - SP
2018

Bruno Hebling Vieira

Estudo da conectividade funcional cerebral em regiões com redução da espessura cortical associadas ao envelhecimento sadio

Versão Corrigida
(Versão original encontra-se na unidade que aloja o Programa de Pós-graduação)

Orientador:
Prof. Dr. **CARLOS ERNESTO GARRIDO SALMON**

Dissertação apresentada à Faculdade de Filosofia, Ciências e Letras de Ribeirão Preto da USP, como parte das exigências para obtenção do título de Mestre em Ciências. Área de concentração: Física Aplicada à Medicina e Biologia

Ribeirão Preto - SP
2018

Vieira, Bruno Hebling
Estudo da conectividade funcional cerebral em regiões com redução da espessura cortical associadas ao envelhecimento sadio. Ribeirão Preto, 2018.
118 p. : il.

Dissertação de Mestrado, apresentada à Faculdade de Filosofia, Ciências e Letras de Ribeirão Preto/USP. Área de concentração: Física Aplicada à Medicina e Biologia.
Orientador: Salmon, Carlos Ernesto Garrido.

1. cérebro 2. conectividade funcional 3. envelhecimento 4. atrofia 5. MRI.

Dedico esse trabalho a minha família: meus pais, Regina e Antonio, e minhas irmãs, Claudia e Carla.

AGRADECIMENTOS

Agradeço primeiramente ao Professor Carlos pela orientação, nesse trabalho e em outros anteriores, durante esses seis anos de minha vida acadêmica. Agradeço também pelo apoio e oportunidades, que tanto me fizeram aprender.

Agradeço também aos colegas do laboratório InBrain, que sempre ali estavam em momentos de descontração e também nas discussões mais produtivas. Durante esses anos amadureci, não só academicamente, e vocês estiveram presentes. Agradeço pelas conversas sobre ciência, política, música, vida, e muitos incontáveis assuntos. Agradeço pelas colaborações quase que diárias. Agradeço pelos conselhos. Agradeço pelas imitações e bordões, aqui inclusos os meus próprios, pelos almoços no bandejão, pelo café a tarde, pelas piadas, pelos memes, que muitas vezes também protagonizei. Agradeço por todas as viagens e aventuras em que estivemos e estaremos juntos, por me ouvirem reclamar incessantemente, por muitas vezes me alegrarem quando nada parece estar dando certo. André, Carlo, Gustavo, Ícaro, Jeam, João, Maíra, et al: a amizade é grande demais para ser descrita aqui.

Agradeço às centenas de amigos com quem vivi e dividi um lar durante tantos anos no Conjunto Residencial do Estudante Universitário; vocês fizeram parte da minha construção, social e cultural, a gratidão é eterna.

Agradeço aos grandes amigos que fiz na XIII Física Médica, com vocês a caminhada foi menos árdua.

Agradeço a todos que em algum momento cruzaram caminhos comigo durante essa jornada, dentro e fora da Universidade.

Agradeço ao Conselho Nacional de Desenvolvimento Científico e Tecnológico (CNPq), que me concedeu bolsa para a realização desse trabalho (processo 132112/2016-7).

E por fim agradeço aos meus familiares, em especial minha mãe, Regina, e meu pai, Antonio, que tanto zelam por mim. Peço desculpa pelas ausências prolongadas durante esses anos. Agradeço por me deixarem seguir o caminho que meu coração manda e fazer o que gosto.

“Far better an approximate answer to the right question, which is often vague, than an exact answer to the wrong question, which can always be made precise”.

(John Wilder Tukey)

RESUMO

Estudo da conectividade funcional cerebral em regiões com redução da espessura cortical associadas ao envelhecimento sadio

O cérebro envelhece, e com isso vêm à tona alterações em sua micro e macroestrutura que se refletem em sua morfologia e funcionamento. Mudanças na estrutura cerebral e acoplamento funcional entre suas regiões podem ser averiguadas através da neuroimagem, e, mais especificamente, imagem por ressonância magnética (IRM). Usando dados de IRM das duas etapas (Pilot and Enhanced) do Nathan Kline Institute – Rockland Sample (NKI-RS), totalizando 613 participantes destros, livres de doenças neurodegenerativas, com idade entre 18 e 85 anos, medimos parâmetros de substância cinzenta como volume, espessura, e área de superfície corticais, e também volume de estruturas subcorticais. Também medimos conectividade funcional cortico-cortical, definida como o coeficiente de correlação de Pearson, coeficiente de correlação parcial de Pearson, causalidade instântanea de Granger e causalidade de Granger bivariadas, e coerência parcial direcionada generalizada (GPDC). A GPDC foi medida em cinco frequências entre quatro pares de regiões que demonstraram a mais forte evidência para diminuição da espessura cortical linearmente, medido pela estatística-t associada, e suas alterações ao longo do envelhecimento foram estudadas usando uma abordagem multivariada baseada na Regressão de Dirichlet. Também estudamos associações espaciais entre padrões de alterações morfométricas e na conectividade. Reproduzimos a atrofia generalizada devido à idade reportada na literatura no volume cortical (90% das estruturas estudadas), área de superfície (68%) e espessura (90%), e atrofia volumétrica de várias estruturas subcorticais. Observamos uma associação positiva na distribuição conjunta do valor esperado da espessura cortical aos 18 anos de idade e a redução percentual anual na espessura cortical. Mostramos, ao projetar ambos em seus eixos principais e analizar a distribuição espacial desses índices, que a primeira componente principal correlaciona-se com a granularidade neocortical enquanto que a segunda componente principal representa o tipo cortical. Sobre a conectividade funcional, colhemos evidências para um aumento geral no coeficiente de correlação de Pearson (6% das conexões no Pilot NKI-RS e 2% no Enhanced NKI-RS), com menor proporção de decréscimos (0.1% no Pilot NKI-RS e 0.3% no Enhanced NKI-RS). O coeficiente de correlação parcial de Pearson entre 12 de 65 pares de regiões homotópicas demonstra um padrão de declínio com a idade, sugerindo desconexão inter-hemisférica. No entanto, a causalidade preditiva, como medida através de ambas as métricas de causalidade de Granger, não aparenta o mesmo grau de mudanças observado nas medidas correlacionais. Observamos aumentos na GPDC de várias regiões para si próprias em muitas frequências (25% de um total de 40 auto-conexões), que indica um grau de disconexão às outras regiões. Dadas regiões semente, revelamos padrões significativos espacialmente

distribuídos de associação entre efeitos padronizados da idade na conectividade para seus alvos e das espessuras dos alvos. Regiões com menor evidência para o desbastamento relacionado com a idade, como várias áreas occipitais, tendem a ter menos alterações em sua conectividade funcional que regiões com maior evidência suportando o desbastamento cortical relacionado à idade, como diversas regiões frontais. Hipotetizamos que regiões cuja associação é negativa (5% das regiões semente) são parte de sistemas compensatórios, estando correlacionadas com regiões que demonstram os maiores graus de atrofia de modo crescente. Regiões cuja associação é positiva (5%) não teriam mecanismos compensatórios à disposição, e portanto perdem conectividade para regiões atróficas. No geral, encontramos evidências para alterações na conectividade e na morfometria cortical e subcortical no cérebro todo ao longo da extensão da vida adulta humana. Também achamos um padrão específico de associações entre tendências atróficas e alterações na conectividade cerebral devido à idade.

Palavras-chave: 1. cérebro 2. conectividade funcional 3. envelhecimento 4. atrofia 5. MRI.

ABSTRACT

Brain functional connectivity in regions that exhibit age-related cortical thinning

The brain ages, and with it come alterations in its micro- and macro-structure which reflect in its morphology and functioning. Changes in the brain structure and functional coupling between regions can be assessed with neuroimaging, and, more specifically, magnetic resonance imaging (MRI). Using MRI data from two stages (Pilot and Enhanced) of the Nathan Kline Institute – Rockland Sample (NKI-RS), totalling 613, free of neurodegenerative diseases, and right-handed, participants aged 18 to 85 years old, we measured gray-matter parameters such as cortical volume, cortical thickness, and cortical surface area, and also volume of subcortical structures. We also measured cortico-cortical functional connectivity, defined either as the Pearson correlation coefficient and partial correlation coefficient, bivariate instantaneous Granger causality and Granger causality, and generalized partial directed coherence (GPDC). GPDC was evaluated in five frequencies between the four pairs of regions displaying the strongest evidence for linear thinning, measured by their associated t-statistic, and its alterations alongside aging were assessed using a multivariate approach based on Dirichlet Regression. We also studied spatial associations between patterns of morphometric and connectivity alterations. We reproduced generalized age-related atrophy reported in the literature in cortical volume (90% of the studied structures), surface area (68%) and thickness (90%), and volumetric atrophy of several subocortical structures. We observe a positive association in the joint distribution of the expected cortical thickness at 18 years old and the yearly percentage reduction in cortical thickness. We showed, projecting these two quantitities into their principal axes and analyzing the spatial distribution of the scores, that the first principal component correlates with neocortical granularity while the second principal component represents cortical type admixture. On functional connectivity, we gathered evidence for overall increased Pearson correlation coefficient (6% of the connections in the Pilot NKI-RS and 2% in the Enhanced NKI-RS), with proportionally smaller number of decreases (0.1% in the Pilot NKI-RS and 0.3% in the Enhanced NKI-RS). The Pearson partial correlation coefficient between 12 out of 65 homotopic region pairs shows a pattern of decline with age, suggesting inter-hemispheric disconnection. However, predictive causality, as measured by both Granger causalities, do not share the same degree of changes observed in the correlational metrics. We observe increased GPDC from several regions to themselves in many frequencies (25% out of a total of 40 self-connections), indicating a degree of disconnection to the other regions. Given seed regions, we uncovered spatially distributed significant patterns of association between the standardized effect of age on the connectivity to its targets and on their targets thicknesses. Regions with smaller evidence for age-related thinning, such as several occipital areas,

tend to have fewer alterations in functional connectivity than regions with greater evidence for age-related thinning, like many frontal regions. We hypothesize that regions showing a negative association (5% of the seed regions) are part of compensatory systems, being increasingly correlated with regions displaying most atrophy. Regions showing a positive association (5%) do not have compensatory mechanisms available, and therefore are losing connectivity to atrophyc regions. Overall, we found evidence for brainwide alterations in connectivity and cortical and subcortical morphometry throughout the human adult lifespan. We also found a specifc pattern of associations between the atrophic trends and age-related alterations in connectivity in the brain.

Keywords: 1. brain 2. functional connectivity 3. aging 4. atrophy 5. MRI.

LIST OF FIGURES

LIST OF TABLES

LIST OF ABBREVIATIONS

AD	Alzheimer's Disease
BOLD	Blood Oxygenation Level Dependent
CSF	Cerebrospinal Fluid
DMN	Default Mode Network
EEG	Electroencephalography
EPI	Echo-Planar Imaging
FDR	False Discovery Rate
GAM	Generalized Additive Model
GLM	Generalized Linear Model
GPDC	Generalized Partial Directed Coherence
GSR	Global Signal Regression
ICA	Independent Component Analysis
IRLS	Iteratively Reweighted Least Squares
MRI	Magnetic Resonance Imaging
NKI-RS	Nathan Kline Institute – Rockland Sample
PDC	Partial Directed Coherence
ROI	Region of Interest
RSFC	Resting-State Functional Connectivity
RSN	Resting-State Network
VAR	Vector Auto-regressive

LIST OF SYMBOLS

2D	Two Dimensional
Hz	Hertz
mm	millimeter
ms	millisecond
T	Tesla

INDEX

1 INTRODUCTION TO BRAIN AGING

Just like the rest of the human body, the brain ages. Cognitive aging has been perceived almost as long as physical aging (SALTHOUSE, 2004).

Due to advances in medicine and sanitation, the average population age is increasing worldwide, and thus the symptoms of aging, and the support they might require, are ever more present on today's daily life (HE; GOODKIND; KOWAL, 2016). Current estimates show the total population aged 65 years or older is expected to surpass the population aged 5 years or less before the 2020's (HE; GOODKIND; KOWAL, 2016). In fact, the growth of the elder population propagates from developed to developing countries, and, as we can see in Figure 1.1, the time required for the population aged 65 years or older to proportionally double, and triple, is decreasing.

Figure 1.1 Years required for the population aged 65 years or older to double and triple from a seven percent baseline in selected countries.

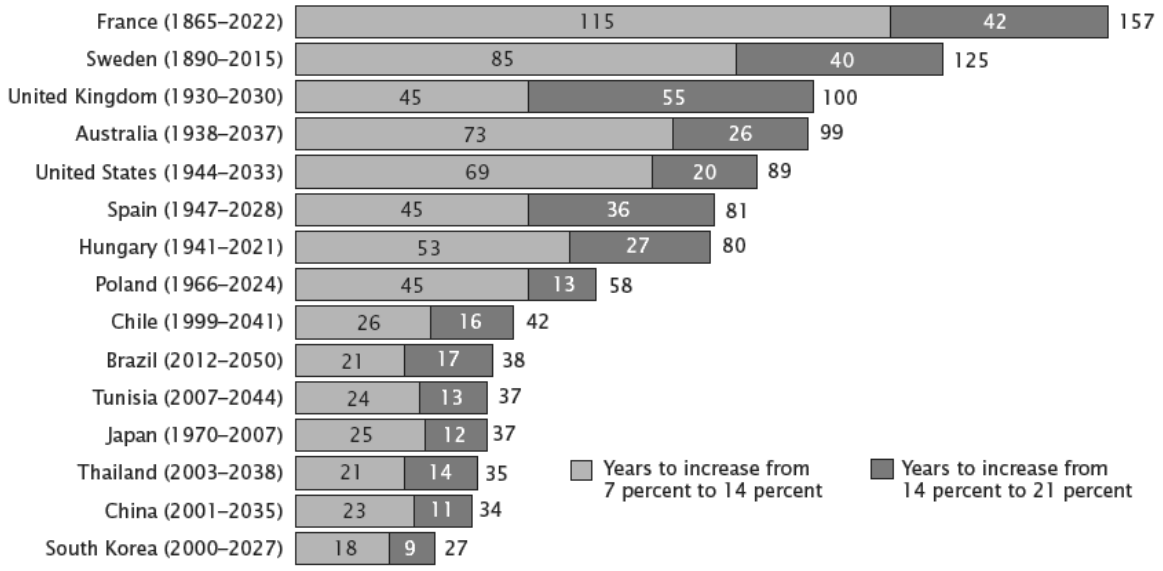

Source: HE, W.; GOODKIND, D.; KOWAL, P. **An Aging World: 2015 International Population Reports**, p. 165, 2016. (Figure 2-7. Number of Years for Percentage Aged 65 and Older in Total Population to Triple: Selected Countries).

This phenomenon is measurable in the most diverse scales of cerebral structure and function and largely affects the way the brain works. Among the most prevalent symptoms of brain aging are declines in memory and executive functions (BUCKNER, 2004; LA CORTE et al., 2016). Language, on the other hand, is often spared (PARK; REUTER-LORENZ, 2009).

Nonetheless, the aging process in the brain is heterogeneous and, to make matters worse, its mechanisms phenocopy symptoms of neurodegenerative diseases (JAGUST, 2013). Some disease factors, such as those from Cerebral Vascular Disease, are asymptomatic and therefore their effects are hard to separate from the effect of aging (LOCKHART; DECARLI, 2014). Parallel to the healthy aging process, elders are more susceptible to slow progressing neurodegenerative diseases (FJELL et al., 2014b). Among the most prevalent, reaching up to around a fifth of the population aged 75 to 84 years (LOCKHART; DECARLI, 2014), Alzheimer's Disease (AD) is biochemically characterized by neuronal and synaptic losses, which manifest as brain atrophy. Apparent atrophy is also detectable in cognitively normal elders, and age is the most significant risk factor for AD, due to a complex mechanism of plasticity capabilities (MESULAM, 2000).

For this reason, the study of brain aging can be contextualized within either normal brain aging or healthy brain aging (LOCKHART; DECARLI, 2014). Normal aging refers to the age-related alterations not associated with neurocognitive impairment, while healthy aging refers to relative preservation of cognitive functions with aging, being less common (LOCKHART; DECARLI, 2014). Other authors distinguish between normal and healthy aging along the lines of undiagnosed or asymptomatic versus absent neurodegenerative effects, respectively. In fact, while the average 79 years old person, approximately the life expectancy of Western countries, has 15% probability of being diagnosed with AD dementia, it also has approximately 30% to 40% chance of presenting AD-related neuropathologic changes (NELSON et al., 2012).

On the study of the neuroscience of aging, a focus exists on the telencephalon, shown in Figure 1.2 as a cerebral hemisphere along other subdivisions of the brain, and more specifically the neocortex, schematically shown in Figure 1.3, due to its higher-order cognitive functionalities, which are often impaired due to neurodegenerative disorders and other biological processes. The neocortex is considered phylogenetically younger than the other form of cortex, the allocortex, and it is present on the outermost surface of the telencephalon (ZILLES; AMUNTS, 2012). On the other hand, the allocortex is present in deep gray matter structures such as the hippocampi, the amygdalae, and the rhinencephalon. The distinction between neocortex and allocortex is the number of cortical layers in their structures. Pure neocortex contains six cortical gray matter layers, whereas pure allocortex has

between three and five layers. There is also a transitional type of cortex, the mesocortex, sharing cytoarchitectonic and histological features of both, being present in the insulas, and entorhinal, cingulate and parahippocampal cortices. In a way, we can see the cortex as three shells, from the inner allocortex, through the mesocortex, to the outer neocortex. The basal ganglia, which are also part of the forebrain, are masses of gray matter buried deep into the forebrain with connections to the cortex, thalamus and brainstem, taking part in many neurochemical pathways.

Figure 1.2 Subdivisions of the brain shown in the mid-sagittal plane.

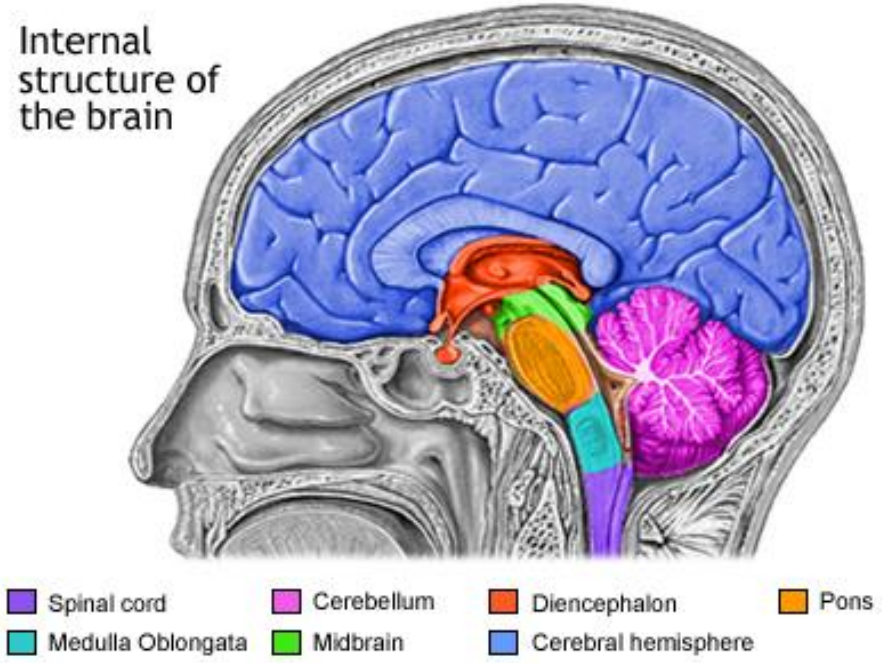

Source: NY Times Health Guide; A.D.A.M., Inc. 2013. Available at: http://www.nytimes.com/health/guides/disease/epilepsy/background.html. Accessed in November 11th, 2017. The diencephalon and the telencephalon, here labeled cerebral hemisphere, constitute the prosencephalon, or forebrain, while the pons, cerebellum and medulla oblongata form the rhombencephalon, or hindbrain.

Figure 1.3 Cortical classifications schematically shown in the mid-sagittal plane.

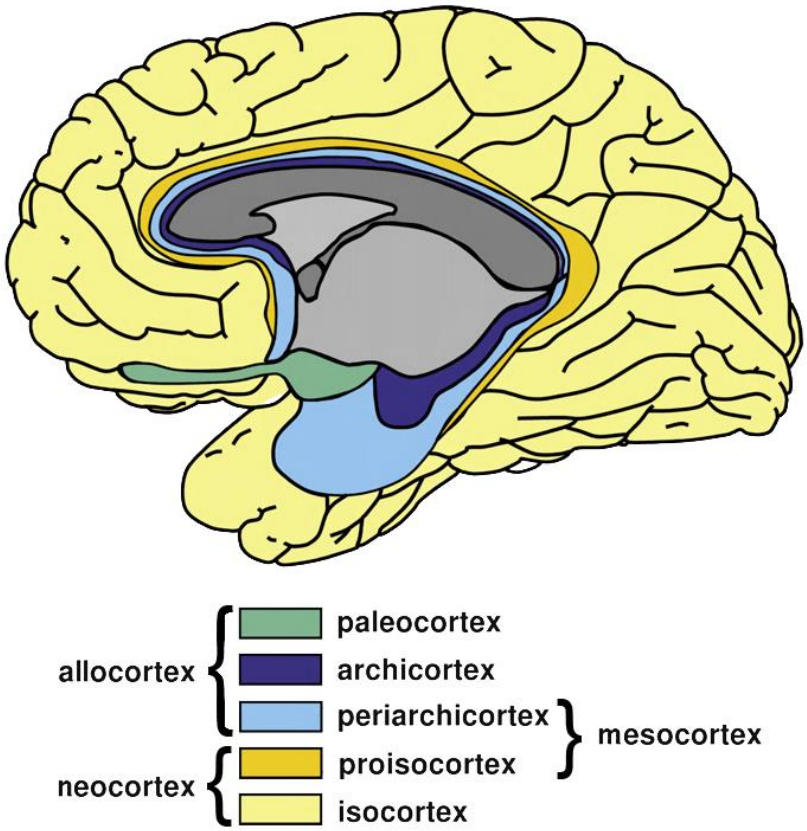

Source: ZILLES, K.; AMUNTS, K. Architecture of the Cerebral Cortex. In: The Human Nervous System. [s.l.] Elsevier, 2012. p. 836–895 (adapted). Peripaleocortex, the transitional mesocortex between paleocortex and proisocortex, is dominant in the anterior insulas, and therefore it is not shown.

Moreover, the isocortex is not homogenous. Its laminar structure varies regionally, with isocortical types being distributed as shown in Figure 1.4. The proportion of granule cells, small sized neurons more abundant in unimodal sensory areas, is a marker of isocortical types (ECONOMO, 2009). For this reason, we can enumerate isocortical types in a scale of granularity, in decreasing order: agranular, frontal, parietal, polar and granular. The agranular and granular isocortices are labeled heterotypic isocortex because, while they initially have the six-layered structure typical of isocortices, during prenatal development some of its layers develop vestigiality and become indiscernible. The converse is true for frontal, parietal and polar isocortical types, which keep the six-layered structure throughout the lifespan.

Figure 1.4 Isocortical laminar architecture types.

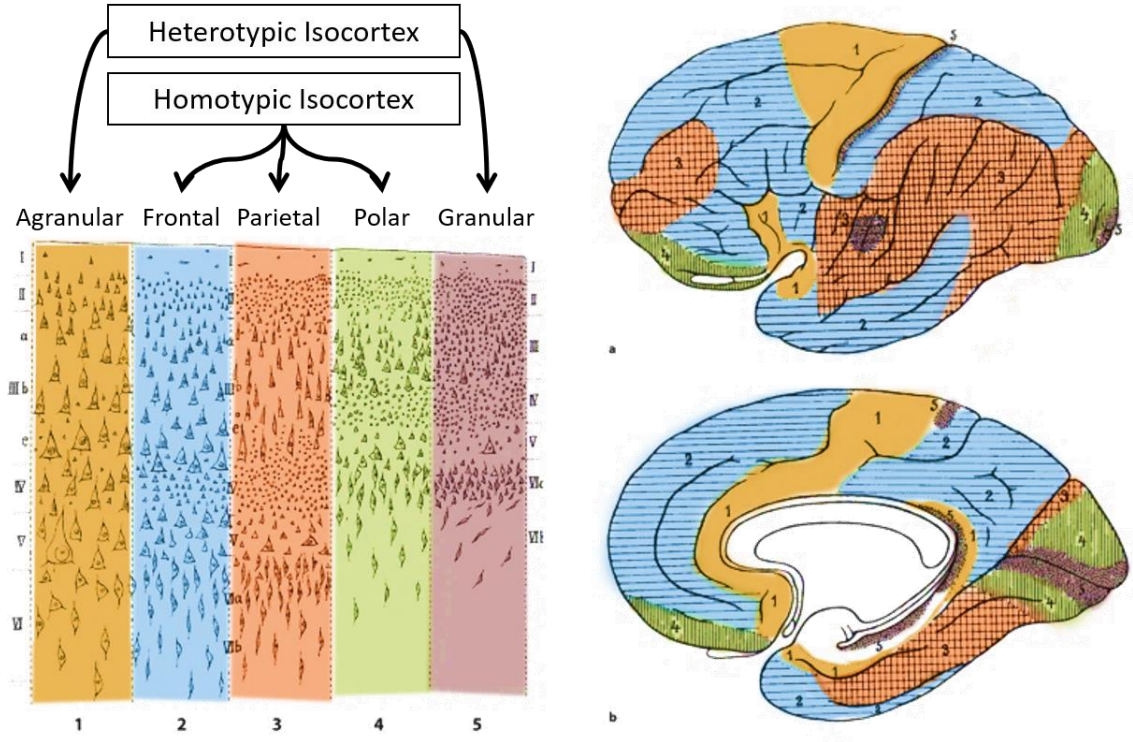

Source: ECONOMO, C. VON. Cellular Structure of the human cerebral cortex. [s.l.] Karger, 2009 (adapted). The five types of isocortical cythoarchitectural configurations are highlighted in colors. Frontal-, parietal- and polar-type isocortices are homotypic while agranular- and granular-type isocortices are heterotypic.

In this chapter, we describe how neuroimaging has been used to study brain aging and what has already been elucidated. We also introduce the concept of connectivity and how it is related to cognitive aging.

1.1 Scientific findings from neuroimaging

An extensive literature has developed from the studies of normal brain aging using neuroimaging (FERREIRA; BUSATTO, 2013; FJELL et al., 2014b; LOCKHART; DECARLI, 2014; SALA-LLONCH; BARTRÉS-FAZ; JUNQUÉ, 2015). In special, high resolution neuroanatomical imaging techniques facilitate the study of the brain morphology and how it changes due to age. Due to its optimal soft-tissue contrast, magnetic resonance imaging (MRI) is today the standard imaging technique in neuroanatomical investigation in vivo.

Usual quantitative descriptors of cortical gray matter shape include thickness and surface area, which have been shown to be genetically distinct (PANIZZON et al., 2009; WINKLER et al., 2010). In fact, there is evidence age-related changes in these,

which are also ontogenetically driven, that is, pertaining to the development of the individual, may reflect different aspects of neurobiological aging (LEMAITRE et al., 2012). Phylogenetically, in other words, referring to the evolution of species, surface area in humans is disproportionally expanded compared to thickness versus other mammals, with a modest two-fold increase in cortical thickness versus a one-thousand-fold increase in surface area from mice to humans (RAKIC, 2009). Cortical gray matter volume forms from the interaction of cortical thickness and surface area (STORSVE et al., 2014), therefore, it is considered a secondary ontogenetic measure (HOGSTROM et al., 2013; WINKLER et al., 2010).

Prominent brainwide age-related cortical thinning has been observed in large scale studies and also in the earlier literature (POTVIN; DIEUMEGARDE; DUCHESNE, 2017a; SALAT et al., 2004). The overall atrophic finding has been widely reaffirmed in the literature (AMLIEN et al., 2016; BAKKOUR et al., 2013; DOUAUD et al., 2014; FJELL et al., 2009a, 2009c, 2010a, 2014a, 2014b, 2015c; LEMAITRE et al., 2012; POTVIN; DIEUMEGARDE; DUCHESNE, 2017a; SALAT et al., 2004; SCAHILL et al., 2003; SHAW et al., 2008; SOWELL et al., 2007; STORSVE et al., 2014; TAMNES et al., 2013; THAMBISETTY et al., 2010; WALHOVD et al., 2011; WESTLYE et al., 2009; ZHOU et al., 2013; ZIELINSKI et al., 2014). This thinning process starts at early age (AMLIEN et al., 2016; TAMNES et al., 2013), as the cortex attains peak thickness in most regions prior to or during puberty (SHAW et al., 2008). However, stereological counting studies show this atrophy is not linked to neuronal cell loss, as the number of neuronal cells remains relatively constant throughout the lifespan of adults free of neurocognitive diseases, nor completely explained by the incidence of pre-symptomatic AD markers (FREEMAN et al., 2008). This fact suggests an increase in gray matter density. Therefore, other factors must account for these age-related changes in cortical morphometry. Changes in synapses and spines and cell body shrinking have been put forward as hypotheses to describe these phenomena (FJELL et al., 2015d). In the case of spines, a major decrease in spines has been observed, regardless of the distance to the neuron body, in the comparison of the cingulate cortex of a middle-aged and an older adult (BENAVIDES-PICCIONE et al., 2013). Increases in glia and small-body neurons and decreases in large cell-body neurons populations are also observed throughout aging, contributing to a near constant cell density (MARTÍNEZ-PINILLA et al., 2016; TERRY; DETERESA; HANSEN, 1987).

While cortical thickness often presents strong atrophic trends in the literature, surface area is a more stable morphological measure. In general, after a period of rapid global increase in the early childhood, global surface area remains relatively spared throughout the adult lifespan after the age of 10 to 15 years, with regional variability and a brainwide mild rate of atrophy (AMLIEN et al., 2016; LEMAITRE et al., 2012; RAZNAHAN et al., 2011). The gyrification, on the other hand, constantly decreases during the adult lifespan, while the same rate of loss is not observed in the cortical convex hull area (RAZNAHAN et al., 2011). A mechanistic interpretation of surface area suggests that its expansion during early development allows the disentangling of cortical connections and better differentiation of afferent signals, resulting in cortical specialization (SELDON, 2005).

Another structural measurement relating to microscopical neuronal organization is cortical myelination. Gray matter to white matter MRI contrast declines with age, with differential rates of decline dependent on the myelination, whereas lighter myelinated areas have higher rates of decline (VIDAL-PIÑEIRO et al., 2016). This might be due to how intracortical myelination correlates with plasticity, less myelin content associated with increased circuit complexity (GLASSER et al., 2014), thereby higher plasticity, which is deeply entwined with age-related cortical morphometric decline (FJELL et al., 2014b).

Even T1-weighted signal intensity is altered during aging, peaking at around 30 years of age for both gray and white matter (WESTLYE et al., 2010).

Subcortical gray matter allows nonlinear age-related volume alterations in several structures.(FJELL et al., 2013; POTVIN et al., 2016a), though their trajectories may vary. Three types of trajectories have been observed in cross-sectional studies validated with longitudinal data: linear reduction, near constant morphometry followed by decline after a certain age, and accentuated nonlinear decline (FJELL et al., 2013).

Hippocampal volume follows a nonlinear age trajectory, with a break point nearing the end of the fourth decade of life (FJELL et al., 2010b). Coincidently, hippocampal volume loss is a neuromarker of AD (SCHUFF et al., 2009) and memory performance in normal subjects (VAN PETTEN, 2004).

No evidence has been established for different rates of yearly change on cortical gray matter thickness nor subcortical gray matter volume between males and females (FJELL et al., 2009b).

Large scale normative studies have established age is a major factor for both subcortical and cortical gray matter morphometry inter-subject variability, compared with sex, estimated intracranial volume, mean field strength, and scanner manufacturer (POTVIN et al., 2016b; POTVIN; DIEUMEGARDE; DUCHESNE, 2017b).

Studies showed cortical thickness, surface area, volume and gyrification are reduced in the whole cortex due to age to varying degrees (FJELL et al., 2009a, 2014b; HOGSTROM et al., 2013; SALAT et al., 2004). However, overlap with areas targeted by AD is not complete (BAKKOUR et al., 2013), with AD reaching up to five times the normal atrophy rates in some regions (FJELL et al., 2014b).

Fronto-temporal areas are especially susceptible to age-related atrophy (FJELL et al., 2014b).

Aging also causes shrinking in metencephalic structures, notably the cerebellum and the vermis, with less noticeable changes in the pons (GAZZALEY; D'ESPOSITO, 2004, cap. 2). Unlike the cerebrum, the cerebellum is susceptible to age-related neuronal loss, and this is hypothesized to be related to observed motor aging, comprising loss of movement speed, precision and stability (BOISGONTIER, 2015).

Brainstem (medulla oblongata, mesencephalon, and pons) and basal ganglia structures are intrinsically related to motor control. Diminished volumes in the former and increased volume, implying over-compensation, in the latter structures have been linked to postural and balance declines in elders (BOISGONTIER et al., 2017).

Basal ganglia and thalamic atrophy also accounts for sensorimotor performance age-related decline, with subregional expansions in the caudate and pallidum (SERBRUYNS et al., 2015).

Morphological changes in the brain occur parallel to alterations in its function, as both are intrinsically linked. To study the brain function through neuroimaging requires a feasible image acquisition technique, susceptible to changes in neuronal activity at some level. Among these neurofunctional techniques displaying some level of sensibility to neuronal activity are electroencephalography (EEG), magnetoencephalography (MEG), near infrared spectroscopy (NIRS), positron emission tomography (PET), single photon emission computed tomography (SPECT), and, at last, functional magnetic resonance imaging (fMRI).

Metabolic imaging with ^{18}F-FDG-PET (fludeoxyglucose) has shown elders have decreased metabolism (BERNIER et al., 2017; CHÉTELAT et al., 2013; MALPETTI et al., 2017). Evidence for sex-specific changes have been found as well (KAKIMOTO et

al., 2016; MALPETTI et al., 2017), but the effect of sex is at an intersection of sociodemographic and biological causes, due to its influence on education and occupation. The spatial extent and gender difference in these changes is not a consensus, as recent literature has left the question open due to different methodologies employed (MALPETTI et al., 2017).

Studies with β-amyloid PET radiotracers have shown between twenty and thirty percent of healthy adults present cortical β-amyloid deposition (HARADA; NATELSON LOVE; TRIEBEL, 2013). The presence of neurofibrillary tangles and amyloid plaques has also been attested in otherwise healthy elders (FREEMAN et al., 2008; MESULAM, 2000), corroborating the notion of an intricate relationship between aging and AD. Therefore, uncovering the brain aging process may bring further advances in the understanding of AD.

Emerging evidences go along with the notion that the brain uses its cognitive reserves to compensate its systems disruption (BUCKNER, 2004). These reserves might underlie the observed increases in activation patterns in task fMRI of older adults, through compensatory mechanisms (BUCKNER, 2003).

Electrophysiological evidence from EEG endorse the theory of decreased hemispheric asymmetric recruitment with aging in motor tasks (LOEHRER et al., 2016).

In the early 20th century, it had already been postulated neurons do not act in isolation, but cooperatively as assemblies, such as described by Hebbian engrams and cell assemblies (HEBB, 1949). Using microelectrodes to simultaneously record activities in small neuronal groups soon allowed the uncovering of the dynamical system. Yet more intriguing, it soon became clear different stimuli induced correlation structures, which was interpreted as organization, defining what is called ‘functional connectivity’ (AERTSEN; PREISSL, 1991).

Indeed, cortico-cortical connections have their basis in the layered organization in the neocortex. Neuronal intra-hemispheric afferents mainly target lamina IV, the internal granular layer. On the other hand, inter-hemispheric cortico-cortical afferents target mainly laminae I through III, the supragranular layers. Cortico-cortical efferents are also mostly sourced from layer III as well (BOLON et al., 2013). Other connections, to supracortical and thalamic structures, are also sourced and target layers differentially. Therefore, connectivity, cortical morphology, and cytoarchitecture are intrinsically linked.

The transition to macroscopical observations on connectivity soon occurred. Functional and effective connectivity were then further defined through a series of papers, first with PET then with fMRI during stimulation or task paradigms, which usually comprise activity and rest blocks alternating in time during an acquisition, such as to measure the effect of the activity on the contrast compared with the baseline set by the rest blocks (FRISTON, 1994; FRISTON et al., 1993). After leaving its infancy, it was then proven such correlation structures existed during rest as well, and were consistent across conditions, as earlier and often dismissed works had studied empirically (BISWAL et al., 1995; BISWAL, 2012). In fact, both the task and the rest signal fluctuations were due to the same mechanism: the blood oxygenation level dependent (BOLD) contrast (OGAWA et al., 1990). The Resting-State Functional Connectivity (RSFC), as the name implies, refers to the functional connectivity estimated from a resting-state paradigm.

From signal processing techniques, especially blind signal separation techniques, such as Principal Component Analysis and Independent Component Analysis (ICA), the so-called resting-state networks (RSN) are defined (DAMOISEAUX et al., 2006; VAN DEN HEUVEL; HULSHOFF POL, 2010), either in spatial or temporal domains. During a resting-state paradigm, RSNs relating to somatosensory functions are also discernible. In special, though, a network strongly active during rest is readily identifiable coupling the angular gyri, posterior cingulate, and medial frontal gyri, the Default Mode Network (DMN) (DAMOISEAUX et al., 2006; HJELM et al., 2014; POWER et al., 2011).

Findings on the effects of age on functional connectivity are varied. Overall, increased connectivity between networks and decreased connectivity within networks, or results otherwise pointing to cortical de-differentiation or de-modularization, have been often noted in brain-wide studies .(BETZEL et al., 2014; CAO et al., 2014; FERREIRA et al., 2016; GEERLIGS et al., 2015; SALA-LLONCH; BARTRÉS-FAZ; JUNQUÉ, 2015; SONG et al., 2014).

It is important to note both age-related alterations on RSFC magnitude and signal when Pearson Correlation is employed as the connectivity metric. The most prevalent change on RSFC due to aging is increased connectivity, either increased magnitude of positive correlations or shifts from negative to positive correlations. These happen mostly in inter-network connectivities. On the other hand, decreased magnitude of positive correlations occurs most often on intra-network connectivities, with emphasis

on the DMN. These findings strengthen the notion that the brain becomes less functionally segregated with aging, as different areas interactions become stronger to the detriment of intraregional interactions (FERREIRA et al., 2016). Studies show inter-hemispheric connections tend to show higher proportions of linearly decreasing connectivities (WANG et al., 2012).

Focusing on the DMN, its anterior and posterior portions exhibit diminished activity with aging (DAMOISEAUX et al., 2008) and also decreased functional connectivity (ANDREWS-HANNA et al., 2007). Other networks are spared from age-related effects, however, such as the visual network (ANDREWS-HANNA et al., 2007).

A possible pitfall of studying functional connectivity between resting state networks derived from group ICA is the assignment of these networks might differ between younger and older participants. This misalignment could induce increased inter-network connectivity and decreased intra-network connectivity. Using personalized regions of interest (ROI), the effect of age on the DMN is attenuated, while other networks still show increased connectivity, resulting in global demodularization (SOHN et al., 2015).

Other findings reported include increased short-range connectivity and decreased long-range connectivity (SALA-LLONCH et al., 2014). This result, however, matches prior results on systematic decreases of long-range correlations and increases of short-range correlations induced purely by subject motion (POWER et al., 2012).

The relationship between network connectivity and cognitive performance is age dependent (TSVETANOV et al., 2016). On function specific studies, putamen-cortical RSFC has been associated with executive function with high replicability in younger and older groups of participants, but with opposite directions of effects, with higher RSFC being associated with faster completion of the Stroop 4 test in the older group and the opposite in the younger group (FJELL et al., 2017a).

Parallel to that, it was already known that diffusion MRI, which had been studied for well over a decade prior to the advent of fMRI, could be used to study white matter fiber orientations in the brain (LE BIHAN, 2014). This area of study developed into tractography, which was used to establish the structural connectivity of the brain, or in other words, the wiring of the axonal fibers, even though some caution is necessary when associating diffusional measurements with white matter microstructure (JONES; KNÖSCHE; TURNER, 2013).

Perhaps not surprisingly, there is some agreement between structural and functional connectivity (SKUDLARSKI et al., 2008), with structural connectivity acting as a moderator and causal driver of functional connectivity (BETZEL et al., 2014) . Indeed, evidences for increases in recruitment from fMRI in areas showing white-matter degeneration have been found (DASELAAR et al., 2015). Parallel to that, white matter morphometric and microstructural properties are related to decreases in executive functions independently of the effect of age (FJELL et al., 2017a).

Global structural connectivity parameters suffer from lasting decline throughout the adult lifespan, including decline in the number of connections, the total number of fibers and fractional anisotropy (BETZEL et al., 2014).

Evidence from the literature suggests functional and structural connectivity and morphometry might interact, but this varies regionally. Over 35 percent of the structural connections are consistent with brain thickness correlation patterns (GONG et al., 2012). Functional networks estimated by glucose consumption assed by FDG-PET and cortical thickness networks interact during aging, with the first acting as a constraint to the latter (ROMERO-GARCIA; ATIENZA; CANTERO, 2014). The relationship between white matter integrity and functional networks is more elusive (ANDREWS-HANNA et al., 2007; FJELL et al., 2015a; TSANG et al., 2017), but there is enough support to the idea that functional connectivity is somewhat dissociated of structural connectivity (FJELL et al., 2017b; TSANG et al., 2017). Multimodal studies fusing structural and functional connectivity and morphometry in aging are scarce, but overall point to compensatory recruitment of areas and also increased functional connectivity with white-matter integrity preservation (BURIANOVÁ et al., 2015; MARSTALLER et al., 2015). Evidence for under- and overactivation due to age-related volumetric atrophy in some areas has been asserted as well (KALPOUZOS; PERSSON; NYBERG, 2012; MAILLET; RAJAH, 2013).

Brain connectivity, structure, and function are intrinsically linked. As either changes due to aging, unveiling the presence, or absence, of alterations in the others, and in their association, could help to better understand the mechanisms of cognition and aging in the brain.

1.2 Objectives

In this work, we aim to further the understanding of the relationship between age-related alterations in brain morphometry and functional connectivity, specifically

defined as the Pearson correlation coefficient, Pearson partial correlation coefficient, Granger causality index, instantaneous Granger causality index, and Generalized Partial Directed Coherence, which has been seldom explored. Establishing if both processes share spatial patterns would help to better understand the what changes in the aging brain. More specifically, we aim to test if changes in gray matter cortical thickness in a given region due to age-related phenomena have an effect on the functional connectivity estimates for this region.

2 RESTING STATE BRAIN FUNCTIONAL CONNECTIVITY AND THE ROLE OF FUNCTIONAL MAGNETIC RESONANCE IMAGING (FMRI)

In this chapter we introduce the methodological foundations of the study of functional connectivity, including the MRI acquisition, spatial and temporal pre-processing to alleviate artifacts and residual variations due to movement and physiological phenomena, processing to obtain workable and meaningful functional connectivity estimators, and analysis to elucidate how these estimates are changing due to other factors.

2.1 Data acquisition

A resting state fMRI experiment usually proceeds as follows: the participant is introduced into the scanner and instructed to not think about anything in special and not fall asleep. The subject is also instructed to either keep their eyes closed or open, in this case including, or not, visual fixation on a visual guide, such as a crosshair on a screen, to differing effects of reliability and consistency (PATRIAT et al., 2013).

During the time that the participant stays in the scanner several procedures are executed. First an automated pre-scan routine is run, for calibration and tuning purposes, typically including quick shimming, coil tuning and matching, center frequency adjustment, and transmitter and receiver gain adjustments, and also including a series of dummy cycles that allow a steady state magnetization to develop, which consists on the application of pulse sequences without acquisition to stabilize the longitudinal magnetization (ELSTER; BURDETTE, 2001; HAASE et al., 2011). After a small amount of time, usually less than a minute, the actual resting state data acquisition starts, often lasting between 5 and 15 minutes, keeping in mind the reliability of connectivity estimates (BIRN et al., 2013). Two-dimensional single shot echo planar imaging (2D EPI) is the most widespread sequence in both academic and clinical applications, consisting in a gradient echo sequence filling the k-space in Euclidean fashion, one slice at a time. Gradient echo sequences are used because their contrast is in T2*, which is a physical property highly susceptible to brain hemodynamic fluctuations, in special the BOLD effect, which shortens the T2* relaxation time with increased deoxyhemoglobin concentration due to higher local field inhomogeneity given by the difference in susceptibility between oxy- and deoxyhemoglobin (OGAWA et al., 1990). In practice, the fMRI signal changes due to the hemodynamic response function,

which supplies blood flow in excess of the local demand. This increases the proton spins availability, and therefore the signal, regionally. Parallel to that, the oxygen saturation of the vessel changes field homogeneity regionally, altering the T2* relaxation time outside the vessel (BROWN et al., 2014).

A structural high-resolution T1-weighted scan is also acquired. This image allows to better discern brain anatomical features due to its improved soft-tissue contrast and spatial resolution.

2.2 Pre-processing

Several problems are likely to arise due to the lengthy scan time which reduces the usefulness of the raw data. To mitigate these, some pre-processing is required (POLDRACK; MUMFORD; NICHOLS, 2011).

The first glaring discrepancy in the scanned volumes is the time of acquisition of different slices. Since in conventional sequences one slice is acquired at each instant, there is a time evolution between the acquisitions of any two slices in the same volume. This is most pronounced when comparing the first slice acquired and the last one in a single TR. Interpolation in time helps to mitigate this effect, and this is commonly called slice timing correction. Slice timing corrections is not always performed, especially in small TR settings, since the errors introduced by the interpolation may surpass the errors due to the timing difference itself.

The next discrepancy is the misalignment of volumes in time, due to the movement of the subject scanned. Indeed, every subject presents involuntary movement inside the scanner, due to physiological tremors and postural adaptation. To correct this defect, scanned volumes are moved in space such that their spatial boundaries coincide approximately with a target volume. Usually, rigid-body transformations are employed, as the brain dimensions do not change during the time-scale of a single scan, comprising three-dimensional translation and rotation, totaling six-parameters. Common choices for target volume include an average volume or the first volume acquired. This comprises the pre-processing step known as realignment.

If both slice timing and realignment are to be applied, there is not a consensus on which order they should be used. In general, though, slice timing is usually performed first. If slice timing correction is performed first, it may interpolate voxels from different regions due to head movement. If it is performed latter,

however, the slices whose time is being corrected may be aggregated from different slices at acquisition time, especially in interleaved acquisition modes, where the difference in time between consecutive slices is bigger than in sequential acquisition modes.

Since the functional acquisition must be fast, spatial resolution is sacrificed. Thus, the high resolution anatomical scan is used to extract segmentation and possibly parcellation masks, which are then co-registered, or, in other words, spatially matched to conform to the functional volumes. Segmentation means determining to which tissue class pertains each voxel. The assignment can be partial, i.e. probabilistic, and is based on both shape and contrast. Parcellation, on the other hand, means subdividing a given tissue into sub-compartments, such as known anatomical regions or Voronoi partitions, for example, and is usually performed based on a template. To a given parcel is commonly ascribed the name Region of Interest (ROI). This structural pre-processing may be performed in surface or volumetric representations of the structural volume and can be done in a common space or in native, i.e. subject, space, that is, with or without normalization (WHITFIELD-GABRIELI; NIETO-CASTANON, 2012).

Depending on the intended purposes of the acquisitions, additional steps in the spatial pre-processing of functional data might include normalization to a template space, allowing direct comparisons between subjects, and spatial smoothing. Normalization is performed first on the anatomical volume. Then, based on the transformation tensor obtained that matches the acquired volume to the template space, the same transformation is performed on the functional volumes, usually requiring additional information, such as the segmentation masks, to ease the process. Smoothing is performed to reduce spatial noise and is a fundamental step for the Random Field Theory parametric method, widely used in model based functional analysis. In connectivity analysis, however, this step is usually skipped.

Even though the realignment helps to mitigate the effects of movement on the voxels timeseries, residual effects might be present on the timeseries signal itself. Also, it is known BOLD-related fluctuations have low amplitude in white matter and are virtually absent in cerebrospinal fluid (CSF) voxels. For these reasons, the timeseries of the movement realignment parameters and representative timeseries from white matter and CSF are included as covariates at the level of the subject, or first-level covariates. Typically, movement parameters include the six-parameter

spatial transformation timeseries, comprising translations and rotations in three-dimensional space, while for white-matter and CSF signal spatial averages or, more commonly, principal components are employed.

The effect of movement, noise components from non-grey matter tissue, and any other known noise timeseries available, such as physiological noise due to the heart cycle and respiration, which are acquired separately with special equipment, and therefore not always available, are removed through linear regression applied to each voxel separately, in what is usually called nuisance regression. The temporal derivatives of these factors may also be included in this step. Prior to that, a procedure known as despiking can be performed to mitigate large sudden variations in the timeseries, which aren't compatible with the theoretical behavior of the BOLD signal.

The magnetic resonance signal may present some drifting behavior, that is, some non-stationarity regarding its expected value. This is removed through detrending the timeseries, usually accounting for linear or polynomial trends.

As the BOLD signal has a frequency signature, signal components whose frequency lie outside this theoretical frequency band are excluded through filtering (WHITFIELD-GABRIELI; NIETO-CASTANON, 2012), as these frequencies might be harmonics of respiratory and cardiac cycles aliased into lower frequencies (CABALLERO-GAUDES; REYNOLDS, 2016).

Timeseries per ROI per subject are extracted by computing the spatial average of the image weighted by the ROI mask. Alternatively, multiple timeseries per ROI can be extracted through source separation methods such as principal components analysis. The timeseries can also be divided into different frequency components.

A typical processing pipeline is shown in Figure 2.1. As shown, functional pre-processing inputs include the functional and structural volumes, ROI definitions and design matrices, in the case of task paradigms, while outputs include the residual BOLD volumes, which can be summarized into ROI timeseries.

Figure 2.1 Schematic view of a pre-processing pipeline.

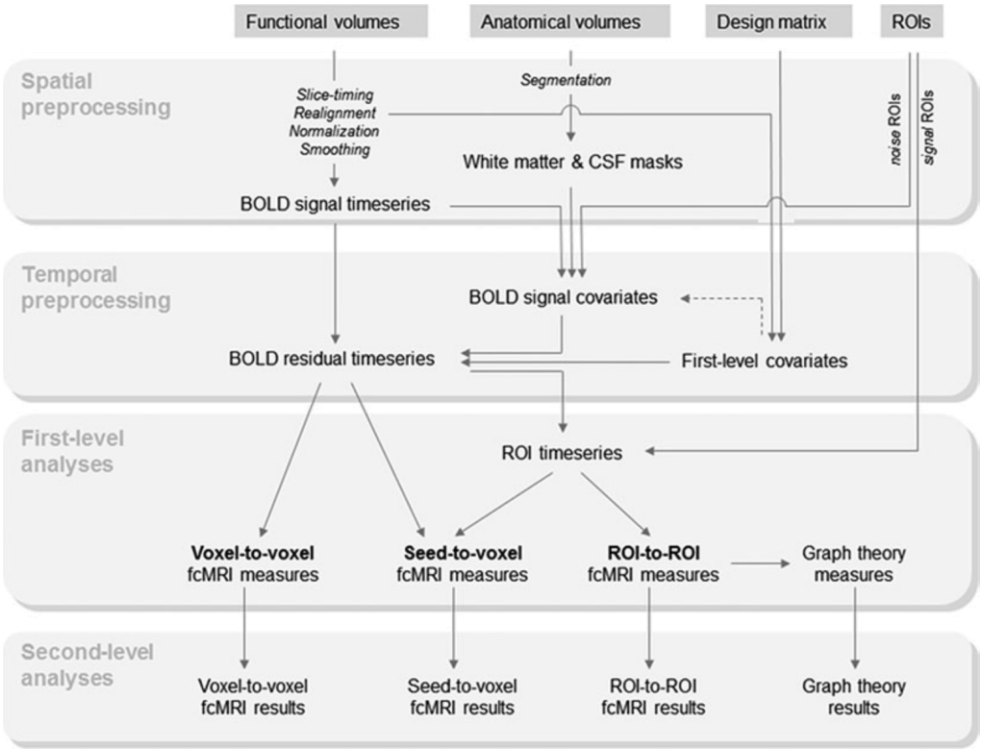

Source: WHITFIELD-GABRIELI, S.; NIETO-CASTANON, A. Conn: A Functional Connectivity Toolbox for Correlated and Anticorrelated Brain Networks. **Brain Connectivity**, v. 2, n. 3, p. 125–141, 2012.

2.3 Processing

After the pre-processing, each ROI per subject is represented as a time series as denoted in Equation 1, in matrix notation, where the matrix $\boldsymbol{X}$ is the concatenation of the timeseries $\boldsymbol{x}_i$ in column matrix format, with n being the number of time samples and m the number of ROIs.

$$\boldsymbol{X} = (\boldsymbol{x}_1, \boldsymbol{x}_2, \ldots \boldsymbol{x}_m) = \{X_{ij}\}_{n \times m} \tag{1}$$

A common and simple measure of functional coupling between scalar timeseries is the Pearson correlation coefficient ρ_{AB} (BISWAL et al., 1995), given indexed timeseries $\boldsymbol{x}_A$ and $\boldsymbol{x}_B$, and having $\sigma(\cdot)$ as the standard deviation function, $\mathbb{E}(\cdot)$ being the expectancy function, and $Cov(\cdot)$ the covariance function between two vectors, as shown in Equation 2.

$$\rho_{A,B} = \frac{\mathbb{E}[(\boldsymbol{x}_A - \mathbb{E}(\boldsymbol{x}_A))(\boldsymbol{x}_B - \mathbb{E}(\boldsymbol{x}_B))]}{\sigma(\boldsymbol{x}_A) \cdot \sigma(\boldsymbol{x}_B)} = \frac{Cov(\boldsymbol{x}_A, \boldsymbol{x}_B)}{\sqrt{Cov(\boldsymbol{x}_A, \boldsymbol{x}_A) \cdot Cov(\boldsymbol{x}_B, \boldsymbol{x}_B)}} \tag{2}$$

These correlation coefficients can be calculated for every pair of ROIs, resulting in $m \times m = m^2$ correlation estimates, with $m \times (m-1)/2$ being unique and potentially different from 1. Arranging these estimates into a matrix, for neurofunctional timeseries, results in the so called functional connectivity matrix, as shown in Equation 3. It can be demonstrated that this matrix is necessarily symmetric, and its diagonal is filled with ones.

$$\boldsymbol{\rho} = \begin{pmatrix} 1 & \cdots & \rho_{1,m} \\ \vdots & \ddots & \vdots \\ \rho_{1,m} & \cdots & 1 \end{pmatrix} \tag{3}$$

If $\boldsymbol{\rho}$ is positive definite, we can calculate its inverse $\boldsymbol{\rho^{-1}}$. This matrix is called the precision matrix $\boldsymbol{R}$, which is also symmetric but whose diagonal is not necessarily populated by ones, as shown in Equation 4.

$$\boldsymbol{R} = \boldsymbol{\rho^{-1}} = \begin{pmatrix} R_{1,1} & \cdots & R_{1,m} \\ \vdots & \ddots & \vdots \\ R_{1,m} & \cdots & R_{m,m} \end{pmatrix} \tag{4}$$

From a normalization of the precision matrix, shown in Equation 5, it is possible to obtain what is called the partial correlation coefficient. This coefficient measures the degree of association between two variables discounting mutual association with other variables. In this specific notation, the correlation coefficient is partial regarding all other variables in the correlation matrix and is shown in Equation 6. Extending this notation to simpler forms, where only specific variables are partialled out, requires just the exclusion of other variables from the correlation matrix prior to the computation of the partial correlation matrix.

$$r_{i,j} = \frac{R_{i,j}}{\sqrt{R_{i,i} \cdot R_{j,j}}} \tag{5}$$

$$\boldsymbol{\rho}^* = 2 \cdot \mathbb{I}_m - \boldsymbol{r} = \begin{pmatrix} 1 & \cdots & -r_{1,m} \\ \vdots & \ddots & \vdots \\ -r_{1,m} & \cdots & 1 \end{pmatrix} \tag{6}$$

Positive definiteness is not achievable when $m > n$. In those cases, the inversion of the correlation matrix can be achieved incorporating assumptions into the problem, leading to shrinkage estimates (LEDOIT; WOLF, 2001, 2004; WANG et al., 2016).

While the correlation coefficients measure linear association, it is important to emphasize such association is simultaneous if the vectors $\boldsymbol{x}_i$ start being measured at the same point in time.

Non-simultaneous associations between the timeseries may be present though, through lagged dependencies. In this case, one might consider modelling one timeseries $\boldsymbol{x}_i$ given past instances of itself and another $\boldsymbol{x}_j$, through Equation 7. Restricting this model to only the original $\boldsymbol{x}_i$ series results in Equation 8. These models are called vector autoregressive (VAR) models, a generalization of the autoregressive model to any number of channels (ROGERS et al., 2010).

$$x_{i,t} = A_0 + \sum_{p=1}^{\tau}\left(A_p \cdot x_{i,t-p} + B_p \cdot x_{j,t-p}\right) + \epsilon_{i,t} \tag{7}$$

$$x_{i,t} = A_0^* + \sum_{p=1}^{\tau}\left(A_p^* \cdot x_{i,t-p}\right) + \epsilon_{i,t}^* \tag{8}$$

The definition of Granger causality is born of the comparison of both models (KIRCHGÄSSNER; WOLTERS, 2007). If the first model explains the variability of $\boldsymbol{x}_i$ better than the second one, we can say that $\boldsymbol{x}_j$ Granger-causes $\boldsymbol{x}_i$. Such comparison can be paraphrased as a likelihood ratio test or as a sequential sum of squares test, and the test statistic can be employed as a coefficient denoting evidence for Granger causality.

Granger causality is directional and therefore asymmetric, which means the Granger causality from A to B and from B to A are not necessarily the same.

This metric of predictive causality has been extensively used in the fMRI literature, but there is no consensus in its validity due to hemodynamic confounding and unclear relationship to underlying neurometabolic processes (SETH; BARRETT; BARNETT, 2015).

On the other hand, augmenting the model in Equation 7 with the inclusion of present states of $\boldsymbol{x}_j$, resulting in the model presented in Equation 9, allows one to test what is called instantaneous Granger causality, if such model is significantly better at prediction $\boldsymbol{x}_i$ than the previous one.

$$x_{i,t} = A_0' + B_0' \cdot x_{j,t} + \sum_{p=1}^{\tau}\left(A_p' \cdot x_{i,t-p} + B_p' \cdot x_{j,t-p}\right) + \epsilon_{i,t}' \tag{9}$$

Instantaneous Granger causality has a sense of immediate coupling and is symmetric.

It is important to note that predictive causality does not allow one to assert true causality. Causality is inferred from randomized controlled experiments, or causal inference accounting for hidden factors.

The previous modelling approach can be generalized to multivariate timeseries, as shown in Equation 10, including other factors besides $\boldsymbol{x}_i$ and $\boldsymbol{x}_j$.

$$\begin{cases} x_{i,t} = A_0 + \sum_{p=1}^{\tau}\left(\sum_{k\neq j}^{m}\left\{A_{p,k}\cdot x_{k,t-p}\right\} + B_p \cdot x_{j,t-p}\right) + \epsilon_{i,t} \\ x_{i,t} = A'_0 + \sum_{p=1}^{\tau}\sum_{k\neq j}^{m}\left(A'_{p,k}\cdot x_{k,t-p}\right) + \epsilon'_{i,t} \end{cases} \tag{10}$$

From these we can also define partial Granger causality and partial instantaneous Granger causality.

The maximum order τ of a VAR model is a hyperparameter that can be chosen using informative criteria (TING et al., 2015). One also has to keep in mind the parsimoniousness of the model, since a VAR model with m timeseries and including τ lags has, in total $k \times k \times \tau$ autoregressive parameters, which quickly saturates the model with increasing k.

Another interesting prospect is to investigate predictive causality in the frequency domain due to the known frequency band of interest inherent to BOLD hemodynamic activity and other bands associated with physiological, non-neuronal, phenomena. Recall that, in the unrestricted VAR formulation, the present state of a factor depends on the previous states of all factors in the past, including itself. We can, therefore, paraphrase this as in Equation 11.

$$\begin{bmatrix} x_{1,t} \\ x_{2,t} \\ \vdots \\ x_{m,t} \end{bmatrix} = \begin{bmatrix} A_{1,0} \\ A_{2,0} \\ \vdots \\ A_{m,0} \end{bmatrix} + \sum_{p=1}^{\tau} \begin{bmatrix} A_{1,1,p} & A_{1,2,p} & \cdots & A_{1,m,p} \\ A_{2,1,p} & A_{2,2,p} & \cdots & A_{2,m,p} \\ \vdots & \vdots & \ddots & \vdots \\ A_{m,1,p} & A_{m,2,p} & \cdots & A_{m,m,p} \end{bmatrix} \begin{bmatrix} x_{1,t-p} \\ x_{2,t-p} \\ \vdots \\ x_{m,t-p} \end{bmatrix} + \begin{bmatrix} \epsilon_{1,t} \\ \epsilon_{2,t} \\ \vdots \\ \epsilon_{m,t} \end{bmatrix} \tag{11}$$

Given autoregressive coefficients $A_{i,j,p}$, $1 \leq p \leq \tau$, these have a dependence on time. Through the Discrete-time Fourier transform of these coefficients we can uncover the signature of these dependencies in the inverse domain. If the direct domain is time, the inverse is one over time, *i.e.* temporal frequency. If we concatenate these coefficients through time into a vector $\boldsymbol{A}_{i,j} = (A_{i,j,1} \quad \cdots \quad A_{i,j,\tau})$, we can denote such transformation as shown in Equation 12.

$$\overline{\boldsymbol{A}}_{i,j} = \mathcal{F}\left(\boldsymbol{A}_{i,j}\right) = \left(\overline{A}_{i,j,1} \quad \cdots \quad \overline{A}_{i,j,\theta}\right) \tag{12}$$

If the length in time between lags is denoted Δt, the maximum unaliased frequency, by the Nyquist-Shannon sampling theorem, is $f_{max} = 1/2 \cdot \Delta t^{-1}$. Frequencies above that are aliased into the $(0, f_{max})$ interval.

The partial directed coherence (PDC) is a normalization of the coefficients in the frequency domain (SAMESHIMA; BACCALÁ, 1999), imbued with meaningful interpretation while preserving the notion of predictive causality. It is often dubbed as the frequency-domain analogue of Granger causality (SATO et al., 2009).

The original PDC is defined as shown in Equation 13, which results in the normalization shown in Equation 14.

$$\pi_{i,j,f} = \frac{\overline{A}_{i,j,f}}{\sqrt{\sum_{l=1}^{m} \left\| \overline{A}_{l,j,f} \right\|_2^2}} \tag{13}$$

$$\sum_{l=1}^{m} \left\| \pi_{l,j,f} \right\|_2^2 = 1 \tag{14}$$

Even though the asymptotic inference for PDC works for every version of this measure (BACCALÁ et al., 2013), the original version of PDC is not invariant to scaling of the input variables. Therefore, a derivative called generalized Partial Directed Coherence (GPDC) has been proposed (BACCALA; SAMESHIMA; TAKAHASHI, 2007), with successful applications in EEG (RODRIGUES; BACCALA, 2015) and fMRI (SATO et al., 2009). Equation 15 shows this generalization, where $\sigma_l^2 = Var(\boldsymbol{\epsilon}_l)$, where $\boldsymbol{\epsilon}_l = (\epsilon_{l,1} \quad \cdots \quad \epsilon_{l,n})$ is the vector of innovations for series $\boldsymbol{x}_l$ in time.

$$\pi_{i,j,f}^{G} = \frac{\frac{1}{\sigma_i} \overline{A}_{i,j,f}}{\sqrt{\sum_{l=1}^{m} \frac{1}{\sigma_l^2} \left\| \overline{A}_{l,j,f} \right\|_2^2}} \tag{15}$$

The GPDC estimate is unique regardless of the scaling of the inputs, which is a desirable property. Besides that, the squared GPDC $\left(\pi_{i,j,f}^{G}\right)^2$ can readily be interpreted as the proportion of the power spectra transferred from $\boldsymbol{x}_j$ to $\boldsymbol{x}_i$ considering all other timeseries in the VAR model (SATO et al., 2009).

Essentially, we can categorize connectivity metrics based on their characteristics, namely multivariate versus bivariate, directed versus symmetric, and operating in the time domain versus operating in the frequency domain. Pearson correlation and instantaneous Granger causality are bivariate, and symmetric connectivity metrics. Granger causality is bivariate and directed. Partial Pearson

correlation is multivariate, and symmetric. All these metrics operate in the time domain. PDC and GPDC are examples of multivariate directed metrics operating in the frequency domain.

2.4 Statistical Analysis

The most common methodology to study the association between a dependent random variable and, possibly many, independent random variables is the Generalized Linear Model (GLM).

The GLM is a widely used statistical framework relating the expectation of a dependent random variable to a linear function of independent random variables. We can describe the conditional expectation $Y_i|X_i$ with the probability density function f, with natural or canonical parameter θ and dispersion parameter ϕ, as in Equation 16

$$Y_i|X_i \sim f(Y_i; \theta_i, \phi_i) \tag{16}$$

If the probability density function f is in the single parameter exponential family, setting the expected value of Y conditional on X as a linear function of X, and the variance of the dependent variable as a function of the linear predictor, as shown in Equation 17, and estimating μ through β is the formal definition of a GLM.

$$\begin{cases} g\big(\mathbb{E}(Y|X)\big) = g(\mu) = \beta X = \eta \therefore \mu = g^{-1}(\eta) \\ \sigma^2 = Var(Y) = v(\mu) = v\big(g^{-1}(\eta)\big) \end{cases} \tag{17}$$

Special choices for g, and v given f turn the estimation easier, which can be carried through employing Iteratively Reweighted Least Squares (IRLS). If f is the Gaussian probability density function, the link function is $g(\mu) = \mu$, and $v(\mu) = \text{cte}$, the resuling GLM is equivalent to an ordinary linear model.

GLM coefficients allow Wald tests given the standard error and mean estimates of the parameters. Analysis of deviance, and consequently joint-tests, can also be performed using the likelihood ratio, based on the χ^2 statistic, or sequential sums of squares, this one resulting in a F-test.

The GLM framework has been extended to support smooth functions of predictors, namely the Generalized Additive Model (GAM). Accounting for intraclass correlation between observations constitutes the Generalized Linear Mixed Model (GLMM), where coefficients are allowed to vary given groupings of samples, becoming what is called a random effect, or in other words an effect that differs from

the population one, the fixed effect, due to sampling. Random effects can be fully segregated and also nested or crossed, fully or partially.

While the single parameter exponential family is really broad, covering the most common choices for the distribution of the dependent variable, for which IRLS can be used to obtain a solution, it doesn't cover all use cases, for example the Beta and Dirichlet distributions. This framework can be extended though.

In the case of the probability density function being the Dirichlet distribution, the resulting model is known as Dirichlet Regression (MAIER, 2014). These modelling approaches are appropriate to proportion data, when the dependent variable is the result of a ratio between two Normal random variables.

3 METHODS

In this chapter, the materials and methods used in our study are detailed, including a description of our sample, data acquisition, image pre-processing and processing, and the statistical analyses used to obtain estimates of effects.

3.1 Casuistry

Phenotypic data from 1148 subjects were retrospectively obtained from the public databases maintained by the Nathan Kline Institute at Orangeburg, NY, that make up the Rockland Sample (NKI-RS) (NOONER et al., 2012), in their Pilot and Enhanced distributions, currently contributing 207 and 941 subjects each respectively, which are distributed through the International Neuroimaging Data-Sharing Initiative (INDI) and the 1000 Functional Connectomes Project (FCP) (MENNES et al., 2013). The NKI-RS is an ongoing large-scale endeavor aimed at phenotyping and imaging neurotypical subjects from the Rockland County, NY.

Our exclusion criteria were age less than 18 years, left-handedness, and perceptible artifacts or defects in either the functional or anatomical scan. Applying these criteria, a final set of 613 subjects was achieved, 483 from the Enhanced NKI-RS and 130 from the Pilot NKI-RS datasets.

Table 3.1 Aging and gender characteristics of the sample

	Enhanced NKI-RS		Pilot NKI-RS	
Age (years since birth)	Male	Female	Male	Female
[18, 27]	53	56	26	19
[28, 37]	19	25	9	9
[38, 47]	18	54	26	6
[48, 57]	13	79	6	5
[58, 67]	26	61	6	6
[68, 77]	19	41	5	5
[78, 87]	7	11	2	0
Mean	44.58*	50.45	40.58*	40.18*
(C.I. 95%)	(41.72, 47.44)	(48.49, 52.42)	(36.60, 44.55)	(35.15, 45.21)
Fisher's exact test	p = 1		p = 1	
Total	155	327	80	50

Source: The author. *: Denotes a significant difference to the age of females in the Enhanced NKI-RS.

The characteristics of the sample are shown in Table 3.1. The Two-Sample Kolmogorov-Smirnov test was employed to test the difference in the distributions of age across genders, resulting in $D = 0.222$, p-value = 0.0000616 for the Enhanced NKI-RS, and $D = 0.148$, p-value = 0.515 for the Pilot NKI-RS.

A type-II two-way ANOVA was conducted to examine any relationship between both dataset, gender, and their interaction with the subject ages. Set and gender demonstrated significant effects at $p = 0.000237$ and $p = 0.00430$, respectively, with no evidence for their interaction at $p = 0.0920$. In this linear model, the expected difference of age between datasets was estimated as 7.1391 years taking into account the effect of gender, with the Pilot NKI-RS presenting, on average, a smaller expected value of age. Females in the Enhanced NKI-RS had age significantly higher than the other groups, as attested by the pairwise comparison of means using Tukey's range test. No other significant difference was present.

Table 3.2 Image acquisition parameters in 3T scanners

Modality	3D MP-RAGE		2D BOLD-EPI	
Dataset	Enhanced	Pilot	Enhanced	Pilot
Voxel size (mm^3)	1 x 1 x 1	1 x 1 x 1	3 x 3 x 3	3 x 3 x 3
TR (ms)	1900	2500	645	2500
TE (ms)	2.52	3.5	30	30
TI (ms)	900	1200	-	-
Flip angle	9°	8°	60°	80°
FOV (mm^3)	250x250x176	256x256x200	222x222x120	216x216x126.21
Number of slices	-	-	40	38
Distance factor	-	-	0%	11%
PA factor	2	-	-	-
MB factor	-	-	4	-
Acquisition mode	Single-shot ascending	Single-shot ascending	Siemens interleaved	Siemens interleaved
Measurements	1	1	900	260
Acquisition time	4’18’’	10’42’’	9’46’’	10’55’’

Source: The author. TR is the repetition time, the time between each volumetric acquisition. TE is the echo time, the time between consecutive echoes in the MP-RAGE acquisition and the time between the excitation pulse and the most intense gradient echo at the center of k-space in 2D BOLD EPI. TI is the inversion time; it is the time between the inversion of the magnetization and the excitation pulse. FOV is the field of view in the antero-posterior, right-left, and foot-head directions, respectively. PA means parallel acquisition acceleration. MB stands for multiband acceleration. The Siemens interleaved slice ordering is one such as that, if the number of slices is even, the even slices in the stack will be acquired first, while if the number of slices is odd, the odd slices in the stack are acquired first instead.

Anatomical scans were comprised of high definition three-dimensional magnetization-prepared rapid gradient-echo imaging (3D MP-RAGE) (MUGLER; BROOKEMAN, 1990; RUNGE et al., 1991) while functional scans were acquired as multi-slice using a 2D EPI sequence. The functional scans we used from the

Enhanced NKI-RS were acquired using a multiband acquisition (FEINBERG; REESE; WEDEEN, 2002). The image acquisition parameters are shown in Table 3.2.

3.2 Pre-processing

All anatomical images were pre-processed in the software Freesurfer v.6.0.0 (FISCHL, 2012) using the default recon-all routine resulting in the segmentation of brain tissue types, and also the automatic whole brain parcellation (FISCHL et al., 2002) of subcortical structures based on the RB_all_2008-03-26.gca atlas distributed with Freesurfer, shown in Figure 3.1, and cortical gray matter into 148 anatomical gyral-sulcal regions of interest (ROIs) according to the Destrieux atlas (DESTRIEUX et al., 2010), shown in Figure 3.2.

Figure 3.1 Selected regions from the RB_all_2008-03-26.gca automatic segmentation atlas.

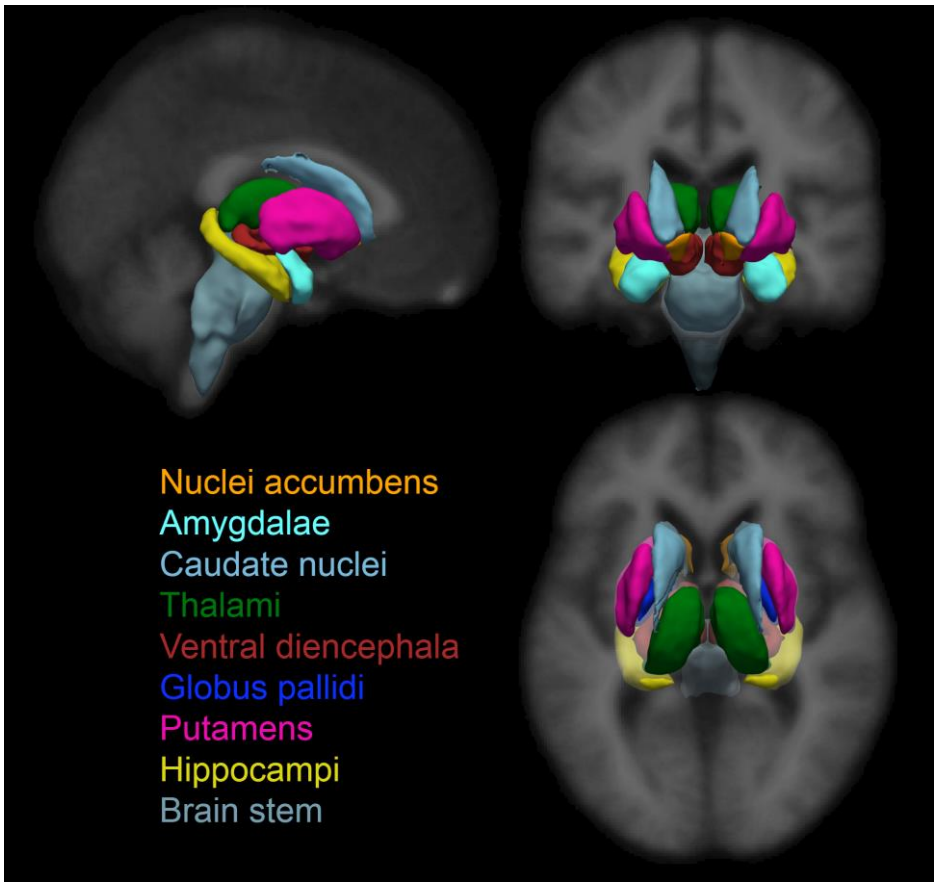

Source: The author. The figure was generated using the visualization toolbox freeview. Ventricular, cerebellar, vascular, and outer cerebral structures not shown. The ventral diencephala consist of several smaller thalamic subdivisions and other small structures which are not discernible in common anatomical MRI contrast and resolution. Brainstem consists of medulla oblongata, pons, and mesencephalon.

Figure 3.2 The Destrieux automatic parcellation atlas.

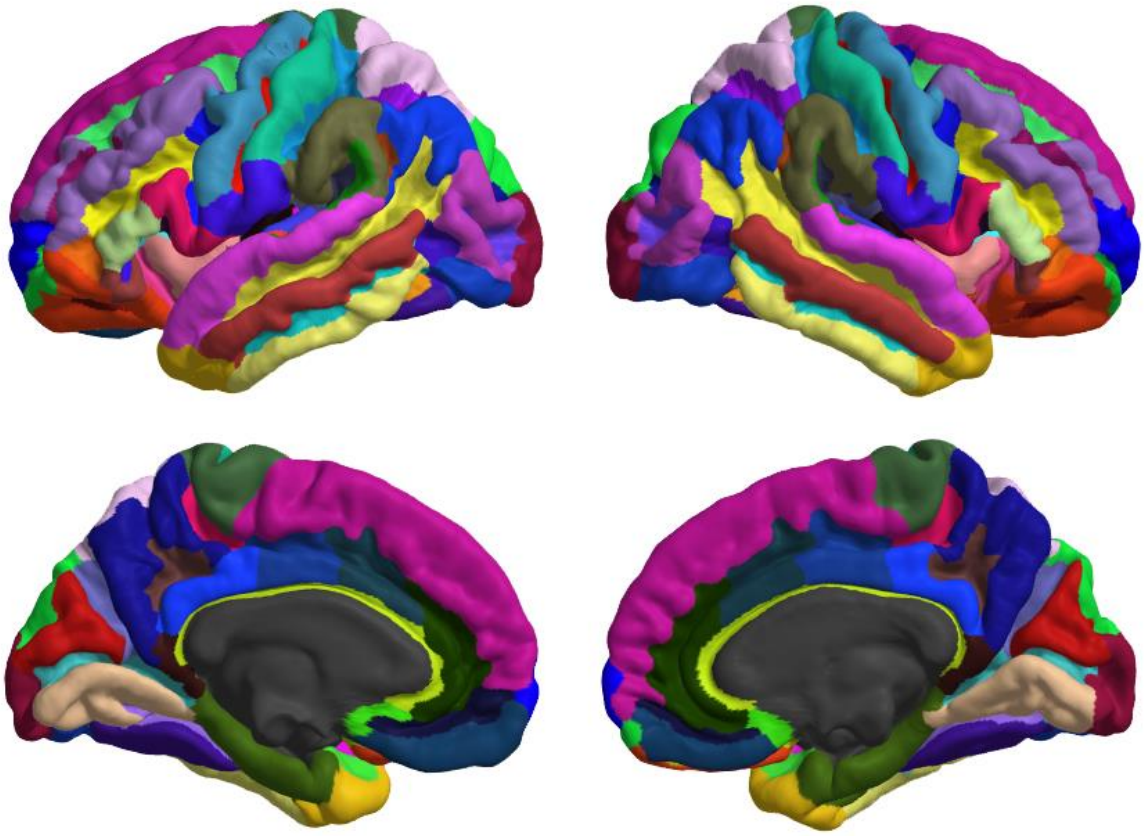

Source: The author. The figure was generated using custom code based on the freesurfer_statsurf_display MATLAB toolbox.

While the RB_all_2008-03-26.gca is the only subcortical atlas distributed with Freesurfer, there are other atlases for the cortical parcellation. The Destrieux atlas has high anatomic specificity and was chosen for this reason.

A single workstation was employed to avoid possible inconsistencies (GRONENSCHILD et al., 2012), which we reproduced between operational system versions (VIEIRA; SALMON, 2017).

In the RB_all_2008-03-26.gca atlas, subcortical structures are defined as in the MGH Center for Morphometric Analysis (CMA) manual segmentation scheme, often employed in the morphometric literature (FILIPEK et al., 1994), with the gray nuclei separated into thalamus proper and a ventral diencephalon, comprised of hypo-, epi-, meta- and subthalamus, substantia nigra, and nucleus ruber (SEIDMAN et al., 1997).

A single subject was removed from the study due to faulty structural pre-processing.

This step of the study was conducted in the High Performance Computing Center of the FAPESP Center for Neuromathematics (grant 2013/07699-0) at USP Ribeirao Preto, in a CentOS Linux 7 (1611), kernel 3.10.0-514, Intel® Xeon® E5-2650 v3 compute cluster. GNU Parallel (TANGE, 2015) was employed to allow pre-processing in parallel, greatly reducing total computation time. Processes were carried through the resource management tool SLURM (JETTE; YOO; GRONDONA, 2002).

Functional scans were pre-processed in the MATLAB toolbox CONN v.16.b (WHITFIELD-GABRIELI; NIETO-CASTANON, 2012) using the default surface-based subject-space pre-processing routine, employing utilities from SPM12 (http://www.fil.ion.ucl.ac.uk/spm/software/spm12/) and Artifact Detection Tools (ART) (https://www.nitrc.org/projects/artifact_detect/) toolboxes, which includes functional volumes realignment and unwarping, slice-timing correction, coregistration to the structural volume and scrubbing. Scrubbing comprises the annotation of functional volumes whose realignment parameters show outlier behavior. Slice time correction was not performed on the functional images from the Enhanced NKI-RS dataset, due to the small repetition time and multiband acquisition.

After the pre-processing, a denoising procedure was conducted. It includes:

- despiking, done through a hyperbolic tangent function applied to the signals standardized by their absolute deviations times four, which should compress the amplitude of the signals, as the function tend to -1 or 1 when the magnitude of the signal is too much higher than the denominator
- nuisance regression, that is, the removal of the effect of first-level covariates, such as the CSF and white matter signal principal components, which is described as the CompCor method (BEHZADI et al., 2007; MUSCHELLI et al., 2014)
- the six rigid-body realignment movement covariates and their derivatives and the scrubbing series
- linear detrending
- bandpass filtering in the 0.008-0.090 Hz band

We did not employ the common pre-processing technique known as global signal regression (GSR) to our analysis. GSR can be carried by simply including the

gray matter temporal averaged timeseries in the CompCor step. GSR reduces the skew of the correlation estimates, mitigating the effects of movement, and therefore shrinking the average correlation towards zero, increasing the number of negative correlations (WHITFIELD-GABRIELI; NIETO-CASTANON, 2012). It is not entirely clear what GSR encompass to the interpretation of the resulting connectivity, and in special the anti-correlations, but it is known the global signal is significantly coupled with neural activity (GEERLIGS et al., 2017; SCHÖLVINCK et al., 2010).

Subsequently to the pre-processing and denoising, the resulting correlation histograms were visually assessed. Some histograms in the Enhanced NKI-RS displayed moderate skewness compared to the rest, which is a symptom of head motion. Three subjects were removed from the Enhanced NKI-RS due to excessive head motion, as verified by the number of temporal volumes marked by the ART procedure, in excess of five percent.

In total, structural data from 612 subjects and functional data from 609 subjects were successfully pre-processed.

3.3 Processing

Morphometric estimates were obtained for every subject in volumetric and superficial subject-space representations, including thickness, volume, and area for cortical structures defined in the Destrieux atlas shown in Figure 3.2, and also subcortical volume estimates based on the RB_all_2008-03-26.gca atlas shown in Figure 3.1.

For each ROI defined in the cortical anatomical atlas, its functional timeseries was defined as the timeseries of voxels inside the ROI averaged through space.

Bivariate connectivity metrics were calculated in pairwise fashion for every combination of the 148 cortical ROIs defined in the Destrieux atlas. These are bivariate Pearson Correlation, Granger Causality, and Instantaneous Granger Causality indexes.

From the Pearson correlation matrices, sparse Partial Correlation matrices were estimated based on a density criterion (WANG et al., 2016). A reduced subset of 130 ROIs was studied, chosen due to the fact that some regions lacked BOLD timeseries in some subjects, most probably due to suboptimal coregistration, which affects smaller regions severely, thus making their connectivity estimates less reliable

due to the reduced sample size. ROIs were kept if both they and their homotopic, i.e. contralateral equivalent, counterpart each had less than forty missing observations.

Four pairs of homotopic ROIs were selected based on the magnitude of the effect of age on cortical thickness t-statistic and GPDC spectra were estimated on fifty frequencies on the normalized frequency band using timeseries from these eight regions.

R package DensParcorr was used to estimate partial correlation matrices (WANG et al., 2016).

The R package vars (PFAFF, 2008a, 2008b) was used to build the bivariate VAR models used to estimate Granger Causality and Instantaneous Granger Causality.

VAR models were estimated to calculate GPDC using AsympPDC Package v. 2b (SAMESHIMA; BACCALÁ, 2011) in MATLAB. VAR(2) models were fitted using the Nutall-Strand algorithm. Order 2 was selected due to the fact that order 2 provided sufficient fit, while informative criteria usually lead to highest order available and therefore overfitted the selection, returning unstable VAR(p) processes. Another practical consideration is the fact that an VAR(2) process in this configuration has 128 parameters already; contrasting that with the 900 samples in the Enhanced NKI-RS and 260 samples in the Pilot NKI-RS makes overfitting a real concern.

3.4 Statistical Analysis

Morphometrical measurements were analyzed in the following fashion, given a morphometric measurement M across subjects, it can be modeled as a linear function of the subjects age, allowing all interactions by subject sex and also the dataset they came from, to account for possible bias in the measurements, as is represented in Equation 18, using Wilkinson-Rogers notation (WILKINSON; ROGERS, 1973):

$$M \sim Age * Sex * Set \tag{18}$$

Equivalently, in conventional notation as shown in Equation 19:

$$M_i = \beta_0 + \beta_{Age} \cdot Age_i + \beta_{Sex} \cdot Sex_i + \beta_{Set} \cdot Set_i + \beta_{Age:Sex} \cdot Age_i \cdot Sex_i + \beta_{Age:Set} \cdot Age_i \cdot Set_i + \beta_{Set:Sex} \cdot Set_i \cdot Sex_i + \beta_{Age:Sex:Set} \cdot Age_i \cdot Set_i \cdot Sex_i + \epsilon_i \tag{19}$$

Analogously, we studied the effect of age on a given bivariate connectivity metric, denoted as C, with the following linear model shown in Equation 20.

$$C \sim Age * Sex \quad (20)$$

Which reduces, in conventional notation, to the expression in Equation 21.

$$C_i = \beta_0 + \beta_{Age} \cdot Age_i + \beta_{Sex} \cdot Sex_i + \beta_{Age:Sex} \cdot Age_i \cdot Sex_i + \epsilon_i \quad (21)$$

As the functional data acquisition differs between the datasets, these were analyzed separately, and therefore no Set_i term appears in Equation 21.

The Pearson correlation coefficient was remapped using the Fisher transformation, i.e. inverse hyperbolic tangent function. Instantaneous Granger Causality and Granger Causality are distributed respectively as Chi-squared and F, and therefore were normalized in all analyses using the normal inverse cumulative distribution function applied to the respective cumulative distribution function applied to the predictive causality estimator.

To study the coupling between connectivity and morphometry, we proposed two seemingly related methods: to study the age-related differential maps of morphometry and ROI-ROI connectivity given a seed ROI, and to study the connectivity given a seed ROI on an intra and inter subject basis with a mixed-effects model. Mixed-effects models were built using the R package lme4 (BATES et al., 2015). Hypothesis testing on the fixed effects was conducted using the normal approximation, made possible due to the large degrees of freedom (BARR et al., 2013), in excess of the hundreds.

To study the differential maps of age-related effects on both cortical thickness and connectivity estimates, the standardized regression coefficients for age were obtained in each connectivity estimate and also in each cortical thickness estimate. Then, given a source ROI, the correlation of the spatial map of the standardized coefficients of its connection to the target ROIs and the standardized coefficients of the cortical thickness of the target ROIs was computed. This procedure was done only for functional connectivity estimates from the Enhanced NKI-RS due to its better temporal resolution and higher number of subjects. The standardized effect of age on cortical thickness was estimated with the union of both data sets.

Given a seed ROI and its connectivity estimates to target ROIs across subjects, the mixed model given in Equation 22 was estimated.

$$C \sim Age * (Sex + TargetThickness + SeedThickness) + (SeedThickness|Target) + (TargetThickness|Subject) \quad (22)$$

Using this specification, a connectivity estimator is allowed to vary given the thickness estimates of both the source and the target ROI, and also the age and sex of the subject. Also, including all first order interactions between the fixed effects with age, the effect of age depends on the sex of the subject and its cortical thickness estimates or, alternatively, the effect of the cortical thickness is allowed to vary linearly with age.

Four pairs of homotopic ROIs were picked based on the t-statistic associated with the effect of age in Equation 19 using thickness as the morphometric measure. This analysis was re-estimated using a robust linear model approach (KOLLER; STAHEL, 2011, 2017).

The Generalized Linear Model (GLM) (MCCULLAGH; NELDER, 1989) using the Logit link is a common and proven method to deal with percentage data (ZHAO; CHEN; SCHAFFNER, 2001). Going further into the theoretical basis, GPDC is a ratio of positive continuous variables. Such type of compositional data has often been studied with Beta Regression, in the bivariate case. The squared GPDC is normalized to sum to one by source, i.e. it is a proportion, naturally leading us to the multivariate generalization of the Beta Regression: the Dirichlet Regression. The Beta and Dirichlet Regressions are not, strictly speaking, Generalized Linear Models due to the non-orthogonal parametrization employed, but in practice, however, they tend to display the same behavior, constituting a GLM-like framework (MAIER, 2014).

We propose the use of Dirichlet Regression to analyze GPDC spectra. A total of forty models were estimated, one per source ROI per frequency. GPDC was estimated for fifty frequencies distributed between 0 Hz and 0.78 Hz, the Nyquist frequency of the Enhanced NKI-RS resting-state acquisition, to better characterize the spectral density. Only the five frequencies within the band of the filter employed in the pre-processing step, approximately 0.016, 0.031, 0.047, 0.062, and 0.078 Hz, were studied. In total, 320 coefficients for the effects of age were estimated.

Robust linear models were fitted using R package robustbase version 0.92-7 (MAECHLER et al., 2016) using the recommended setting “KS2014”.

Dirichlet Regression was performed using R package DirichletReg version 0.6-3 (MAIER, 2014, 2015).

Statistical analyses were conducted in the GNU distribution of the statistical language and environment R version 3.4.1 (R CORE TEAM, 2018), unless otherwise stated.

Statistical maps on the fsaverage cortical surface were generated using custom code based on the freesurfer_statsurf_display MATLAB toolbox (DEVELOPMENTAL IMAGING GROUP - MCRI, 2017).

Tukey's range test on the distribution of age across samples was performed using R package lsmeans (LENTH, 2016).

Multiple comparisons were adjusted at the sub-analysis level, meaning that each result presented has been individually adjusted, using the Benjamini-Hochberg False Discovery Rate (FDR) controlling procedure, as it is valid under positive dependency (BENJAMINI; HOCHBERG, 1995; BENJAMINI; YEKUTIELI, 2001).

4 RESULTS

4.1 Morphometry

The morphometric analysis corroborates the general age-related cerebral atrophy process. Cortical and subcortical gray-matter structures have their dimensions consistently diminished with aging. Some white matter structures are also consistently diminished. Among the increased structures are the choroid plexuses, ventricular cavities and the optic chiasm.

The linear effect of age on the volume of regions defined in the automatic segmentation provided by Freesurfer is shown in Figure 4.1. Linear coefficients are represented as percentage change from the expected value of volume at a reference age, 18 years, as $\beta_{age}/(\beta_0 + 18 \cdot \beta_{age})$ in the notation introduced in Equation 19. Only significant effects at a 0.05 FDR significance level are colored.

Figure 4.1 Effect of age on the volume of the structures defined in the automatic segmentation atlas shown as yearly percentage change with 18 years old as reference

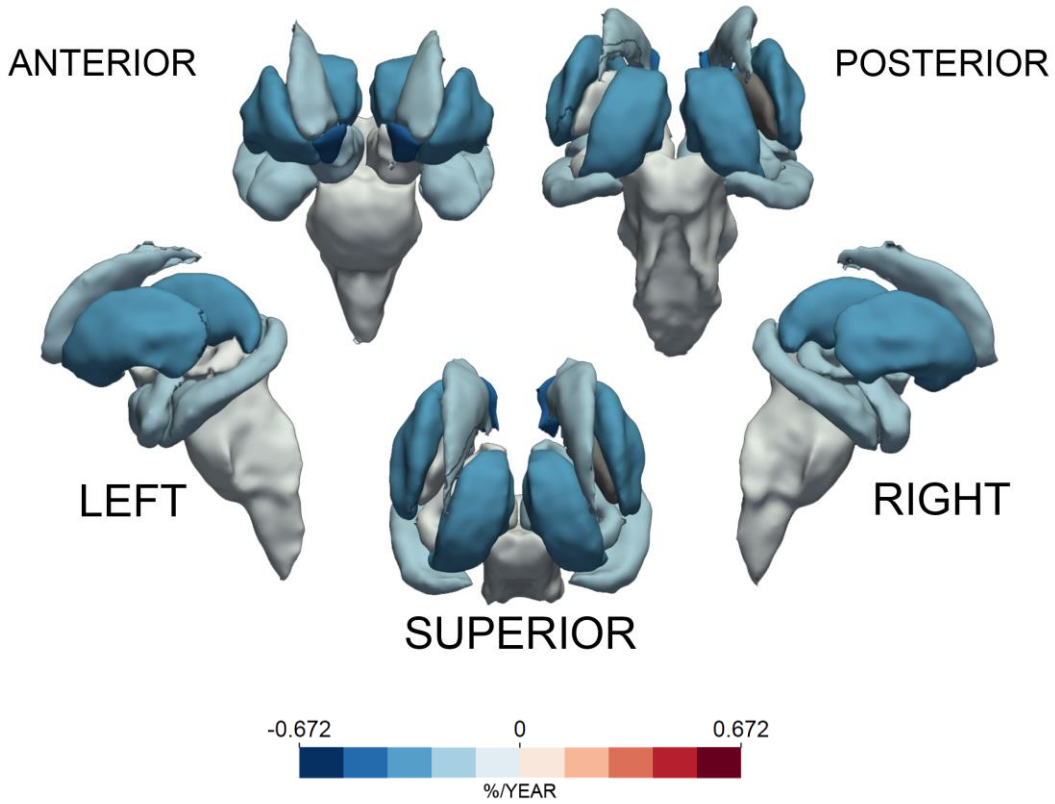

Source: The author. The structures are defined in Figure 3.1. Cerebellar, vascular, and ventricular structures not shown. No significant effect of age was observed on the Right pallidum, shown in gray.

Age-related alterations on cortical thickness for the automatic parcellation done in Freesurfer are presented in Figure 4.2. Linear coefficients are represented as percentage change from the expected value of volume at the same reference age of 18 years, as introduced in Equation 19. Only significant effects at a 0.05 FDR significance level are colored.

Figure 4.2 Effect of age on the cortical thickness of the structures in the automatic parcellation atlas shown as yearly percentage change with 18 years old as reference

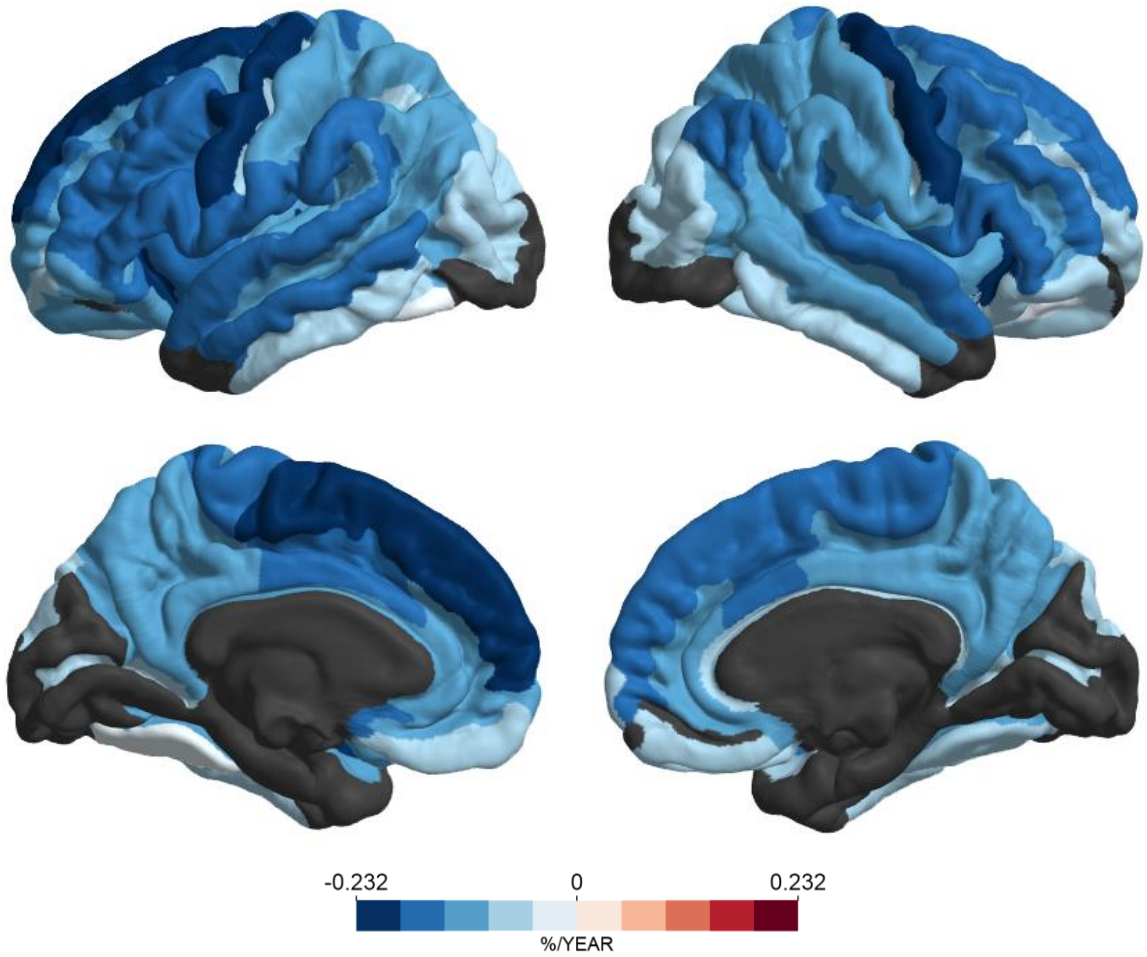

Source: The author.

In total, 133 ROIs showed a significant effect of age on cortical thickness at the 0.05 FDR level. These ROIs are equivalent to 89.9 percent of the cortical structures studied, 88.7 percent of the cortical volume, and 88.9 percent of the cortical surface area. All of them had thinning cortices with aging on the average of the groups studied.

Analogously, results for cortical surface area and cortical gray matter volume are shown in Figure 4.3 and Figure 4.4, respectively.

Figure 4.3 Effect of age on the cortical surface area of the structures in the automatic parcellation atlas shown as yearly percentage change with 18 years old as reference

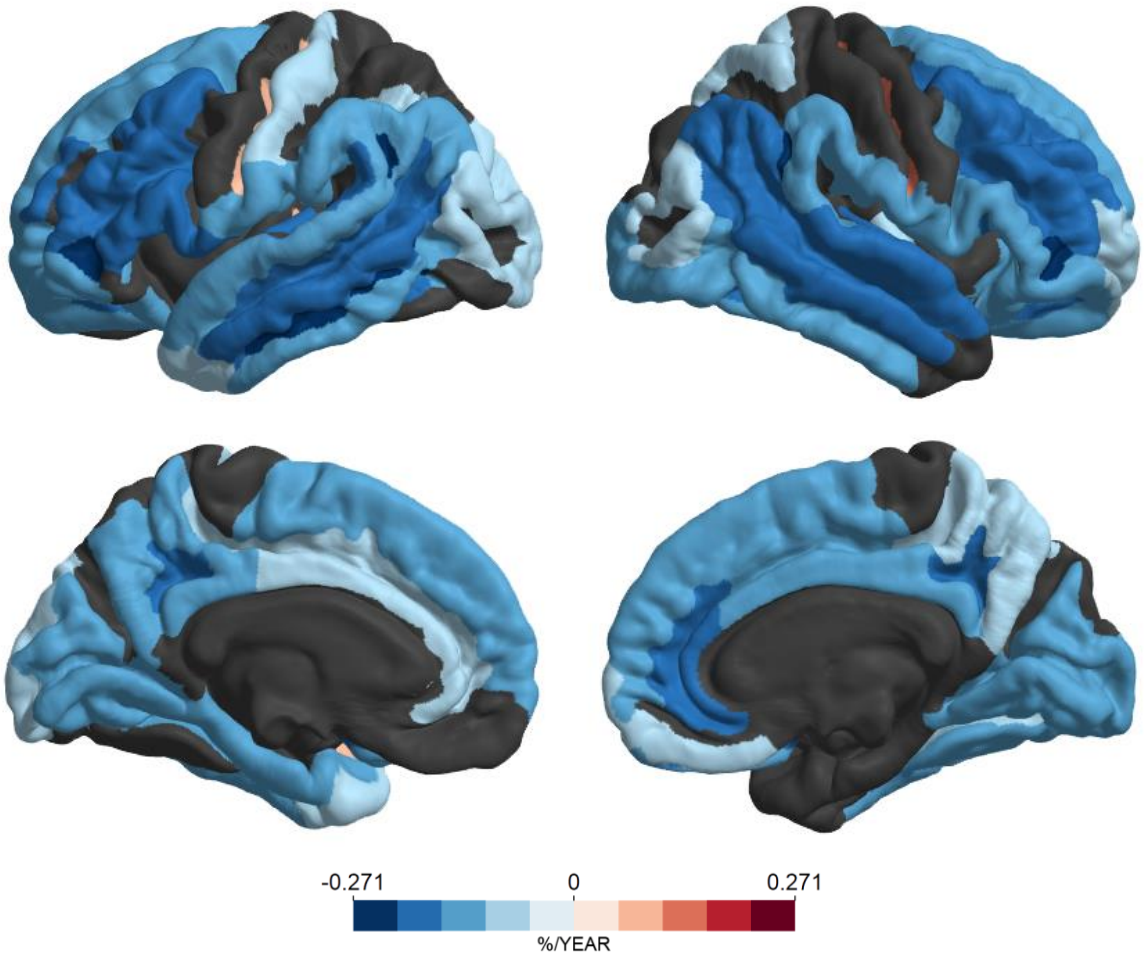

Source: The author.

In total, 101 ROIs showed a significant effect of age on cortical surface area at the 0.05 FDR level. These ROIs are equivalent to 68.2 percent of the cortical structures studied, 76.8 percent of the cortical volume, and 75.1 percent of the cortical surface area. Of these, only three small ROIs had increasing area with age.

Figure 4.4 Effect of age on the cortical gray matter volume of the structures in the automatic parcellation atlas shown as yearly percentage change with 18 years old as reference

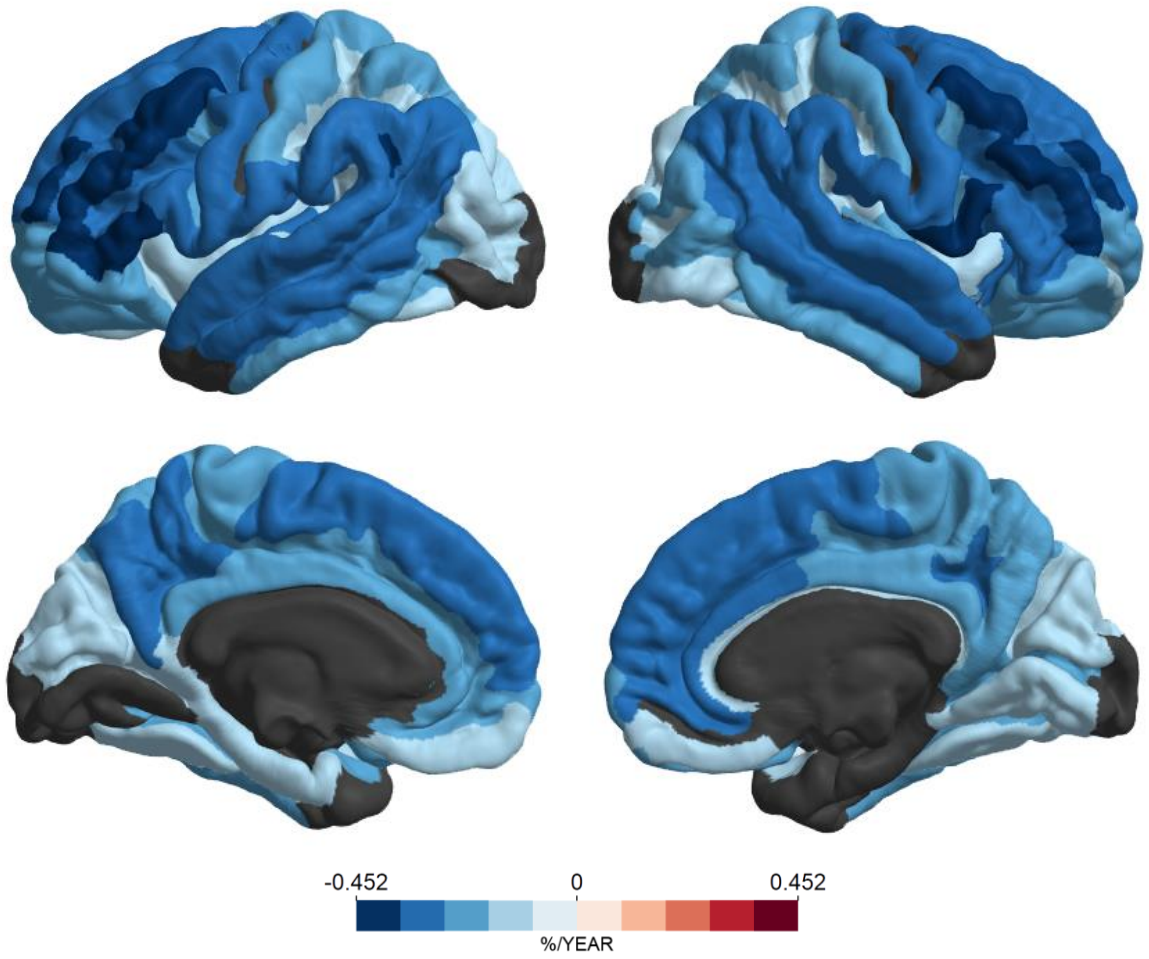

Source: The author.

For the cortical grey matter volume, age had a significant effect on 133 ROIs, i.e. 89.9 percent of the cortical structures. Albeit a coincident number with the cortical thickness, the effect was not in exactly the same regions. All regions had significant decreases in cortical grey matter volume with age at the 0.05 FDR level, covering 90.5 percent of the cortical volume and 89.6 percent of the cortical surface area.

The relationship between expected rate of change in thickness, $\beta_{age}/(\beta_0 + 18 \cdot \beta_{age})$, and the initial expected value of thickness, $\beta_0 + 18 \cdot \beta_{age}$, as represented in Equation 19, is shown in Figure 4.5, for each ROI from the Destrieux cortical atlas.

Figure 4.5 Annual percentage change in thickness versus the expected thickness at 18 years old for the 148 parcels defined in the Destrieux atlas.

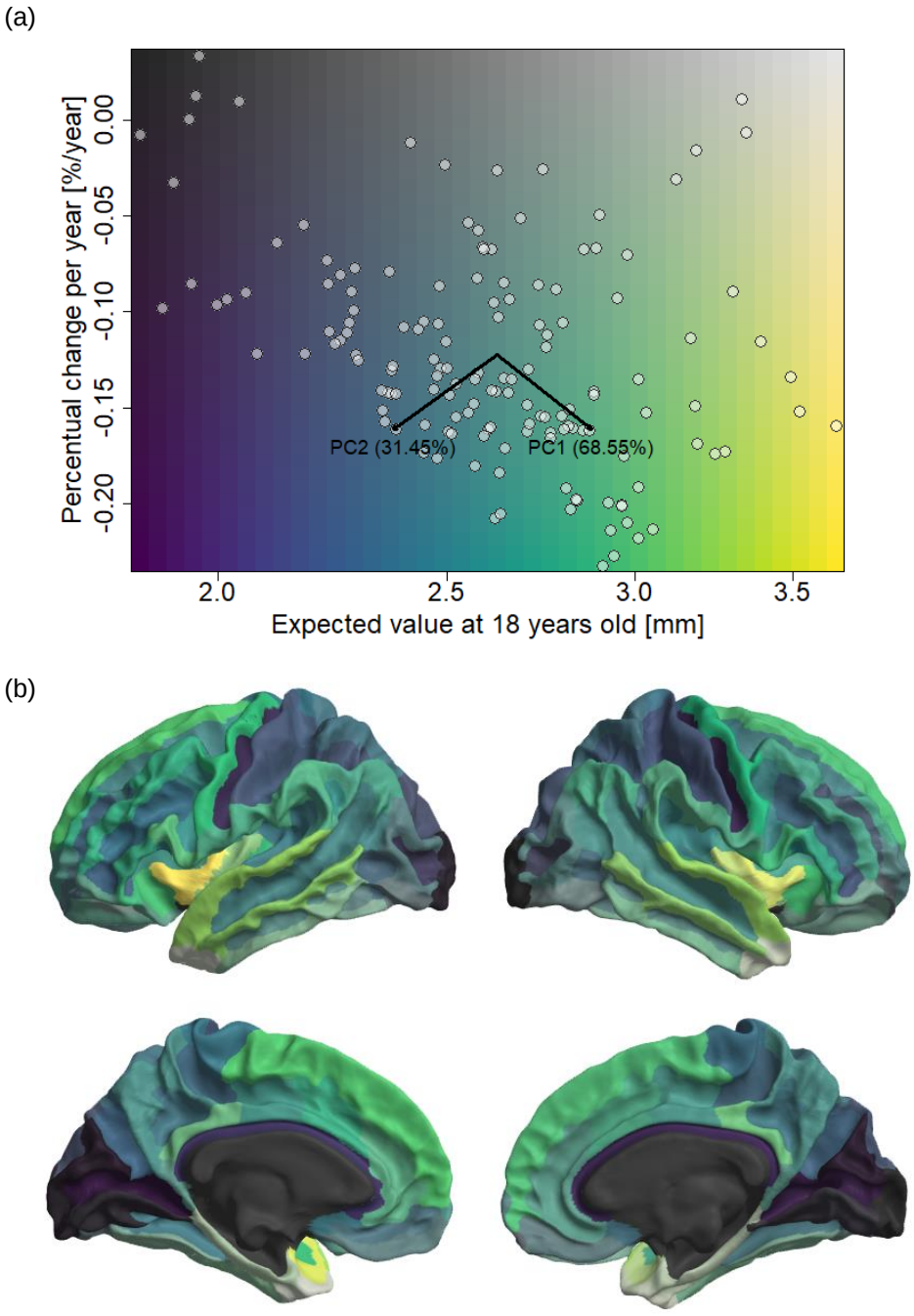

Source: The author. (a) The 148 regions from the Destrieux atlas are represented given their expected thickness at 18 years old and the percentage change per year after that age. First and second principal components are shown as arrows with their respective explained variance between parentheses (b) The regions are represented on the white matter surface of the fsaverage template space using the same colors they were assigned on the first plot.

Analogously, the same results are shown for cortical surface area, in Figure 4.6, and cortical volume, in Figure 4.7. The representations on the cortical surface for

these variables have been omitted because no clear patterns of dependence were observed.

Figure 4.6 Annual percentage change in surface area versus the expected surface area at 18 years old for the 148 parcels defined in the Destrieux atlas.

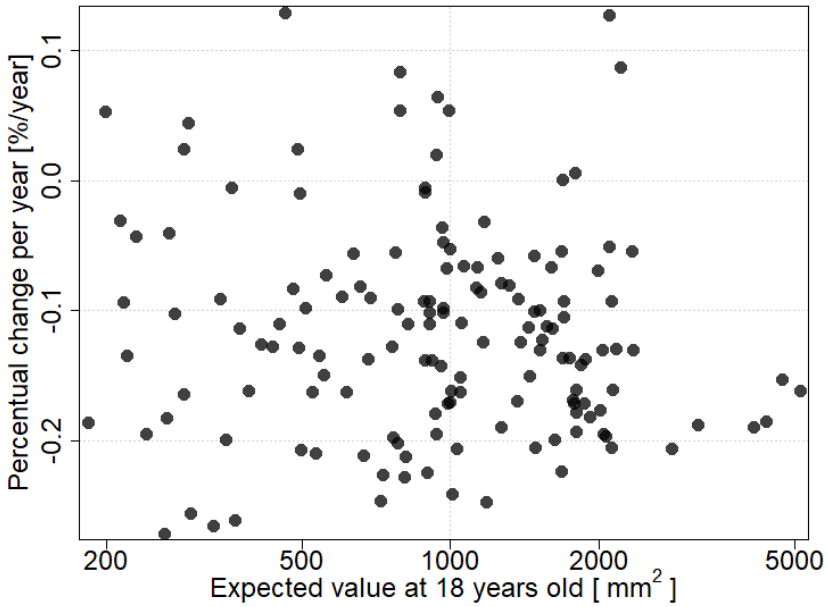

Source: The author.

Figure 4.7 Annual percentage change in volume versus the expected volume at 18 years old for the 148 parcels defined in the Destrieux atlas.

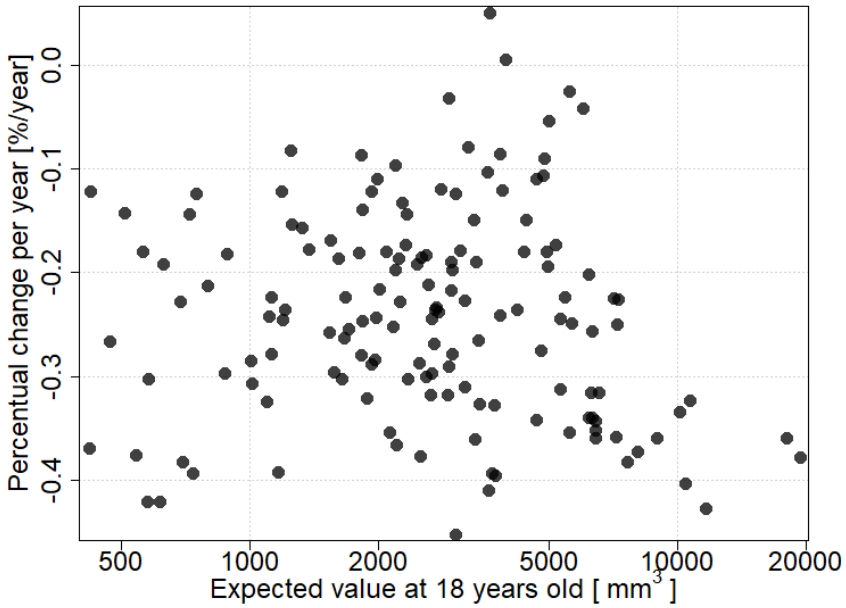

Source: The author.

Exploring the scores in the principal directions shown in Figure 4.5 allow us to study the main apparent effect, encoded in the first principal component, and the secondary effect, which is a perceptive deviation from the norm, as encoded in the second principal component. These scores are detailed in Figure 4.8. In (a), we see how cortices are positioned regarding their alignment to the linear association between atrophy and initial thickness. In (b) we see the direction orthogonal to the main effect, or in other words the deviations from the preferential direction.

Figure 4.8 Principal component scores in the interaction between cortical thickness and rate of atrophy in standardized units.

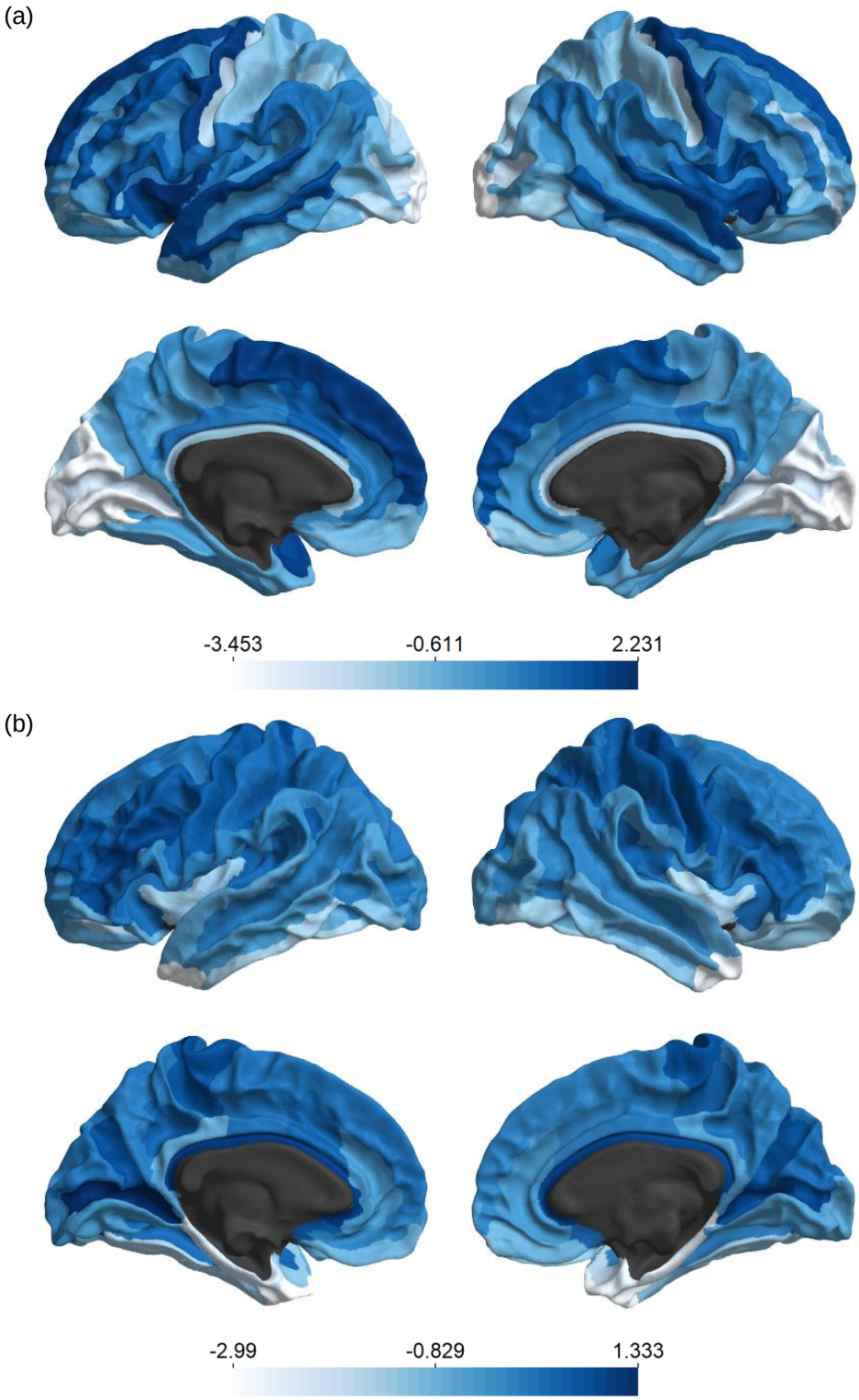

Source: The author. (a) The scores of the first principal component, which accounts for 68.55% of the variance. (b) Scores in the second principal component, accounting for 31.45% of the variance.

As shown in Equation 18, sex and dataset where also present in the morphometric linear models. The expected value of thickness at 18 years old is significantly different between sexes in 12 regions of the Destrieux atlas and also different between the two datasets, Pilot and Enhanced NKI-RS, in 72 ROIs. No significant difference in the age-related thickness rate of change was observed between sexes. The effect of age differed significantly between the datasets in a single region, the right Inferior segment of the circular sulcus of the insula (*S_circular_insula_inf*). For cortical surface area the same significant effects were observed, with 114 regions showing differences between sexes, 50 regions showing differences between datasets, 2 regions showing differences in the coefficient for the effect of age between sexes, and no regions displaying different effects of age between datasets. 137 regions had different expected values between sexes for volume at 18 years of age and 23 regions had different expected values for volume between datasets. 50 subcortical structures had different expected values of volume between sexes at 18 years, 17 had significant differences between datasets, 2 had different effects of age between sexes and had 7 different rates of age-related change between datasets.

4.2 Functional Connectivity: Pearson Correlation Coefficient

Results for the Pilot NKI-RS and Enhanced NKI-RS are explored separately due to the different resting-state functional acquisition sequences used.

The effect of age on the undirected connections measured by the Pearson correlation coefficient is shown in Figure 4.9 for the Pilot NKI-RS as the *t*-statistic associated with the coefficient β_{Age} in Equation 21.

Figure 4.9 Effect of age on the bivariate functional connectivity estimated as the Pearson correlation coefficient in the Pilot NKI-RS

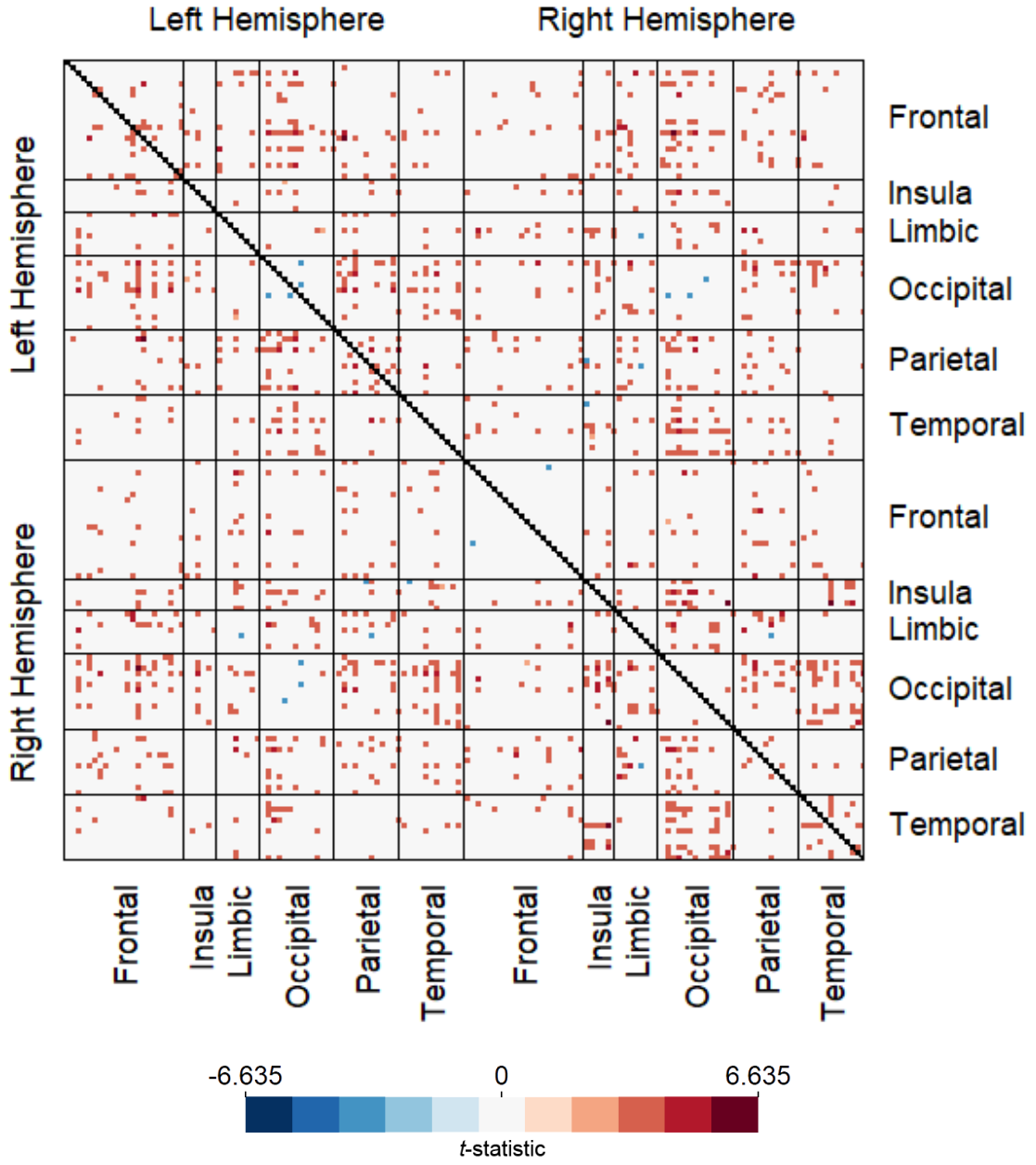

Source: The author.

Only 691 connections from the 10878 total had a significant effect of age, i.e. 6.4 percent of the connections, 680 increases and 11 decreases.

Likewise, for the Enhanced NKI-RS, the effect of age on the same connections is shown in Figure 4.10.

Figure 4.10 Effect of age on the bivariate functional connectivity estimated as the Pearson correlation coefficient in the Enhanced NKI-RS

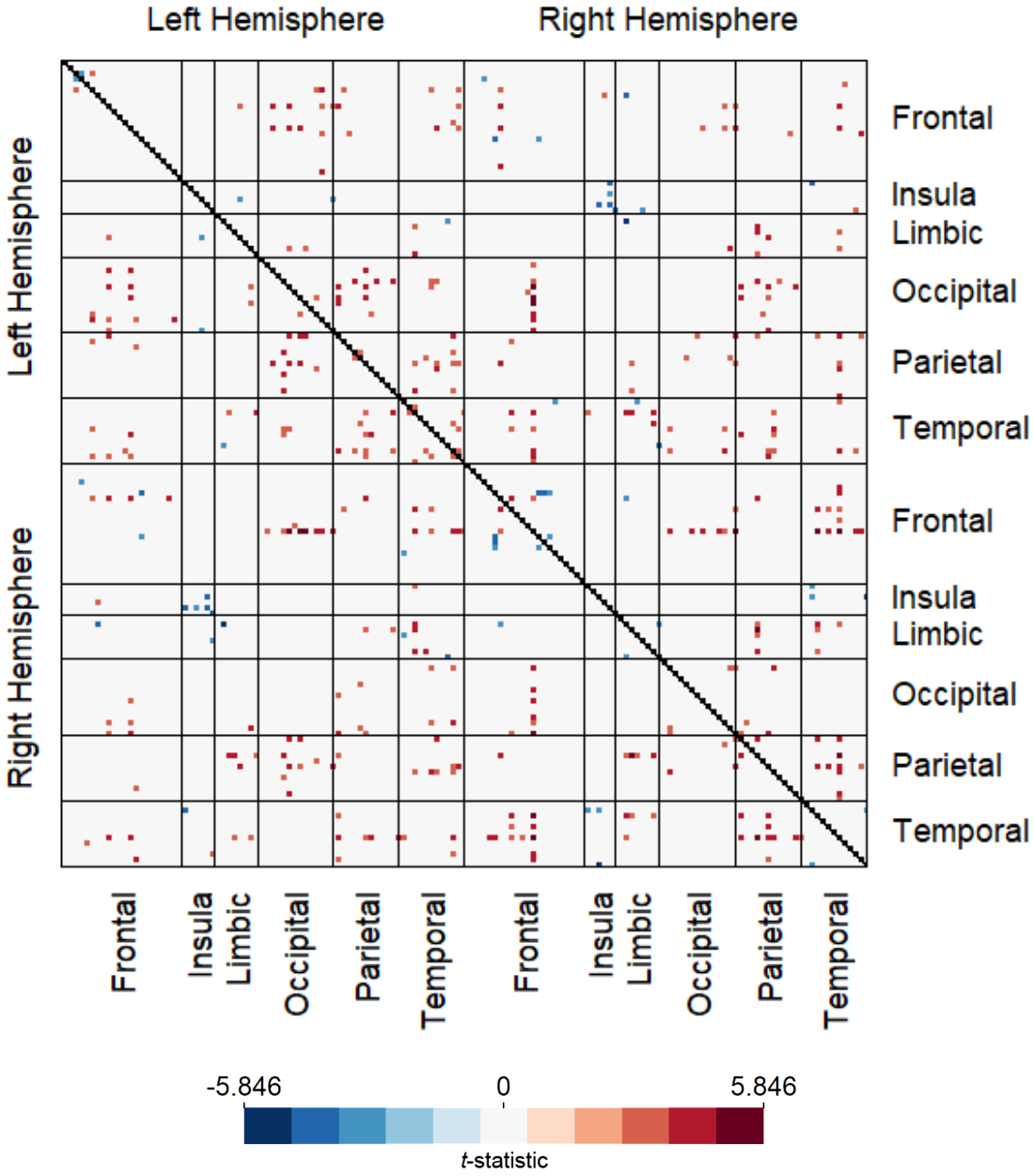

Source: The author.

Less connections than in the Pilot NKI-RS, 214 out of the 10878 connectivity estimates, i.e. 1.97 percent of the connections, had a significant effect of age. Out of these, 185 had increased Pearson correlation coefficients while 29 had decreased coefficients.

The effect of age on homotopic connectivity estimated as the Pearson partial correlation coefficient is shown in Figure 4.11. As only connections between homotopic regions are shown we can represent them on the brain surface.

Figure 4.11 Effect of age on the bivariate functional connectivity estimated as the Pearson partial correlation coefficient between homotopic ROIs in the Enhanced NKI-RS.

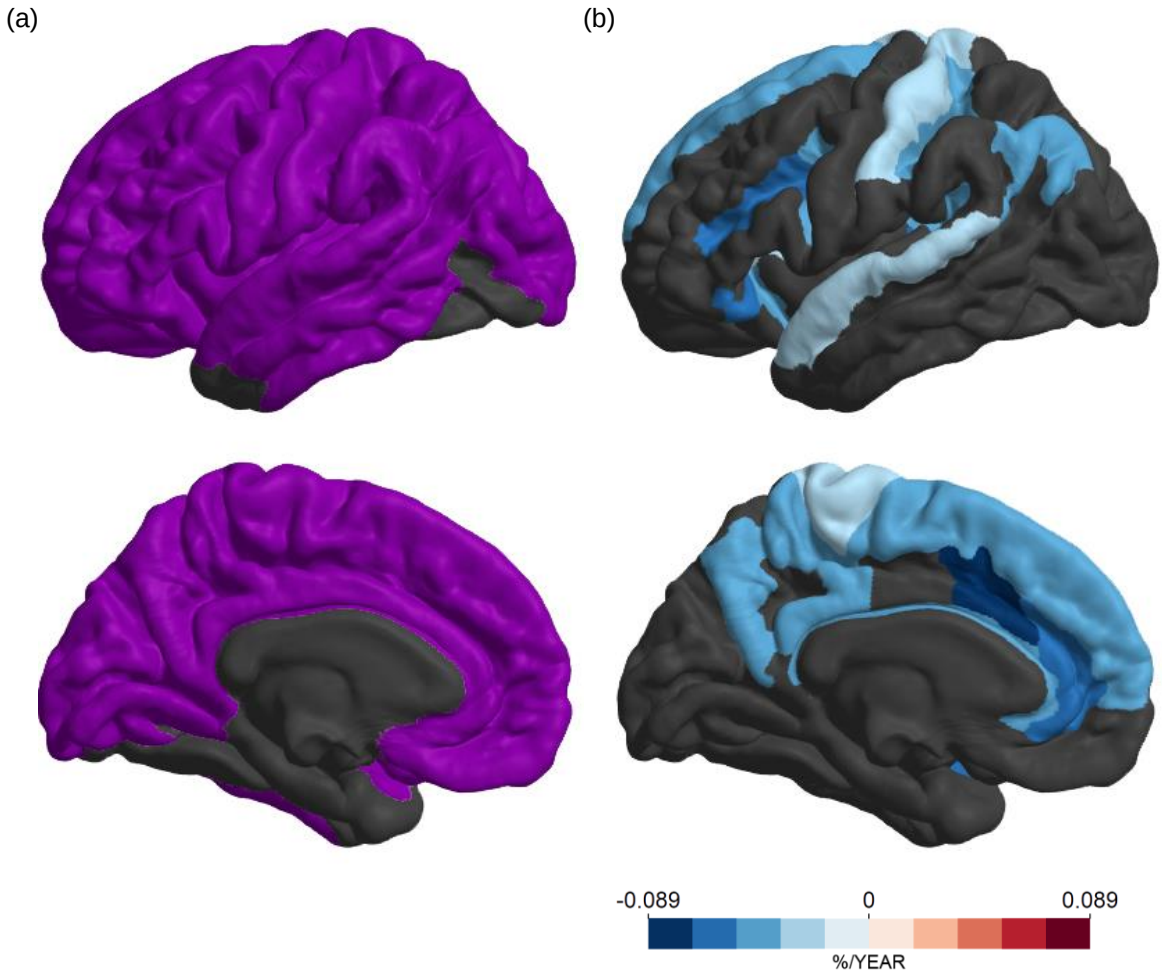

Source: The author. (a) Regions selected for the analysis. (b) Effect of age on the homotopic connectivity. For illustrative purposes, the result is presented on the right hemisphere.

Out of the 65 connections, 12 had significant decreases along aging. No significant difference between sexes at 18 years of age nor a different rate of change was observed.

The expected value of Pearson correlation coefficient at 18 years of age is shown in Figure 4.12, while the same is done for Pearson partial correlation coefficient in Figure 4.13.

Figure 4.12 Expected Pearson correlation connectivity matrix at the age of 18 years

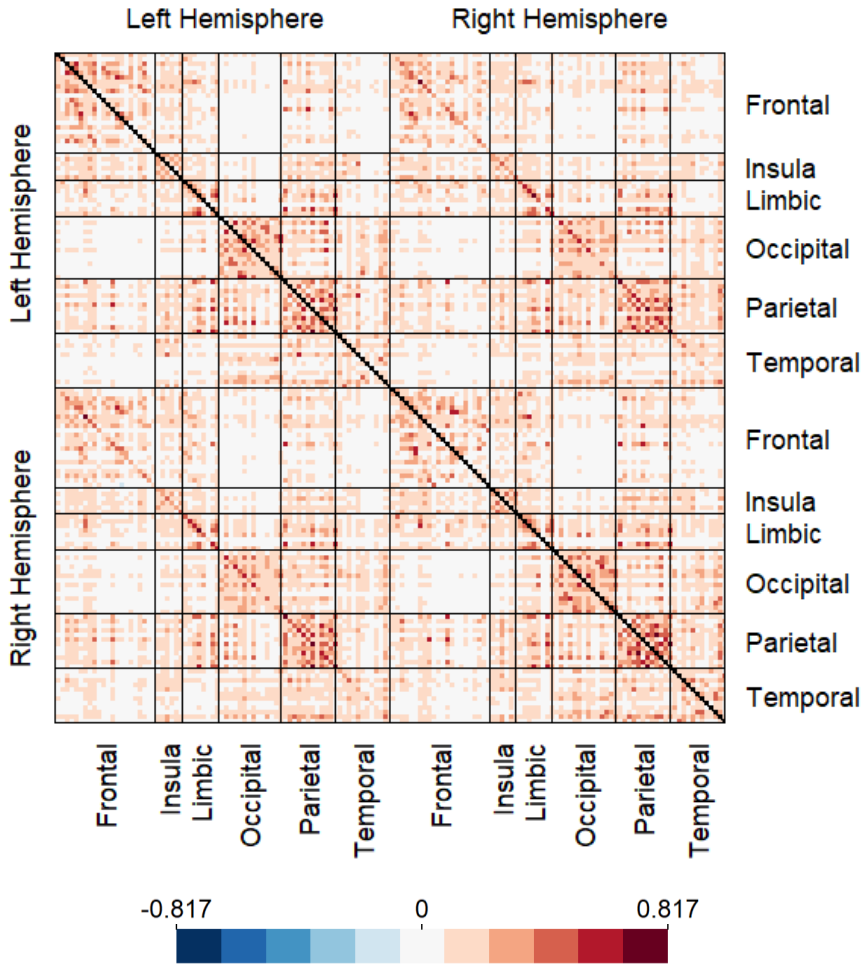

Source: The author. Pearson correlation is defined between -1 and 1.

Figure 4.13 Expected Pearson partial correlation connectivity matrix at the age of 18 years

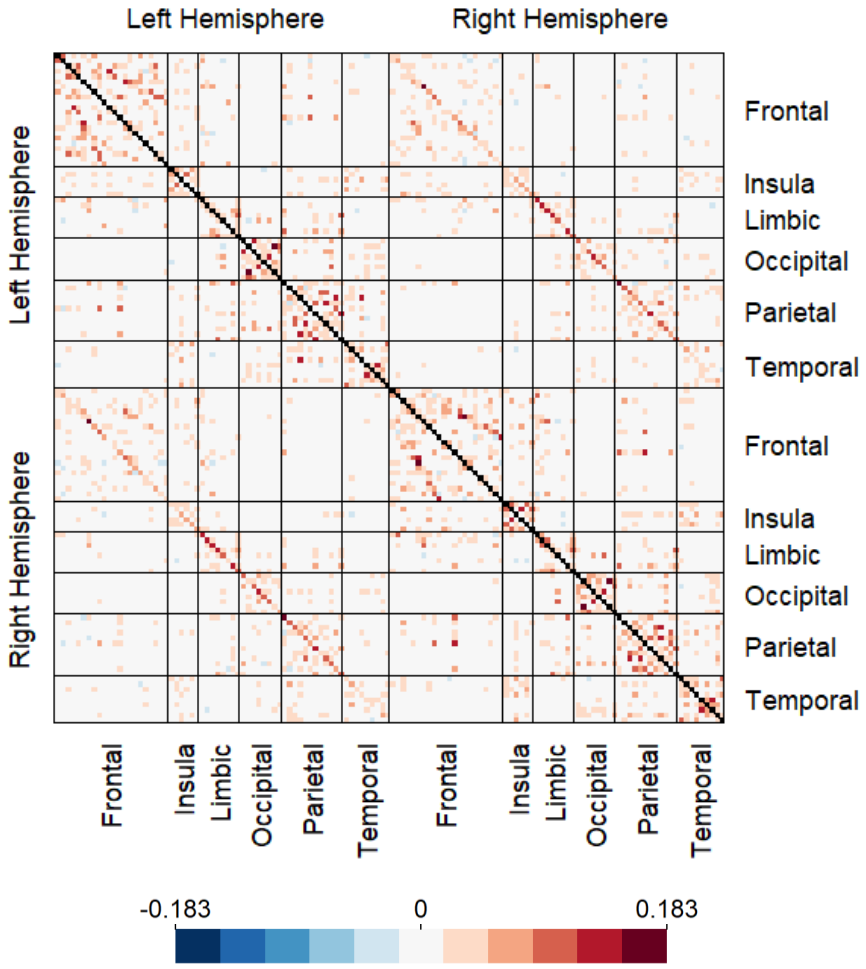

Source: The author. Pearson partial correlation is defined between -1 and 1.

4.3 Functional Connectivity: Causality Analysis

The effect of age on the directed connectivity estimated through Granger causality testing in the Pilot NKI-RS was significative in the connectivity from the right Occipital Pole (*Pole_occipital*) to the right Orbital Gyri (*G_orbital*), and from the left Sulcus intermedius primus (*S_interm_prim-Jensen*) to the right Pericallosal sulcus (*S_pericallosal*), both increased along aging. On the Enhanced NKI-RS, no effect of age was constated.

For the undirected connectivity estimate of instantaneous Granger causality, age-related effects for the Pilot NKI-RS were present in four connections, between the right Anterior occipital sulcus (*S_occipital_ant*) and left Posterior-dorsal part of

the cingulate gyrus (dPCC) (*G_cingul-Post-dorsal*), right Medial orbital sulcus (*S_orbital_med-olfact*) and right Orbital part of the inferior frontal gyrus (*G_front_inf-Orbital*), right Inferior temporal gyrus (*G_temporal_inf*) and right Short insular gyri (*G_insular_short*), and right Inferior temporal gyrus (*G_temporal_inf*) and right Inferior segment of the circular sulcus of the insula (*S_circular_insula_inf*), all showing increased connectivity with age.

The effect of age on the instantaneous Granger causality coefficient in the Enhanced NKI-RS is shown in Figure 4.14.

Figure 4.14 Effect of age on the bivariate connectivity estimated as the instantaneous Granger causality coefficient in the Enhanced NKI-RS

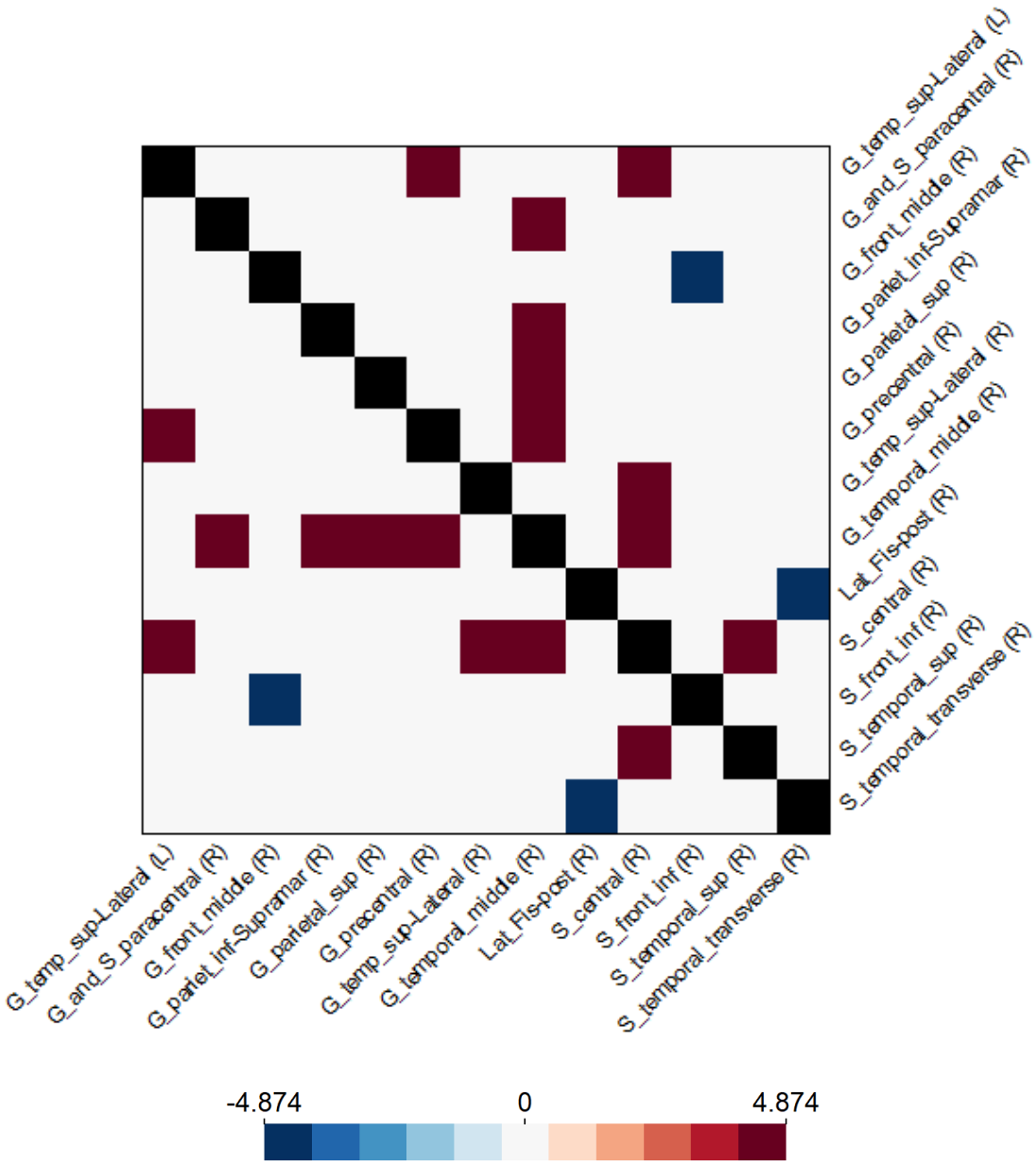

Source: The author. Only regions with at least one significant effect are shown.

4.4 Partial Directed Coherence

Middle-anterior part of the cingulate gyri and sulci (*G_and_S_cingul.Mid.Ant*), middle frontal gyri (*G_front_middle*), superior frontal gyri (*G_front_sup*), inferior segments of the circular sulci of the insulas (*S_circular_insula_sup*), and the opercular part of the inferior frontal gyri (*G_front_inf.Opercular*) were selected as ROIs based on the t-statistic for the effect of age on each of these.

While they demonstrated consistent thinning, the opercular gyri (*G_front_inf.Opercular*) were excluded from the GPDC analysis due to the lower concordance index exhibited by their right counterpart, under 0.8 (DESTRIEUX et al., 2010).

The map for the t-statistic of the effect of age on cortical thickness and the selected regions are therefore shown in Figure 4.15.

Figure 4.15 The effect of age of cortical thickness of the Destrieux ROIs.

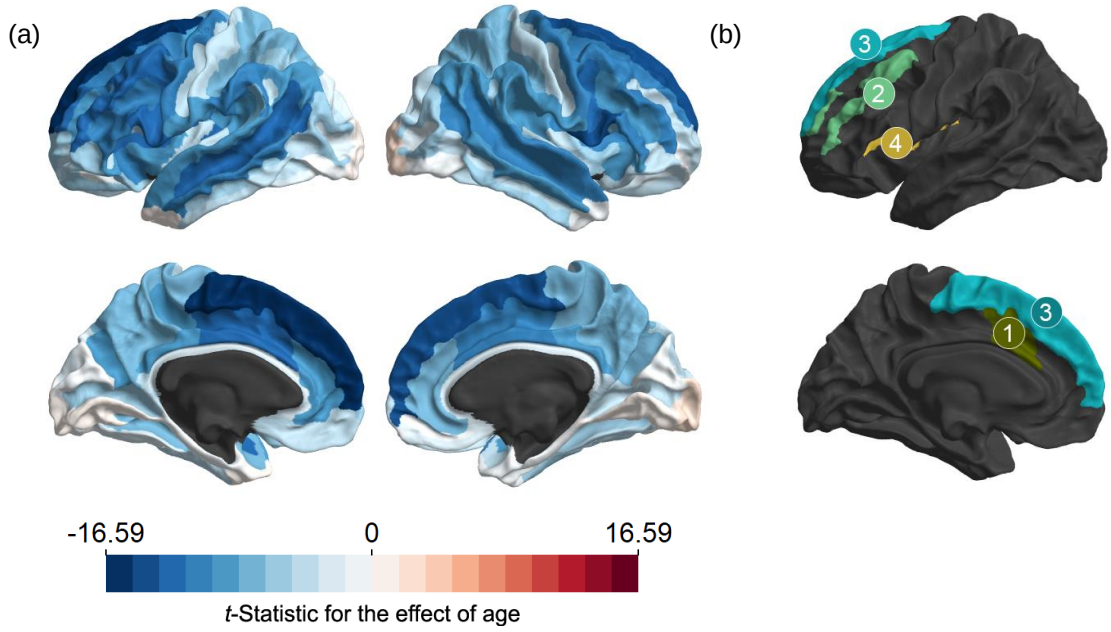

Source: The author. (a) t-statistic for the linear effect of age on the cortical thickness of the structures in the automatic parcellation atlas. (b) four pairs of bilateral ROIs selected for the analysis of GPDC, shown in a single hemisphere for illustrative purposes, namely: (1) middle-anterior part of the cingulate gyri and sulci, (2) middle frontal gyri, (3) superior frontal gyri, and (4) superior segments of the circular sulci of the insulas.

The effect of age on the GPDC between the eight ROIs is shown in Figure 4.16, for each of the five frequencies.

Figure 4.16 Effect of age on the squared GPDC in eight thinning ROIs and five frequencies, from the Enhanced NKI-RS.

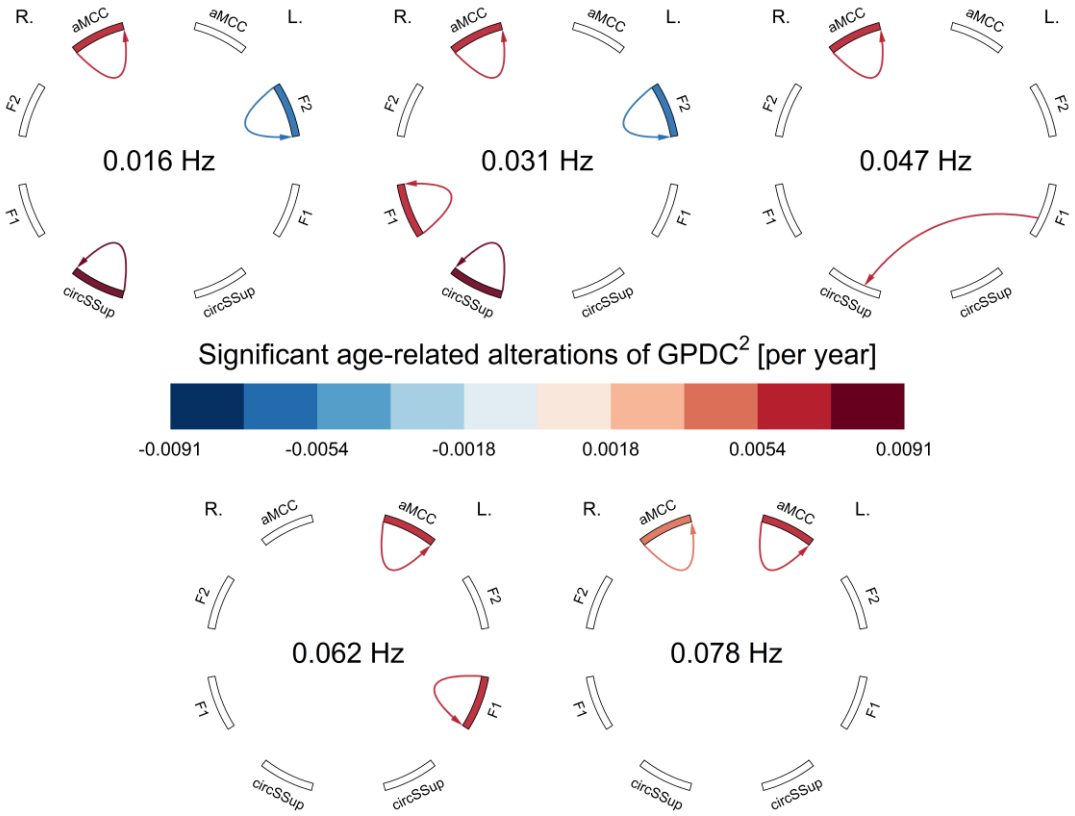

Source: The author. Only connections where the effect of age is significantly different from zero are colored. Regions are: Middle-anterior part of the cingulate gyri and sulci (aMCC), middle frontal gyri (F2), superior frontal gyri (F1), superior segments of the circular sulci of the insulas (circSSup).

The GPDC from the left middle frontal gyrus to the right inferior segment of the circular sulcus of the insula varies significantly with age. A strong, albeit not significant, age-related effect is also present in the GPDC from the right middle frontal gyrus to the right inferior segment of the circular sulcus of the insula, not shown in Figure 4.16.

The expected distribution of Pearson correlation, Pearson partial correlation, and squared GPDC at 18 years of age is shown in Figure 4.17.

Figure 4.17 Connectograms of the expected value of squared GPDC at the age of 18 years.

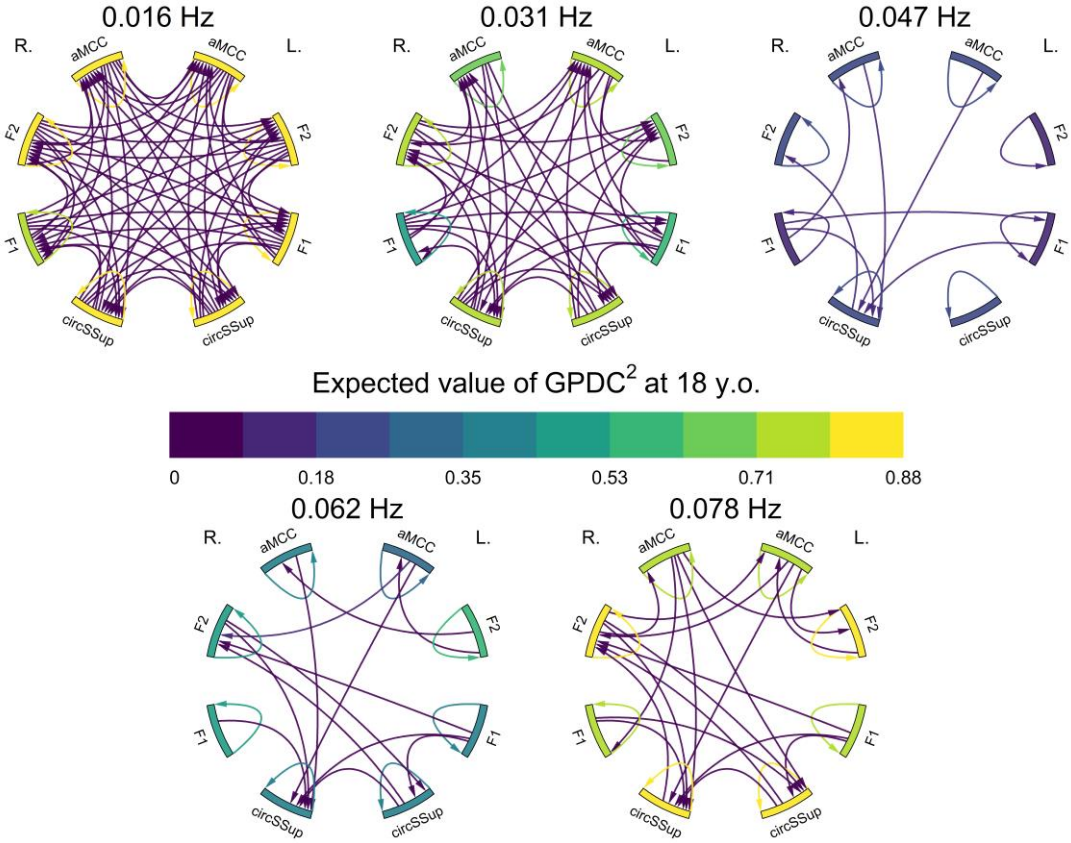

Source: The author. GPDC is defined between 0 and 1. Only connections significantly different from zero are shown, and each ROI area is colored as the GPDC from the ROI to itself. Regions are: Middle-anterior part of the cingulate gyri and sulci (aMCC), middle frontal gyri (F2), superior frontal gyri (F1), superior segments of the circular sulci of the insulas (circSSup).

4.5 On the Association Between Alterations in Cortical Thickness and Functional Connectivity

The association of the effect of age on the functional connectivity and on the cortical thickness of the target ROIs, given a seed ROI, is shown in Figure 4.18 for the Enhanced NKI-RS. Standardized coefficients of the effect of age on thickness estimates of a seed ROI and the effect of age of functional connectivity from this seed ROI to all other ROIs are computed as the β_{age} in Equations 19 and 21, though now the numerical dependent and independent variables are centered and scaled to have variance equal to one. This way, the coefficients become unitless. Then, the

effect of age on the 147 connectivities from a seed ROI is regressed on the effect of age on the 147 target ROIs thicknesses.

Figure 4.18 Association of the effect of age on the bivariate connectivity, estimated as the Pearson correlation coefficient, and the effect of age on cortical thickness, in the Enhanced NKI-RS

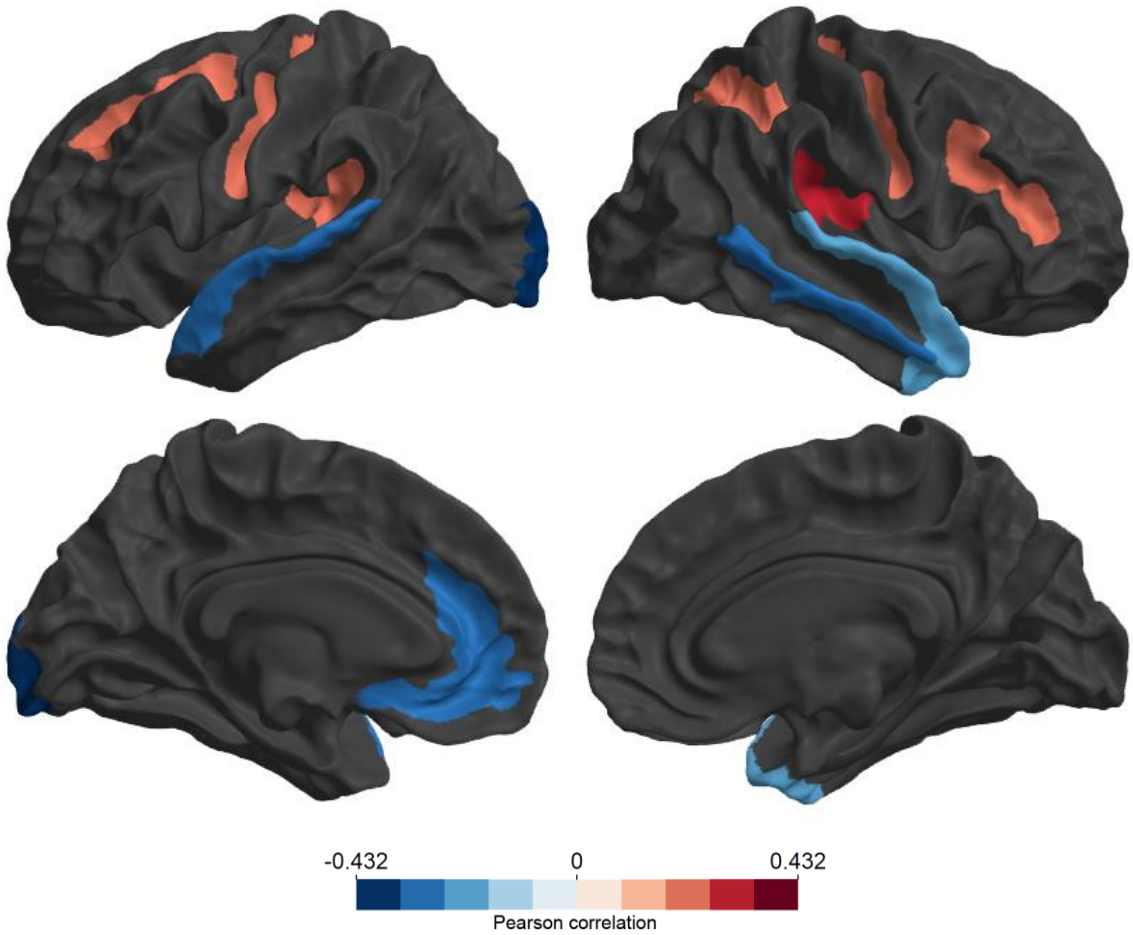

Source: The author. Positive association for a seed ROI means the stronger the thinning rate of the target ROIs, the smaller, numerically, the rate of change in connectivity between this seed and the targets.

In the Enhanced NKI-RS, 15 seed regions had significantly correlated effects of age on cortical thickness and functional connectivity estimates.

When studying the connectivity measures from a seed ROI with mixed effects models in both datasets, almost no effect survives the correction for multiple comparisons in the type II ANOVA. At a significance level of 0.05, the effect of age on the Pearson correlation from the left Paracentral lobule and sulcus (*G_and_S_paracentral*) and the effect of the interaction between age and seed thickness on the Instantaneous Granger Causality from the right collateral sulcus and

lingual sulci (*S_oc-temp_med_and_Lingual*, a single ROI in the Destrieux parcellation) are significant.

We also tested the joint effect of age, seed thickness, and target thickness, and the relevant interactions. No significant effect was found in any of the six analyses.

5 DISCUSSION AND CONCLUSION

In all analyses, age was entered as an independent variable. In both NKI-RS datasets, age is recorded as a positive integer. This small interval-censoring was not accounted for in the models and should not alter the results.

Our study, as many others in the area of human brain mapping, is at risk of hidden variable bias. Sociodemographic factors, which have some correlation with sex and age, are unaccounted for, and these have some bearing on neuroimaging findings.

As we performed all analyses on native space with personalized ROI selection, the effects of subject variability are mitigated on our results (SOHN et al., 2015).

Our morphometric results support the notion of generalized age-related atrophy in the brain, with diminishing dimensions in gray and white matter structures and increased ventricular structures. These findings have been widely reported in the literature (BAKKOUR et al., 2013; FJELL et al., 2009a, 2009c, 2010a, 2010b, 2013, 2014a, 2014b, 2015d; GOODRO et al., 2012; HARADA; NATELSON LOVE; TRIEBEL, 2013; LEMAITRE et al., 2012; LOCKHART; DECARLI, 2014; MEIER-RUGE et al., 1992; POTVIN; DIEUMEGARDE; DUCHESNE, 2017a; SALAT et al., 2004; SCAHILL et al., 2003; SOWELL et al., 2007; STORSVE et al., 2014; THAMBISETTY et al., 2010; WALHOVD et al., 2011; WESTLYE et al., 2009; ZHOU et al., 2013; ZIELINSKI et al., 2014). While almost the whole cortex present evidence for age-related thinning, frontal gyri, superior and middle temporal gyri, the temporoparietal junctions and pre- and postcentral gyri display highly consistent thinning across samples, with relative sparing of inferior temporal lobes and anterior cingulate cortices (FJELL et al., 2009a).

Particularly, as seen in Figure 4.2, thinning attains higher yearly rates in the Precentral gyri (*G_precentral*) and the Superior frontal gyri (*G_front_sup*), in accordance with the literature (FJELL et al., 2009a). Spared areas include several bilateral Occipital gyri and sulci with some Temporal gyri also being present, more specifically the temporal poles and parahippocampal gyri.

Cortical surface area reductions are highlighted in Subparietal sulci (*S_subparietal*), Lateral orbital sulci (*S_orbital_lateral*) and several Temporal and

Frontal gyri and sulci, as in Figure 4.3. Area is significantly increased with age in the Central sulci (*S_central*).

Cortical surface area and cortical thickness age-related changes do not match exactly spatially, with most areas even displaying inverted effects, with area expansion and cortical thinning (HOGSTROM et al., 2013). This phenomenon could be following the phylogenetical principle of area maximization instead of cortical thickening for better functional organization (SELDON, 2005).

Age-related alterations in cortical regions thickness interact with alterations in area explaining most alterations in volume of Figure 4.4.

On subcortical structures, most gray matter structures display age related atrophy in their volumes, with pallidi, caudate nuclei and amygdalae having lower age-related effects sizes (GOODRO et al., 2012). In our results, illustrated in Figure 4.1, the right pallidum did not significantly diminish with age, and the left pallidum displayed a small rate of atrophy. Amygdalae and caudate nuclei also had small rates of atrophy, alongside the hippocampi, though there exists strong evidence the hippocampi follow a nonlinear trajectory at advanced age, and therefore our linear model incurs some bias (FJELL et al., 2010b). The volumetric increase of ventricular structures we reported is consistent with the literature as well (FJELL et al., 2013; WALHOVD et al., 2011).

A relationship has been noted in the literature between the decline observed during normal aging and related conditions, such as AD, and the evolutionary expansion of brain areas, with high expanding regions exhibiting on average increased morphometric decline (FJELL et al., 2014b, 2015b).

A possible caveat in our morphometric analysis is the non-linear behavior of age-related phenomena in several brain structures, as reported in the literature (FJELL et al., 2009c, 2014a; GOODRO et al., 2012; SCAHILL et al., 2003; STORSVE et al., 2014; WALHOVD et al., 2011; ZIELINSKI et al., 2014), present even in brain weight (DEKABAN; SADOWSKY, 1978). At the degrees of freedom afforded by the large sample size, we believe the linear models sufficiently capture the direction of effects, even though rates of change might be off at different ages. The linear hypothesis is a reasonable choice to the study of cortical thinning across the adult lifespan (FJELL et al., 2009a; RAZNAHAN et al., 2011).

We noted a dependence on the percentage yearly rate of change on cortical thickness and the expected value of cortical thickness at 18 years old, shown in

Figure 4.5, which is not so readily perceived in cortical surface area, in Figure 4.6, or volume measurements, in Figure 4.7.

The expected value of thickness can be thought of as a stand in for the granularity of the cortex, as agranular cortices are thicker whereas granular cortices are thinner. Therefore, as our results suggest, the thicker a cortex is, the faster it thins out during the adult lifespan.

Previous results from the literature suggested the developmental trajectories of different cortices closely resemble their granularity (SHAW et al., 2008), with agranular cortices, being phylogenetically younger and performing higher cognitive functions, having more complex trajectories, closely matching the association cortices, which are expanded in humans in comparison to other mammals (CROXSON et al., 2017). Our results demonstrate these cortices are also likely to show higher rates of atrophy due to aging.

This result matches the hypothesis known in the literature as “last-in first-out”, where regions maturing, phylogenetically and ontogenetically, last are the most likely to be affected by age-related declines (RAZ, 2000).

The observed sparing of the temporal poles in Figure 4.2 and Figure 4.4 is elusive though, as it is among the thickest cortices in the brain. It is a mixed cortex in the temporal lobe, containing granular, dysgranular, and agranular cortical sub-fields (KONDO; SALEEM; PRICE, 2003; PASCUAL et al., 2015). The temporal pole has been implicated in memory and high order cognitive functions, and its cytoarchitectonic subfields present different anatomical and functional cortico-cortical connectivity patterns (FAN et al., 2014).

Figure 4.8 shows how the cortices are arranged according to their initial thickness and their rate of atrophy. In (a) we argue this distribution closely resembles neocortical granularity, with more agranular cortices being blue and granular cortices white. This indicated agranular cortices have higher rates of atrophy as well. In (b), since most superior cortices, mostly neocortical, have high scores in this scale and that the anterior insulas, temporal poles and parahippocampal gyri, which are known to contain meso- and even allocortex, have low scores, which means that while they are thicker they present smaller rates of atrophy, we hypothesize this direction correlates cortical type admixture, suggesting regions which score higher in this direction are more likely to contain pure neocortex.

On the analysis of the functional connectivity estimated by the Pearson correlation coefficient, the data in the Pilot NKI-RS and the Enhanced NKI-RS exhibit different effects. The number of connections significantly altered due to aging is expressively higher in the Pilot NKI-RS, seen in Figure 4.9, than in the Enhanced NKI-RS, in Figure 4.10. On the other hand, the number of significant decreases with age is higher in the Enhanced NKI-RS, while the Pilot NKI-RS has mostly increases with age. These differing results have their counterparts in the literature, with generalized increases of connectivity with aging being widely reported, as well as a higher prevalence of decreases.

Increased functional connectivity between areas, or more specifically brain networks, is called the demodularization or dedifferentiation process of cognitive aging. Our results do not allow inference on network modularization as we did not parcellate network units, but specific anatomical structures. This hypothesis maintains that the brain loses some of its segregation with aging due to compensatory mechanisms, with more areas having to work in tandem to perform the same functions than what is observed in the younger adults, thus increasing the temporal correlations between them. Results in this same vein have been previously reported (FERREIRA et al., 2016; GEERLIGS et al., 2015; SONG et al., 2014), though contrasting our specific results, such as proportions of increased or decreased correlations, with the literature is made difficult due to the different ROI definitions, e.g. studies using random parcellations tend to have uniformly sized ROIs, while our anatomical ROIs have diverse sizes.

Connections between intra-hemispheric and inter-hemispheric insular ROIs are decreased with aging in Figure 4.10. This is also observed in connections between the insular lobe and other lobes. Totaling twelve connections involving either insula being decreased with aging, including five inter-hemispheric connections between the insulas themselves, over forty percent of the decreased connections involve the insular cortices. The insulas are cortices of mixed type, implicated in several disparate functions, including being responsible for mediation between large scale networks in the brain (MENON; UDDIN, 2010). Their structures are among the thickest cortices, but their rate of atrophy is proportionally smaller than what is expected, as seen in Figure 4.5. Indeed, the functional disconnection of the insula has been attested in the transition from old to very old age (MULLER; MÉRILLAT; JÄNCKE, 2016).

Contrary to the morphometric analyses, here the linear hypothesis is much more reasonable and parsimonious due to the sheer number of hypotheses being tested, which is equal to 10878, even though evidences of nonlinear functional connectivity trajectories exist (WANG et al., 2012).

The Enhanced NKI-RS has better temporal resolution, which diminishes the aliasing effects of high frequency noise components in the BOLD timeseries. In practice, in the Pilot NKI-RS the frequencies in the band between 0.310 Hz and 0.391 Hz are aliased into the filter band, while for the Enhanced NKI-RS aliasing occurs at higher frequencies, between 1.461 Hz and 1.542 Hz. Harmonics of cardiac and respiratory cycles, with fundamentals respectively around 1 Hz and 0.3 Hz, are aliased into the band of interest more prominently in the Pilot NKI-RS (CABALLERO-GAUDES; REYNOLDS, 2016). Also, the realignment of functional volumes is easier in the Enhanced NKI-RS due to the smaller framewise displacement between consecutive volumes. Another observed behavior was that subjects in the Enhanced NKI-RS presented smaller movement components than subjects in the Pilot NKI-RS. This should mimic the effect that GSR has on behavioral studies.

Due to the general appearance of the average Pearson Correlation connectivity matrix, which usually presents stronger intra hemispheric and homotopic connectivities, to study an estimate of direct correlation, that is, accounting for all the information shared in the system, becomes of interest. We hypothesized inter hemispheric connectivities through the commissural fiber systems between non-homotopic regions could be driven mostly by an indirect phenomenon, with direct inter hemispheric connections being present strongly between homotopic regions. In other words, a sparse connectivity matrix should ensue. Incorporating this assumption into the partial correlation estimation revealed a different view of the human connectome.

The first thing that becomes clear is that inter hemispheric non-homotopic connections, even if non-zero, are not consistent, i.e. they have near zero magnitude for the majority of connections and subjects. This happens because the Pearson correlation between two non-homotopic regions is captured by the correlation between them and their homotopic counterpart and from these counterparts to the other region, now an intra-hemispheric connection, resulting in estimates shrunk to near-zero or zero, as we impose a sparse partial correlation matrix. Therefore, we studied the effect of age on the connections between homotopic regions only, totaling

65 connections. Using this strategy, we uncovered a different phenomenon, shown in Figure 4.11: the interhemispheric connections between homotopic regions estimated as the partial Pearson correlation coefficient tend to exhibit significant age-related effects, and those exhibiting such effect have decreased connectivity with aging. In total, twelve connections out of a sixty-five total were significantly reduced with aging, and all these have positive expected values at eighteen years old.

Looking at the same connectivities estimated through the Pearson correlation coefficient, two are positively correlated with age: the Sulcus intermedius primus (*S_interm_prim-Jensen*) and the Inferior temporal sulcus (*S_temporal_inf*). Further, another ten connections are significantly reduced with aging. Of these, seven also display decreased partial correlations with aging.

This brings an accessory hypothesis to the age-related dedifferentiation hypothesis observed in functional connectivity. It is known non-adjacent cortical brain areas are connected by axon fiber bundles, which form into tracts. Through the study of the diffusion properties of these fibers, an aging related decline has been observed suggesting the degradation of the myelin sheath of the axons in several of these tracts (BENNETT et al., 2010). This suggests a loss in the capability of direct communication between regions, and, due to compensatory mechanisms, the information flow could follow through indirect ways, thus demonstrating higher functional coupling between regions, in a way that the functional connectivity between the terminal regions and regions along the path are increased, e.g. connection between arbitrary regions A and B is maintained during aging despite loss of structural connectivity due to a compensatory mechanism directing information to a region C, therefore functional connectivity between A and B does not change while connectivity between A and C and C and B is increased. Inter hemispheric connections are viable only through commissural tracts, such as anterior and posterior commissures and the corpus callosum, though. Therefore, a general decline in these fibers would signify a decline in the information flow between the hemispheres, as no other path could be taken between regions. This would explain why we observe diminished partial correlations in the homotopic connections, while the effect of age on intrahemispheric correlations is less robust, due to the fact that they have the availability of more indirect paths to compensate.

Our results here have resemblances with the literature, since reduced intra networks connectivities with aging have been reported (FERREIRA et al., 2016), and homotopic contralateral regions are likely part of the same resting state network.

We also note the regions displaying reduced partial Pearson interhemispheric correlation are likely to display cortical thinning, per Figure 4.2. Inter-hemispheric afferents and efferents are sourced and target the supragranular layers of the cortex, mostly layer III. Synaptic spine loss in layers I/III has been observed alongside aging, where nearly half of spine loss is from thin spines, which are associated with short-term plasticity and learning (MORRISON; BAXTER, 2012).

Our study did not attempt to elucidate if reduced use of axonal connections causes their atrophy or if it is the other way around, and therefore it remains to be tested as a hypothesis.

Due to the fact that negative bivariate correlation between timeseries can arise due to a lagged dependence structure (GOELMAN; GORDON; BONNE, 2014; MESZLÉNYI et al., 2017), studying predictive-causal relations become interesting. Here we emphasize predictive-causality does not allow one to assert true causal relations between phenomena. Having said that, we observed that the connectivities based on predictive-causality do not show age-related effects.

No significant effect of age was observed for Granger causality in the Enhanced NKI-RS while only two connectivities had significant effects of age in the Pilot NKI-RS. For instantaneous Granger causality, four and eleven connections had significant effects of age for the Pilot and Enhanced datasets respectively, the latter shown in Figure 4.14. None of these connectivities had significant effects when studying Pearson correlation.

The study of causality metrics on these data brings us to another realization: functional neuroimaging tends to exhibit high temporal autocorrelation (EKLUND et al., 2012; GEERLIGS et al., 2017), effectively reducing the degrees of freedom provided by the data even without any temporal processing in the study of BOLD connectivity (POWER; SCHLAGGAR; PETERSEN, 2014). If the past states of a timeseries are enough to reasonably describe its own states, then other timeseries cannot add enough information to the predictive problem. We observed this phenomenon in the Enhanced NKI-RS, which presents heavy non-stationarity due to the time resolution, the temporal filtering of underlying phenomena due to the hemodynamic response, and the filter band used. In Pilot NKI-RS, which does not

present as much non-stationarity, even though predictive causality could be attested, there was no obvious effect of age in its magnitude. Vector moving average (VMA) terms could help mitigate these phenomena, being incorporated into a Vector Auto-Regressive Moving Average (VARMA) modelling framework. This flexible strategy, however, further increases the number of parameters to be estimated.

The instantaneous Granger causality estimates have some resemblance to the absolute value of the Pearson correlation coefficient in the same series. A comparison is presented in Figure 5.1. This makes sense, since strong instantaneous Granger causality implies the simultaneous coupling between series, which in turn describes a high absolute value of Pearson correlation. A major difference between both is the fact that instantaneous Granger causality has no notion of reverse coupling, which is captured by a negative Pearson correlation coefficient. Also, as can be seen in Figure 5.1, even though there is high coupling between the metrics, there is also large deviations. This could explain the differing results on the effect of age on Instantaneous Granger Causality versus Pearson Correlation Coefficient. A last, and perhaps the most important point, is that Instantaneous Granger Causality accounts for some autocorrelation in both timeseries, which is not accounted for in Pearson correlation. If the autocorrelation is the driving force behind age-related alterations in Pearson correlation, then Instantaneous Granger causality mitigates that effect.

Figure 5.1 Pearson correlation coefficient plotted against instantaneous Granger causality index for all connections, in all subjects.

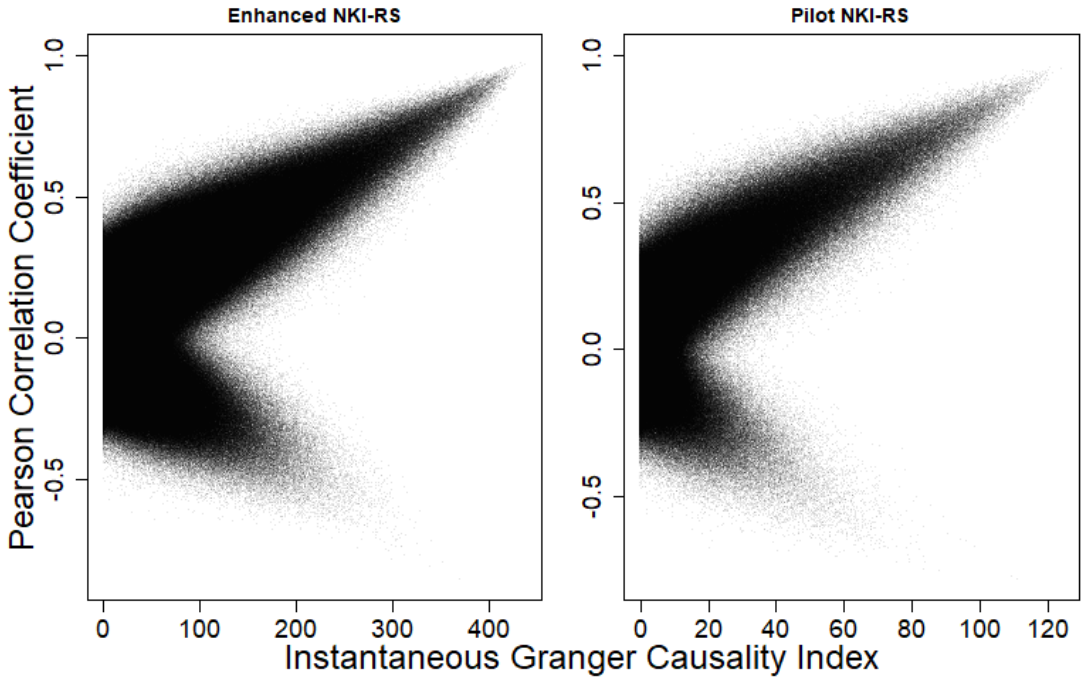

Source: The author.

The Granger Causality index, on the other hand, does not follow that trend, as can be seen in Figure 5.2.

Figure 5.2 Pearson correlation coefficient plotted against Granger causality index for all connections, in all subjects.

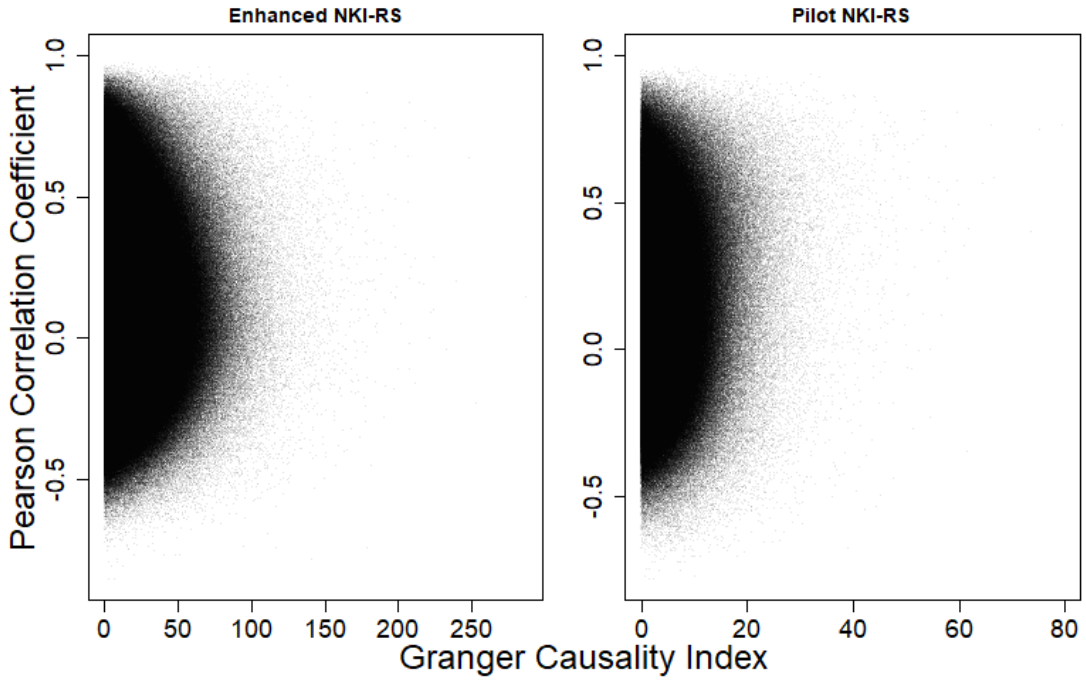

Source: The author.

Another consideration is that, due to the fact that the Granger causality connectivity matrix is full, that is, the upper triangle and the lower triangle are different, the multiple comparison correction is much more severe than in the case of the Pearson correlation coefficient or instantaneous Granger causality, requiring a higher level of evidence to attest significance.

A drawback of our approach is that indirect predictive causality paths are hidden from our analysis. Only a full multivariate approach including all known factors would help to elucidate direct predictive causality, and here we could probably include the movement and physiological noise acquisitions. The problem is this full model would be saturated; the amount of data acquired in a common functional neuroimaging study is not enough to identify the parameters of this model, at least not without incurring heavy bias through assumptions in a regularization framework. The bivariate approach is commonplace in the literature, but the researcher must know what this kind of inference actually allows. We did not attempt to model all timeseries at the same time for lack of enough effective degrees of freedom in our data. Regularized VAR modelling, using Partial Least Squares (PLS) or Tikhonov regularization, i.e. the ridge estimator, or mixed effects VAR modelling are viable approaches to this.

The GPDC is altered in several connections, in different frequencies. In total, 13 connections out of 320 exhibit significant effects of age. GPDC increases with age in 11 stances, and the remaining two are decreasing GPDC from a ROI to itself in two different frequencies. It is important to note that increasing GPDC from a ROI to itself necessarily means that GPDC is reduced from this very same ROI to all others, but if this is not homogeneously distributed along individuals then these connections won't be significantly altered due to age. The converse is also true for decreasing GPDC.

Among the common forms of PDC, GPDC was selected due to the scaling by the covariance matrix, which should make the magnitude of GPDC comparable between subjects.

GPDC reveals another type of functional coupling between different regions, namely a partial predictive causality index distributed in the frequency domain. Reducing the matrix shown in Figure 4.10 to only the ROIs shown in Figure 4.16 results in Figure 5.3. We can see the Pearson correlation coefficients involving the Middle frontal gyrus are not reduced, and even an increase is observed between the left Middle frontal gyrus and the right Superior frontal gyrus. Indeed, the only significant effects of age on the Middle frontal gyrus GPDC are decreases in GPDC in the left Middle frontal gyrus at 0.016 Hz and 0.031 Hz, which signifies the power it transfers to other ROIs is increased with aging.

Figure 5.3 Effect of age on the Pearson correlation coefficient between the same eight ROIs used to study the effect of age on GPDC, from the Enhanced NKI-RS

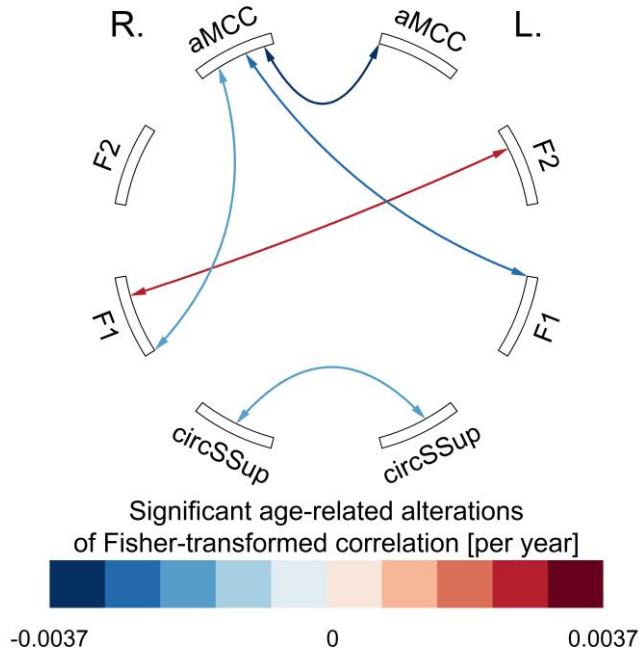

Source: The author. Regions are: Middle-anterior part of the cingulate gyri and sulci (aMCC), middle frontal gyri (F2), superior frontal gyri (F1), superior segments of the circular sulci of the insulas (circSSup).

We proposed a novel method accounting for the multivariate structure and theoretical distribution of the GPDC estimator. To the best of our knowledge, no prior study employed Beta or Dirichlet Regression to the study of the many variants of PDC. Our approach allows the study of PDC against the most diverse dependent variables in regression scenarios, not being limited to group comparisons.

Possible caveats of our analysis include the fact that GPDC estimates can be contaminated by hidden, unaccounted for, sources, which comprise the many other factors not included in the analysis. Therefore, the observed effects might be indirect.

Looking at the number of significant alterations in connectivities from a given ROI and ordering ROIs such that regions showing less atrophy are to the left and regions with more atrophy are to the right results in Figure 5.4. We can qualitatively perceive some dependence, even if small, on the number of altered connections and the degree of age-related atrophy.

Figure 5.4 Proportion of connectivities altered per ROI

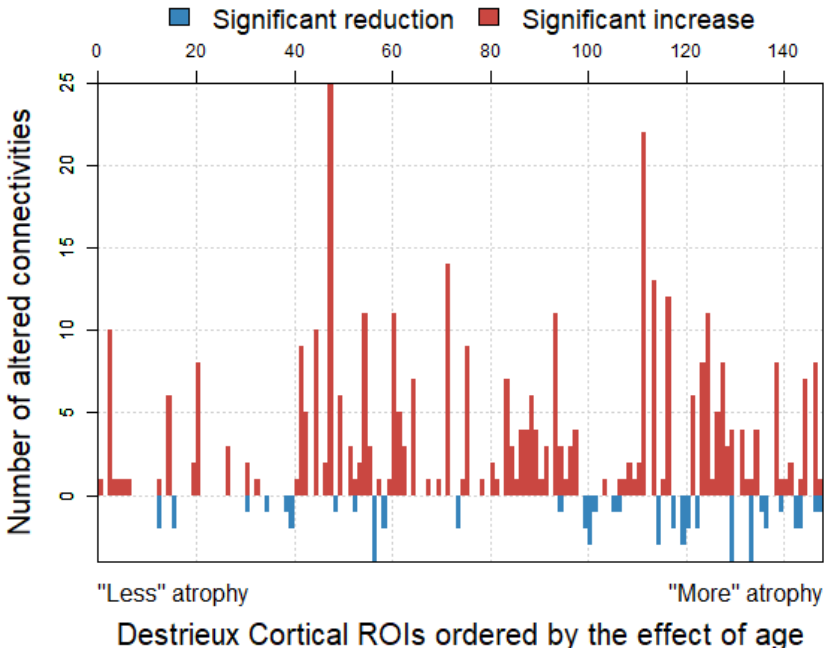

Source: The author. All 148 cortical ROIs from the Destrieux atlas are shown. Regions with more negative t-statistics are shown to the right.

Following this logic, a particularly interesting effect observed in our study is in the proportion of the positive and negative effects of age on the Pearson Correlation coefficient considering only regions whose effect of age on cortical thickness is under a certain rank, compared to other regions. Starting with regions with higher, therefore positive, t-statistics for alterations in cortical thickness, which are nearer zero since we observe most regions have negative effects of age, resulting in Figure 5.5.

Figure 5.5 Proportion of connectivities altered as a function of a maximal rank of cortical thickening during aging

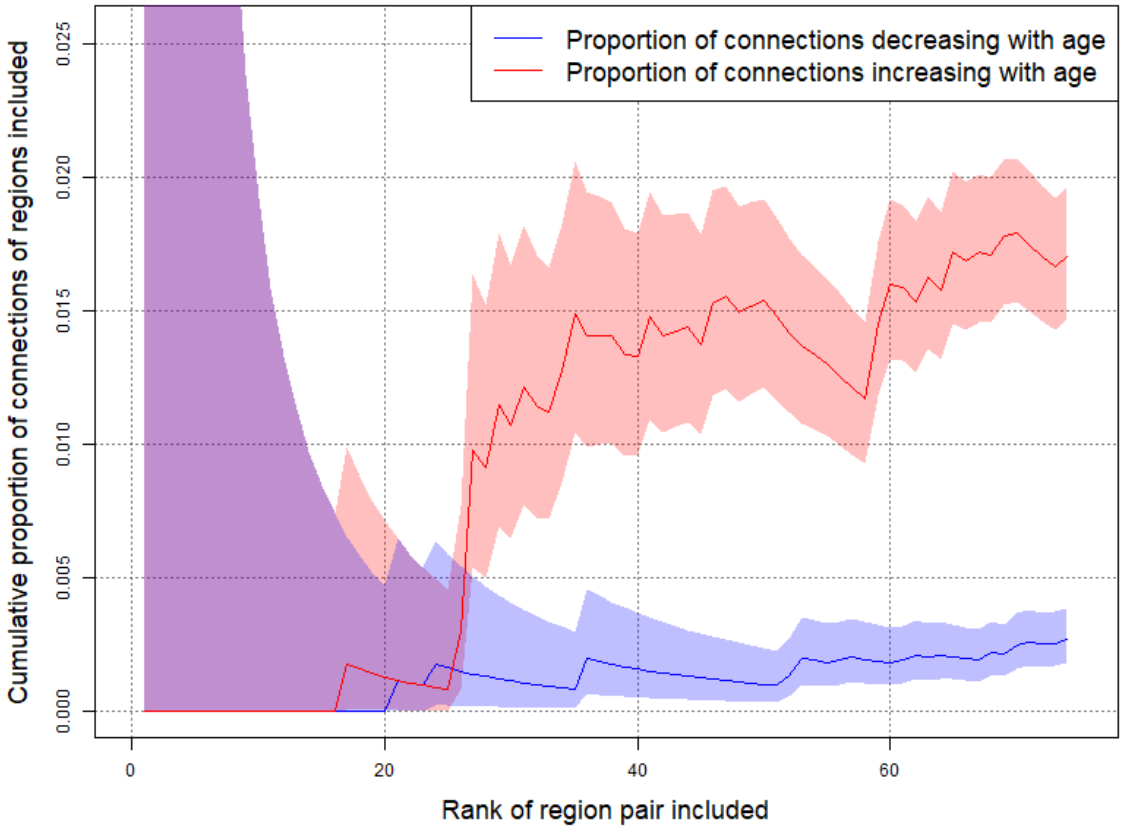

Source: The author. Binomial proportion confidence intervals are shown as the shaded regions and were calculated as the Clopper–Pearson interval. Homotopic regions are assigned the minimum t-statistic of either, and therefore enter the graph together.

Looking at Figure 5.5 we visually identify three regions: the leftmost one, where regions have no effect of age on thickness and also do not display age-related alterations in connectivity, lasting to around the inclusion of pair number 25; the central one where there is an intermediary negative effect of age on thickness, and now there is a constant small number of connections decreasing with aging plus a higher proportion of connections increasing with age, and starting shortly after the inclusion of pair 50, there is a steady albeit small increase in the proportion of connections decreasing with age plus an increase in the proportion of connections increasing with age. This effect is well illustrated in Figure 5.6.

Figure 5.6 Altered functional connectivities with regions ordered by the effect of age on their cortical thickness

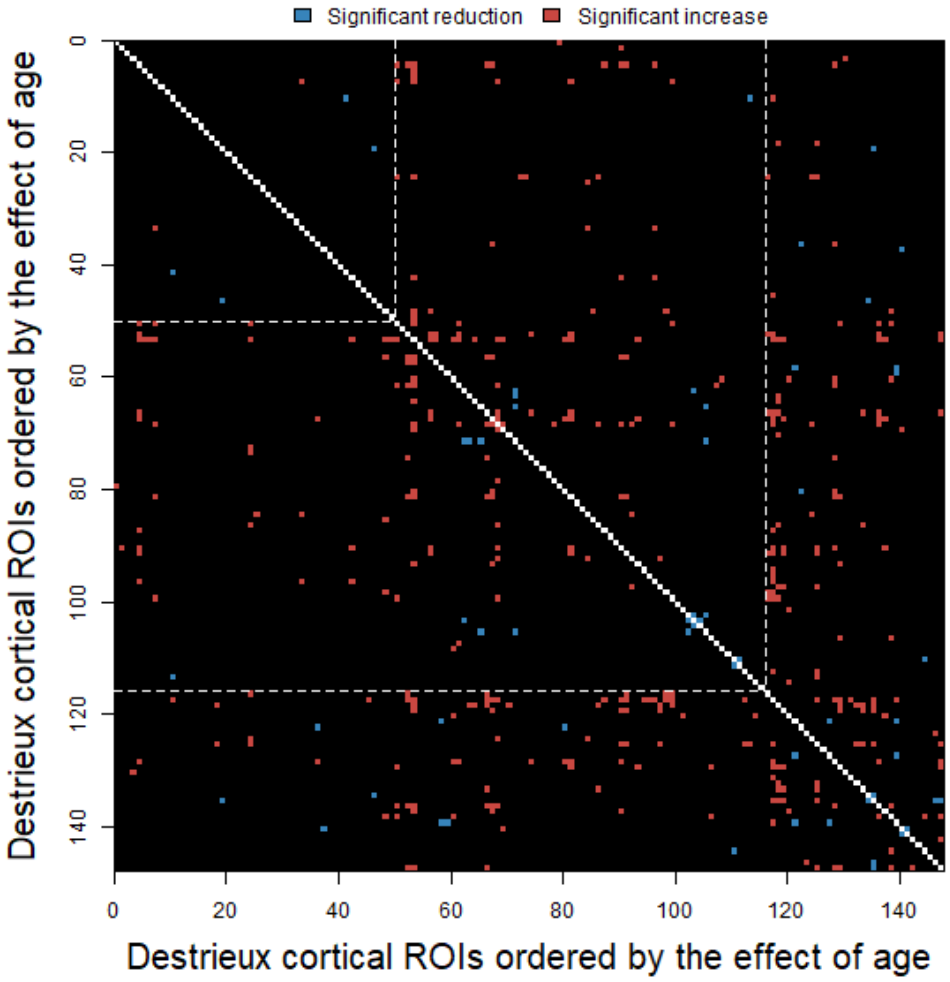

Source: The author. Higher t-statistics are at the start of the axes, while smaller or, better worded, more negative t-statistics are at the end. Homotopic regions are assigned the highest effect among both, so that they enter the graph together. Dashed lines represent the 25th and 58th pairs of regions.

Dividing the brain cortex along the dashed lines of Figure 5.6 results in the brain shown in Figure 5.7.

Figure 5.7 Brain regions divided by the order of the effect of age on cortical thickness

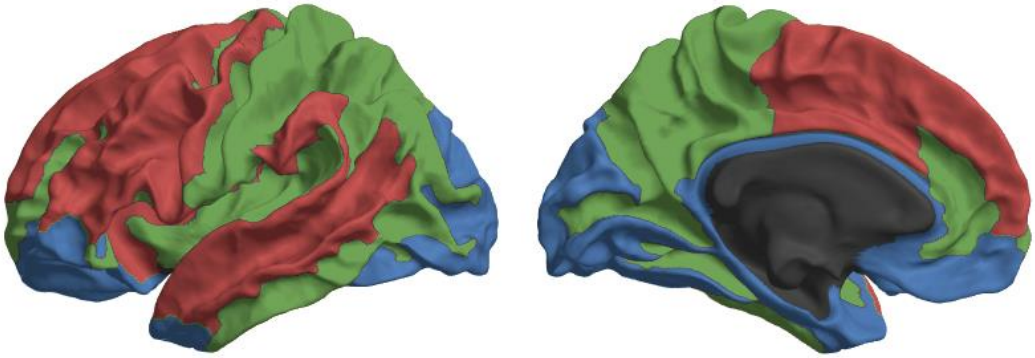

Source: The author. Regions are colored according to the white dashed lines shown in Figure 5.6, where blue represents region pairs ranked less than 25, green represents region pairs ranked between 26 and 58, and red represents region pairs ranked above 58.

From Figure 5.7 we see, for example, that occipital regions are ranked lower than frontal regions. These occipital regions in blue are responsible for many secondary visual functions, and there is smaller evidence for thickness atrophy as well as few alterations in connectivity between them. The frontal regions sustain many high-order cognitive functions and have strong evidence for thickness atrophy and the highest proportion of altered connectivities. Visual networks are not likely to be altered by aging (ZHANG et al., 2014), while alterations in frontal connectivity are commonplace and might signal increased demand or an anterior-posterior shift in brain activity due to age (SALA-LLONCH et al., 2014).

On the association between alterations in cortical thickness and functional connectivity, we first notice 15 regions exhibiting significant associations in the Enhanced NKI-RS, with 7 being positive. A positive association means that the effects of age on the connectivities given a seed has the same direction of the effects of age on the cortical thickness of the target regions, i.e. higher rates of change in thickness implying higher rates of change in functional connectivity. On the other hand, a negative association implies opposite direction of the effects, i.e. higher rates of change in thickness imply smaller rates of change in functional connectivity. As an example, the association for the left Occipital Pole (*Pole_occipital*), from the Enhanced NKI-RS, is shown in Figure 5.8, with a coefficient of -0.432, $p(FDR) < 0.001$.

Figure 5.8 Association between age-related effects on target cortical thickness and functional connectivity given the left occipital pole as seed.

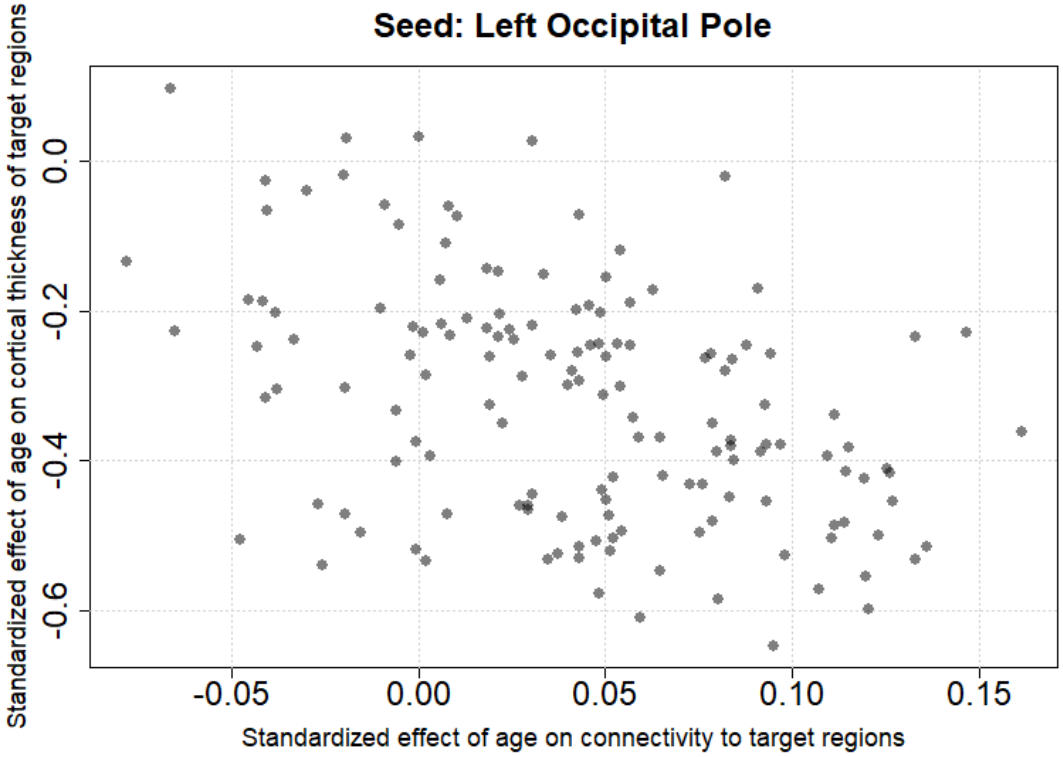

Source: The author.

If a region shows a negative association between the standardized effects of age on target thickness and functional connectivity to the targets, such as the example shown in Figure 5.8, it means that region becomes more connected with regions showing the highest degrees of atrophy. We hypothesize these regions are part of compensatory systems, as they become more connected with regions whose cortical organization suffers most with aging, perhaps helping to relay information. The converse is also true, regions showing a positive association between said effects become less connected with the regions showing the highest degrees of atrophy. These might be regions where compensatory mechanisms are not available and show the effects of disconnection associated with atrophy.

Studying the association directly at the subject level as the mixed-effect previously described allows one to directly estimate the sway cortical thickness has on connectivity, and also how much this effect varies with age, if at all. However, it is important to note that, due to the inclusion of interactions, the main effects are estimates when all other independent variables are null. For this reason, thickness

effects might come into and leave significance at different ages, for example. To overcome this issue, the type II ANOVA was performed instead.

A problem with this procedure is that cortical gray matter thickness is strongly correlated with age on most of the cortex. Therefore, when a model without the effect of age is fitted, most of its explanatory power is retained by the mere inclusion of cortical thickness estimates.

Besides that, even when testing the joint effect of the inclusion of age, seed thickness, and target thickness on the models, no significant effect was found. This is simply due to the fact that the average connectivity from a seed ROI does not change with age or cortical thickness. This does not imply, however, that its connectivities are unaltered. The number of ROIs in the atlas has an impact on this. Proposed methodological adaptations include mediation analysis and fully multivariate analysis.

Concluding, our results support gray-matter atrophy in the whole brain, affecting cortical thickness, surface area, and volume, and also in supracortical volume. In particular, we show how the cortical age-related thinning profiles have some association to the starting cortical thickness, with thicker cortex displaying, proportionally, higher rates of thinning. We propose the relationship between initial cortical thickness and rate of thinning is associated with cortical granularity and also cortical type admixture. Under this light, pure neocortex presents higher rates of atrophy, higher still in agranular than in granular neocortex, than mixed cortices. We also found a moderate proportion of age-related alterations in cortico-cortical connectivities. Increases in the functional coupling between regions measured by Pearson correlation, which are more prevalent than decreases, can be interpreted as a mechanism compensating brain aging. Our results, of course, cannot be so readily compared to the rest of the literature without taking into account different cortical parcellations used, but overall the main findings are consistent, with overall increase in functional connectivity. On the other hand, we did not observe many effects of age on predictive causality indices, bivariate Granger causality and instantaneous Granger causality, which mitigate the effect of autocorrelation between series. The non-stationarity of timeseries might be a cause for this. We also studied the functional coupling in the frequency domain between the regions most affected by age-related cortical thinning with GPDC, uncovering increased power spectral density retained in several regions across the frequencies analyzed using a multivariate approach that best matches the specificities of squared GPDC. We

believe this new approach, using Dirichlet Regression, is useful for a broad selection of applications of GPDC in neuroscience. Moreover, associations between age-related changes in functional connectivity from a seed region and cortical thinning of the target regions has been found, suggesting an underlying, overarching, phenomenon, where regions specially targeted by age-related atrophy tend to present more alterations in functional connectivity.

Even though we thoroughly studied the subject of our research, successfully reproducing several results from the literature while adding several findings of our own, there are still questions to be answered. Topics for future research include allowing the estimation of non-linear effects of age on morphometry and perhaps even connectivity, which could be studied through non-parametric models such as GAMs, and the effect of age on combined phase-frequency functional connectivity estimates, such as window functions decomposition approaches (GOELMAN et al., 2017). Cortical thickness measurements aggregate myelinated and unmyelinated gray matter (ROWLEY et al., 2015), and these might be affected by aging differentially. The increasing number of large scale datasets on aging also allows confirmatory studies on the results here presented. Apart from the study of aging, the methods here presented allow for the principled study of several other cognitive phenomena.

REFERENCES

AERTSEN, A.; PREISSL, H. Dynamics of Activity and Connectivity in Physiological Neuronal Networks. **Nonlinear dynamics and neuronal networks**, v. 13, n. August 2016, p. 281–302, 1991.

AMLIEN, I. K. et al. Organizing Principles of Human Cortical Development - Thickness and Area from 4 to 30 Years: Insights from Comparative Primate Neuroanatomy. **Cerebral Cortex**, v. 26, n. 1, p. 257–267, 2016.

ANDREWS-HANNA, J. R. et al. Disruption of Large-Scale Brain Systems in Advanced Aging. **Neuron**, v. 56, n. 5, p. 924–935, 6 dez. 2007.

BACCALÁ, L. A. et al. Unified asymptotic theory for all partial directed coherence forms. **Philosophical transactions. Series A, Mathematical, physical, and engineering sciences**, v. 371, n. 1997, p. 20120158, 28 ago. 2013.

BACCALA, L. A.; SAMESHIMA, K.; TAKAHASHI, D. Y. **Generalized Partial Directed Coherence**. 2007 15th International Conference on Digital Signal Processing. **Anais**...IEEE, jul. 2007Disponível em: <http://ieeexplore.ieee.org/document/4288544/>

BAKKOUR, A. et al. The effects of aging and Alzheimer's disease on cerebral cortical anatomy: specificity and differential relationships with cognition. **NeuroImage**, v. 76, p. 332–44, 1 ago. 2013.

BARR, D. J. et al. Random effects structure for confirmatory hypothesis testing: Keep it maximal. **Journal of Memory and Language**, v. 68, n. 3, p. 255–278, 2013.

BATES, D. et al. Fitting Linear Mixed-Effects Models Using lme4. **Journal of Statistical Software**, v. 67, n. 1, p. 51, 2015.

BEHZADI, Y. et al. A component based noise correction method (CompCor) for BOLD and perfusion based fMRI. **NeuroImage**, v. 37, n. 1, p. 90–101, 1 ago. 2007.

BENAVIDES-PICCIONE, R. et al. Age-based comparison of human dendritic spine structure using complete three-dimensional reconstructions. **Cerebral cortex (New York, N.Y. : 1991)**, v. 23, n. 8, p. 1798–810, ago. 2013.

BENJAMINI, Y.; HOCHBERG, Y. Controlling the False Discovery Rate: a Practical and Powerful Approach to Multiple Testing. **Journal of the Royal Statistical Society**, v. 57, n. 1, p. 289–300, 1995.

BENJAMINI, Y.; YEKUTIELI, D. The control of the false discovery rate in multiple testing under depencency. **The Annals of Statistics**, v. 29, n. 4, p. 1165–1188,

2001.

BENNETT, I. J. et al. Age-related differences in multiple measures of white matter integrity: A diffusion tensor imaging study of healthy aging. **Human Brain Mapping**, v. 31, n. 3, p. 378–390, 2010.

BERNIER, M. et al. Spatial distribution of resting-state BOLD regional homogeneity as a predictor of brain glucose uptake: A study in healthy aging. **NeuroImage**, v. 150, n. January, p. 14–22, 15 abr. 2017.

BETZEL, R. F. et al. Changes in structural and functional connectivity among resting-state networks across the human lifespan. **NeuroImage**, v. 102, n. P2, p. 345–357, nov. 2014.

BIRN, R. M. et al. The effect of scan length on the reliability of resting-state fMRI connectivity estimates. **NeuroImage**, v. 83, p. 550–558, dez. 2013.

BISWAL, B. et al. Functional connectivity in the motor cortex of resting human brain using echo-planar MRI. **Magnetic resonance in medicine**, v. 34, n. 4, p. 537–41, out. 1995.

BISWAL, B. B. Resting state fMRI: a personal history. **NeuroImage**, v. 62, n. 2, p. 938–44, 15 ago. 2012.

BOISGONTIER, M. P. Motor aging results from cerebellar neuron death. **Trends in neurosciences**, v. 38, n. 3, p. 127–8, mar. 2015.

BOISGONTIER, M. P. et al. Individual differences in brainstem and basal ganglia structure predict postural control and balance loss in young and older adults. **Neurobiology of Aging**, v. 50, p. 47–59, 2017.

BOLON, B. et al. Chapter 52 - Nervous System. In: HASCHEK, W. M. et al. (Eds.). . **Haschek and Rousseaux's Handbook of Toxicologic Pathology, 3rd edition**. 3. ed. [s.l.] Academic Press, 2013. p. 2005–2093.

BROWN, R. W. et al. **Magnetic Resonance Imaging: Physical Principles and Sequence Design**. Chichester, UK: John Wiley & Sons Ltd, 2014.

BUCKNER, R. L. Functional-anatomic correlates of control processes in memory. **The Journal of neuroscience : the official journal of the Society for Neuroscience**, v. 23, n. 10, p. 3999–4004, 15 maio 2003.

BUCKNER, R. L. Memory and Executive Function in Aging and AD. **Neuron**, v. 44, n. 1, p. 195–208, set. 2004.

BURIANOVÁ, H. et al. The relation of structural integrity and task-related functional connectivity in the aging brain. **Neurobiology of aging**, v. 36, n. 10, p. 2830–7, out.

2015.

CABALLERO-GAUDES, C.; REYNOLDS, R. C. Methods for cleaning the BOLD fMRI signal. **NeuroImage**, n. December, p. 0–1, 9 dez. 2016.

CAO, M. et al. Topological organization of the human brain functional connectome across the lifespan. **Developmental Cognitive Neuroscience**, v. 7, n. 16, p. 76–93, 2014.

CHÉTELAT, G. et al. Relationships between brain metabolism decrease in normal aging and changes in structural and functional connectivity. **NeuroImage**, v. 76, p. 167–77, 1 ago. 2013.

CROXSON, P. L. et al. Structural Variability Across the Primate Brain: A Cross-Species Comparison. **Cerebral Cortex**, p. 1–13, 2017.

DAMOISEAUX, J. S. et al. Consistent resting-state networks across healthy subjects. **Proceedings of the National Academy of Sciences of the United States of America**, v. 103, n. 37, p. 13848–53, 2006.

DAMOISEAUX, J. S. et al. Reduced resting-state brain activity in the “default network” in normal aging. **Cerebral Cortex**, v. 18, n. 8, p. 1856–1864, 2008.

DASELAAR, S. M. et al. Less wiring, more firing: low-performing older adults compensate for impaired white matter with greater neural activity. **Cerebral cortex (New York, N.Y. : 1991)**, v. 25, n. 4, p. 983–90, abr. 2015.

DEKABAN, A. S.; SADOWSKY, D. Changes in brain weight during the span of human life: relation of brain weight to body height and body weight. **Ann. Neurol.**, v. 4, p. 345, 1978.

DESTRIEUX, C. et al. Automatic parcellation of human cortical gyri and sulci using standard anatomical nomenclature. **NeuroImage**, v. 53, n. 1, p. 1–15, 15 out. 2010.

DEVELOPMENTAL IMAGING GROUP - MCRI. **freesurfer_statsurf_display Freesurfer surface results display in MATLAB**. Disponível em: <https://chrisadamsonmcri.github.io/freesurfer_statsurf_display>. Acesso em: 6 out. 2017.

DOUAUD, G. et al. A common brain network links development, aging, and vulnerability to disease. **Proceedings of the National Academy of Sciences of the United States of America**, v. 111, n. 49, p. 17648–53, 9 dez. 2014.

ECONOMO, C. VON. **Cellular Structure of the human cerebral cortex**. [s.l.] Karger, 2009.

EKLUND, A. et al. Does parametric fMRI analysis with SPM yield valid results?-An

empirical study of 1484 rest datasets. **NeuroImage**, v. 61, n. 3, p. 565–578, 2012.

ELSTER, A.; BURDETTE, J. **Questions and Answers in MRI**. 2nd ed ed. St. Louis: Mosby, 2001.

FAN, L. et al. Connectivity-based parcellation of the human temporal pole using diffusion tensor imaging. **Cerebral Cortex**, v. 24, n. 12, p. 3365–3378, 2014.

FEINBERG, D. A.; REESE, T. G.; WEDEEN, V. J. Simultaneous echo refocusing in EPI. **Magnetic Resonance in Medicine**, v. 48, n. 1, p. 1–5, 2002.

FERREIRA, L. K. et al. Aging effects on whole-brain functional connectivity in adults free of cognitive and psychiatric disorders. **Cerebral Cortex**, v. 26, n. 9, p. 3851–3865, 2016.

FERREIRA, L. K.; BUSATTO, G. F. Resting-state functional connectivity in normal brain aging. **Neuroscience and Biobehavioral Reviews**, v. 37, n. 3, p. 384–400, 2013.

FILIPEK, P. A. et al. The young adult human brain: an MRI-based morphometric analysis. **Cerebral cortex (New York, N.Y. : 1991)**, v. 4, n. 4, p. 344–60, 1994.

FISCHL, B. et al. Whole brain segmentation: Automated labeling of neuroanatomical structures in the human brain. **Neuron**, v. 33, n. 3, p. 341–355, 2002.

FISCHL, B. FreeSurfer. **NeuroImage**, v. 62, n. 2, p. 774–781, 2012.

FJELL, A. M. et al. High consistency of regional cortical thinning in aging across multiple samples. **Cerebral Cortex**, v. 19, n. 9, p. 2001–2012, 2009a.

FJELL, A. M. et al. Minute effects of sex on the aging brain: a multisample magnetic resonance imaging study of healthy aging and Alzheimer's disease. **The Journal of neuroscience : the official journal of the Society for Neuroscience**, v. 29, n. 27, p. 8774–83, 8 jul. 2009b.

FJELL, A. M. et al. One-year brain atrophy evident in healthy aging. **The Journal of neuroscience : the official journal of the Society for Neuroscience**, v. 29, n. 48, p. 15223–31, 2 dez. 2009c.

FJELL, A. M. et al. Cortical gray matter atrophy in healthy aging cannot be explained by undetected incipient cognitive disorders: a comment on Burgmans et al. (2009). **Neuropsychology**, v. 24, n. 2, p. 258-263-266, 2010a.

FJELL, A. M. et al. When does brain aging accelerate? Dangers of quadratic fits in cross-sectional studies. **NeuroImage**, v. 50, n. 4, p. 1376–83, 1 maio 2010b.

FJELL, A. M. et al. Critical ages in the life course of the adult brain: nonlinear subcortical aging. **Neurobiology of aging**, v. 34, n. 10, p. 2239–47, out. 2013.

FJELL, A. M. et al. Accelerating cortical thinning: Unique to dementia or universal in aging? **Cerebral Cortex**, v. 24, n. 4, p. 919–934, 2014a.

FJELL, A. M. et al. What is normal in normal aging? Effects of aging, amyloid and Alzheimer's disease on the cerebral cortex and the hippocampus. **Progress in neurobiology**, v. 117, p. 20–40, jun. 2014b.

FJELL, A. M. et al. Functional connectivity change across multiple cortical networks relates to episodic memory changes in aging. **Neurobiology of Aging**, v. 36, n. 12, p. 3255–3268, 2015a.

FJELL, A. M. et al. The roots of Alzheimer's disease: Are high-expanding cortical areas preferentially targeted? **Cerebral Cortex**, v. 25, n. 9, p. 2556–2565, 2015b.

FJELL, A. M. et al. High-Expanding Cortical Regions in Human Development and Evolution Are Related to Higher Intellectual Abilities. **Cerebral Cortex**, v. 25, n. 1, p. 26–34, 1 jan. 2015c.

FJELL, A. M. et al. Development and aging of cortical thickness correspond to genetic organization patterns. **Proceedings of the National Academy of Sciences of the United States of America**, v. 112, n. 50, p. 15462–7, 15 dez. 2015d.

FJELL, A. M. et al. The Disconnected Brain and Executive Function Decline in Aging. **Cerebral cortex (New York, N.Y. : 1991)**, v. 27, n. 3, p. 2303–2317, 2017a.

FJELL, A. M. et al. Relationship between structural and functional connectivity change across the adult lifespan: A longitudinal investigation. **Human Brain Mapping**, v. 38, n. 1, p. 561–573, 2017b.

FREEMAN, S. H. et al. Preservation of neuronal number despite age-related cortical brain atrophy in elderly subjects without Alzheimer disease. **Journal of neuropathology and experimental neurology**, v. 67, n. 12, p. 1205–12, dez. 2008.

FRISTON, K. J. et al. Functional Connectivity: The Principal-Component Analysis of Large (PET) Data Sets. **Journal of Cerebral Blood Flow & Metabolism**, v. 13, n. 1, p. 5–14, 29 jan. 1993.

FRISTON, K. J. Functional and Effective Connectivity: A Review. **Brain Connectivity**, v. 1, n. 1, p. 13–36, jan. 1994.

GAZZALEY, A. H.; D'ESPOSITO, M. BOLD Functional MRI and Cognitive Aging. In: **Cognitive Neuroscience of Aging**. [s.l.] Oxford University Press, 2004. v. 163p. 107–131.

GEERLIGS, L. et al. A Brain-Wide Study of Age-Related Changes in Functional Connectivity. **Cerebral Cortex**, v. 25, n. 7, p. 1987–1999, 2015.

GEERLIGS, L. et al. Challenges in measuring individual differences in functional connectivity using fMRI: The case of healthy aging. **Human brain mapping**, v. 0, 23 maio 2017.

GLASSER, M. F. et al. Trends and properties of human cerebral cortex: Correlations with cortical myelin content. **NeuroImage**, v. 93, p. 165–175, 2014.

GOELMAN, G. et al. Frequency-phase analysis of resting-state functional MRI. **Scientific reports**, v. 7, n. January, p. 43743, 8 mar. 2017.

GOELMAN, G.; GORDON, N.; BONNE, O. Maximizing negative correlations in resting-state functional connectivity MRI by time-lag. **PloS one**, v. 9, n. 11, p. e111554, 2014.

GONG, G. et al. Convergence and divergence of thickness correlations with diffusion connections across the human cerebral cortex. **NeuroImage**, v. 59, n. 2, p. 1239–1248, 2012.

GOODRO, M. et al. Age effect on subcortical structures in healthy adults. **Psychiatry research**, v. 203, n. 1, p. 38–45, 30 jul. 2012.

GRONENSCHILD, E. H. B. M. et al. The effects of FreeSurfer version, workstation type, and Macintosh operating system version on anatomical volume and cortical thickness measurements. **PLoS ONE**, v. 7, n. 6, 2012.

HAASE, A. et al. FLASH imaging: rapid NMR imaging using low flip-angle pulses. 1986. **Journal of magnetic resonance (San Diego, Calif. : 1997)**, v. 213, n. 2, p. 533–41, dez. 2011.

HARADA, C. N.; NATELSON LOVE, M. C.; TRIEBEL, K. L. Normal cognitive aging. **Clinics in geriatric medicine**, v. 29, n. 4, p. 737–52, nov. 2013.

HE, W.; GOODKIND, D.; KOWAL, P. An Aging World : 2015 International Population Reports. p. 165, 2016.

HEBB, D. O. **The organization of behavior: A neuropsychological theory**. New York: Wiley, 1949.

HJELM, R. D. et al. Restricted Boltzmann machines for neuroimaging: an application in identifying intrinsic networks. **NeuroImage**, v. 96, p. 245–60, 1 ago. 2014.

HOGSTROM, L. J. et al. The structure of the cerebral cortex across adult life: Age-related patterns of surface area, thickness, and gyrification. **Cerebral Cortex**, v. 23, n. 11, p. 2521–2530, 2013.

JAGUST, W. Vulnerable Neural Systems and the Borderland of Brain Aging and Neurodegeneration. **Neuron**, v. 77, n. 2, p. 219–234, jan. 2013.

JETTE, M. A.; YOO, A. B.; GRONDONA, M. **SLURM: Simple Linux Utility for Resource Management**. In Lecture Notes in Computer Science: Proceedings of Job Scheduling Strategies for Parallel Processing (JSSPP) 2003. **Anais**...Springer-Verlag, 2002

JONES, D. K.; KNÖSCHE, T. R.; TURNER, R. White matter integrity, fiber count, and other fallacies: the do's and don'ts of diffusion MRI. **NeuroImage**, v. 73, p. 239–54, jun. 2013.

KAKIMOTO, A. et al. Age-Related Sex-Specific Changes in Brain Metabolism and Morphology. **Journal of nuclear medicine : official publication, Society of Nuclear Medicine**, v. 57, n. 2, p. 221–5, 1 fev. 2016.

KALPOUZOS, G.; PERSSON, J.; NYBERG, L. Local brain atrophy accounts for functional activity differences in normal aging. **Neurobiology of Aging**, v. 33, n. 3, p. 623.e1-623.e13, 2012.

KIRCHGÄSSNER, G.; WOLTERS, J. **Introduction to Modern Time Series Analysis**. Berlin, Heidelberg: Springer-Verlag Berlin Heidelberg, 2007.

KOLLER, M.; STAHEL, W. A. Sharpening Wald-type inference in robust regression for small samples. **Computational Statistics & Data Analysis**, v. 55, n. 8, p. 2504–2515, ago. 2011.

KOLLER, M.; STAHEL, W. A. Nonsingular subsampling for regression S estimators with categorical predictors. **Computational Statistics**, v. 32, n. 2, p. 631–646, 3 jun. 2017.

KONDO, H.; SALEEM, K. S.; PRICE, J. L. Differential connections of the temporal pole with the orbital and medial prefrontal networks in macaque monkeys. **The Journal of comparative neurology**, v. 465, n. 4, p. 499–523, 27 out. 2003.

LA CORTE, V. et al. Cognitive Decline and Reorganization of Functional Connectivity in Healthy Aging: The Pivotal Role of the Salience Network in the Prediction of Age and Cognitive Performances. **Frontiers in aging neuroscience**, v. 8, n. AUG, p. 204, 2016.

LE BIHAN, D. Diffusion MRI: what water tells us about the brain. **EMBO molecular medicine**, v. 6, n. 5, p. 569–73, maio 2014.

LEDOIT, O.; WOLF, M. Improved Estimation of the Covariance Matrix of Stock Returns With an Application to Portfolio Selection. p. 1–19, 2001.

LEDOIT, O.; WOLF, M. A well-conditioned estimator for large-dimensional covariance matrices. **Journal of Multivariate Analysis**, v. 88, n. 2, p. 365–411,

2004.

LEMAITRE, H. et al. Normal age-related brain morphometric changes: Nonuniformity across cortical thickness, surface area and gray matter volume? **Neurobiology of Aging**, v. 33, n. 3, p. 617.e1-617.e9, 2012.

LENTH, R. Least-Squares Means: The R Package lsmeans. **Journal of Statistical Software, Articles**, v. 69, n. 1, p. 1–33, 2016.

LOCKHART, S. N.; DECARLI, C. Structural imaging measures of brain aging. **Neuropsychology review**, v. 24, n. 3, p. 271–89, set. 2014.

LOEHRER, P. A. et al. Ageing changes effective connectivity of motor networks during bimanual finger coordination. **NeuroImage**, v. 143, p. 325–342, 2016.

MAECHLER, M. et al. **robustbase: Basic Robust Statistics**, 2016. Disponível em: <http://robustbase.r-forge.r-project.org/>

MAIER, M. J. **DirichletReg : Dirichlet Regression for Compositional Data in R**. [s.l: s.n.]. Disponível em: <http://epub.wu.ac.at/4077/>.

MAIER, M. J. **DirichletReg: Dirichlet Regression in R**, 2015. Disponível em: <http://dirichletreg.r-forge.r-project.org/>

MAILLET, D.; RAJAH, M. N. Association between prefrontal activity and volume change in prefrontal and medial temporal lobes in aging and dementia: A review. **Ageing Research Reviews**, v. 12, n. 2, p. 479–489, 2013.

MALPETTI, M. et al. Gender differences in healthy aging and Alzheimer's Dementia: A ^{18} F-FDG-PET study of brain and cognitive reserve. **Human Brain Mapping**, v. 0, n. October 2016, p. 4212–4227, 2017.

MARSTALLER, L. et al. Aging and large-scale functional networks: White matter integrity, gray matter volume, and functional connectivity in the resting state. **Neuroscience**, v. 290, p. 369–378, 2015.

MARTÍNEZ-PINILLA, E. et al. Regional and gender study of neuronal density in brain during aging and in alzheimer's disease. **Frontiers in Aging Neuroscience**, v. 8, n. SEP, p. 1–12, 2016.

MCCULLAGH, P.; NELDER, J. A. **Generalized Linear Models**. Boston, MA: Springer US, 1989.

MEIER-RUGE, W. et al. Age-related white matter atrophy in the human brain. **Annals of the New York Academy of Sciences**, v. 673, p. 260–9, 26 dez. 1992.

MENNES, M. et al. Making data sharing work: The FCP/INDI experience. **NeuroImage**, v. 82, p. 683–691, 2013.

MENON, V.; UDDIN, L. Q. Saliency, switching, attention and control: a network model of insula function. **Brain Structure and Function**, v. 214, n. 5–6, p. 655–667, 2010.

MESULAM, M. M. A plasticity-based theory of the pathogenesis of Alzheimer's disease. **Annals of the New York Academy of Sciences**, v. 924, n. 1, p. 42–52, 2000.

MESZLÉNYI, R. J. et al. Resting State fMRI Functional Connectivity Analysis Using Dynamic Time Warping. **Frontiers in Neuroscience**, v. 11, n. FEB, p. 1–17, 17 fev. 2017.

MORRISON, J. H.; BAXTER, M. G. The ageing cortical synapse: Hallmarks and implications for cognitive decline. **Nature Reviews Neuroscience**, v. 13, n. 4, p. 240–250, 2012.

MUGLER, J. P.; BROOKEMAN, J. R. Three-dimensional magnetization-prepared rapid gradient-echo imaging (3D MP RAGE). **Magnetic Resonance in Medicine**, v. 15, n. 1, p. 152–157, jul. 1990.

MULLER, A. M.; MÉRILLAT, S.; JÄNCKE, L. Small changes, but huge impact? The right anterior insula's loss of connection strength during the transition of old to very old age. **Frontiers in Aging Neuroscience**, v. 8, n. MAY, p. 1–20, 2016.

MUSCHELLI, J. et al. Reduction of motion-related artifacts in resting state fMRI using aCompCor. **NeuroImage**, v. 96, p. 22–35, 1 ago. 2014.

NELSON, P. T. et al. Correlation of Alzheimer disease neuropathologic changes with cognitive status: a review of the literature. **Journal of neuropathology and experimental neurology**, v. 71, n. 5, p. 362–81, maio 2012.

NOONER, K. B. et al. The NKI-Rockland Sample: A Model for Accelerating the Pace of Discovery Science in Psychiatry. **Frontiers in Neuroscience**, v. 6, n. OCT, p. 152, 2012.

OGAWA, S. et al. Brain magnetic resonance imaging with contrast dependent on blood oxygenation. **Proceedings of the National Academy of Sciences of the United States of America**, v. 87, n. 24, p. 9868–72, dez. 1990.

PANIZZON, M. S. et al. Distinct genetic influences on cortical surface area and cortical thickness. **Cerebral Cortex**, v. 19, n. 11, p. 2728–2735, 2009.

PARK, D. C.; REUTER-LORENZ, P. The adaptive brain: aging and neurocognitive scaffolding. **Annual review of psychology**, v. 60, n. 1, p. 173–96, 2009.

PASCUAL, B. et al. Large-scale brain networks of the human left temporal pole: a

functional connectivity MRI study. **Cerebral cortex (New York, N.Y. : 1991)**, v. 25, n. 3, p. 680–702, mar. 2015.

PATRIAT, R. et al. The effect of resting condition on resting-state fMRI reliability and consistency: a comparison between resting with eyes open, closed, and fixated. **NeuroImage**, v. 78, p. 463–73, set. 2013.

PFAFF, B. **Analysis of Integrated and Cointegrated Time Series with R**. Second ed. New York: Springer, 2008a.

PFAFF, B. VAR, SVAR and SVEC Models: Implementation Within R Package vars. **Journal of Statistical Software**, v. 27, n. 4, 2008b.

POLDRACK, R. A.; MUMFORD, J. A.; NICHOLS, T. E. **Handbook of functional MRI data analysis**. [s.l.] Cambridge University Press, 2011.

POTVIN, O. et al. Normative data for subcortical regional volumes over the lifetime of the adult human brain. **NeuroImage**, v. 137, p. 9–20, 15 ago. 2016a.

POTVIN, O. et al. FreeSurfer subcortical normative data. **Data in Brief**, v. 9, p. 732–736, dez. 2016b.

POTVIN, O.; DIEUMEGARDE, L.; DUCHESNE, S. Normative morphometric data for cerebral cortical areas over the lifetime of the adult human brain. **NeuroImage**, v. 156, n. May, p. 315–339, ago. 2017a.

POTVIN, O.; DIEUMEGARDE, L.; DUCHESNE, S. Freesurfer cortical normative data for adults using Desikan-Killiany-Tourville and ex vivo protocols. **NeuroImage**, v. 156, n. May, p. 43–64, ago. 2017b.

POWER, J. D. et al. Functional Network Organization of the Human Brain. **Neuron**, v. 72, n. 4, p. 665–678, nov. 2011.

POWER, J. D. et al. Spurious but systematic correlations in functional connectivity MRI networks arise from subject motion. **NeuroImage**, v. 59, n. 3, p. 2142–54, 1 fev. 2012.

POWER, J. D.; SCHLAGGAR, B. L.; PETERSEN, S. E. Studying brain organization via spontaneous fMRI signal. **Neuron**, v. 84, n. 4, p. 681–696, 2014.

R CORE TEAM. **R: A Language and Environment for Statistical Computing**Vienna, Austria, 2018. Disponível em: <https://www.r-project.org/>

RAKIC, P. Evolution of the neocortex: A perspective from developmental biology. **Nature Reviews Neuroscience**, v. 10, n. 10, p. 724–735, 2009.

RAZ, N. Aging of the brain and its impact on cognitive performance: integration of structural and functional findings BT - Handbook of Aging and Cognition. In:

Handbook of Aging and Cognition - II. [s.l: s.n.]. v. 2p. 1–90.

RAZNAHAN, A. et al. How Does Your Cortex Grow? **The Journal of Neuroscience**, v. 31, n. 19, p. 7174–7177, 2011.

RODRIGUES, P. L. C.; BACCALA, L. A. **A new algorithm for neural connectivity estimation of EEG event related potentials**. 2015 37th Annual International Conference of the IEEE Engineering in Medicine and Biology Society (EMBC). **Anais**...IEEE, ago. 2015Disponível em: <http://ieeexplore.ieee.org/document/7319218/>

ROGERS, B. P. et al. Functional MRI and multivariate autoregressive models. **Magnetic Resonance Imaging**, v. 28, n. 8, p. 1058–1065, 2010.

ROMERO-GARCIA, R.; ATIENZA, M.; CANTERO, J. L. Predictors of coupling between structural and functional cortical networks in normal aging. **Human Brain Mapping**, v. 35, n. 6, p. 2724–2740, 2014.

ROWLEY, C. D. et al. Assessing intracortical myelin in the living human brain using myelinated cortical thickness. **Frontiers in Neuroscience**, v. 9, n. OCT, p. 1–14, 2015.

RUNGE, V. M. et al. Clinical comparison of three-dimensional MP-RAGE and FLASH techniques for MR imaging of the head. **Journal of Magnetic Resonance Imaging**, v. 1, n. 4, p. 493–500, 1991.

SALA-LLONCH, R. et al. Changes in whole-brain functional networks and memory performance in aging. **Neurobiology of aging**, v. 35, n. 10, p. 2193–202, out. 2014.

SALA-LLONCH, R.; BARTRÉS-FAZ, D.; JUNQUÉ, C. Reorganization of brain networks in aging: a review of functional connectivity studies. **Frontiers in psychology**, v. 6, n. May, p. 663, 2015.

SALAT, D. H. et al. Thinning of the cerebral cortex in aging. **Cerebral Cortex**, v. 14, n. 7, p. 721–730, 2004.

SALTHOUSE, T. A. What and When of Cognitive Aging. **Current Directions in Psychological Science**, v. 13, n. 4, p. 140–144, 23 ago. 2004.

SAMESHIMA, K.; BACCALÁ, L. A. Using partial directed coherence to describe neuronal ensemble interactions. **Journal of Neuroscience Methods**, v. 94, n. 1, p. 93–103, 1999.

SAMESHIMA, K.; BACCALÁ, L. A. **AsympPDC Package v. 2b User Guide**, 2011.

SATO, J. R. et al. Frequency domain connectivity identification: An application of partial directed coherence in fMRI. **Human Brain Mapping**, v. 30, n. 2, p. 452–461,

fev. 2009.

SCAHILL, R. I. et al. A Longitudinal Study of Brain Volume Changes in Normal Aging Using Serial Registered Magnetic Resonance Imaging. **Archives of Neurology**, v. 60, n. 7, p. 989, 1 jul. 2003.

SCHÖLVINCK, M. L. et al. Neural basis of global resting-state fMRI activity. **Proceedings of the National Academy of Sciences of the United States of America**, v. 107, n. 22, p. 10238–43, 1 jun. 2010.

SCHUFF, N. et al. MRI of hippocampal volume loss in early Alzheimers disease in relation to ApoE genotype and biomarkers. **Brain**, v. 132, n. 4, p. 1067–1077, 2009.

SEIDMAN, L. J. et al. Reduced subcortical brain volumes in nonpsychotic siblings of schizophrenic patients: a pilot magnetic resonance imaging study. **American journal of medical genetics**, v. 74, n. 5, p. 507–14, 19 set. 1997.

SELDON, H. L. Does brain white matter growth expand the cortex like a balloon? Hypothesis and consequences. **Laterality**, v. 10, n. 1, p. 81–95, 2005.

SERBRUYNS, L. et al. Subcortical volumetric changes across the adult lifespan: Subregional thalamic atrophy accounts for age-related sensorimotor performance declines. **Cortex**, v. 65, p. 128–138, 2015.

SETH, A. K.; BARRETT, A. B.; BARNETT, L. Granger Causality Analysis in Neuroscience and Neuroimaging. **Journal of Neuroscience**, v. 35, n. 8, p. 3293–3297, 2015.

SHAW, P. et al. Neurodevelopmental Trajectories of the Human Cerebral Cortex. **Journal of Neuroscience**, v. 28, n. 14, p. 3586–3594, 2008.

SKUDLARSKI, P. et al. Measuring brain connectivity: Diffusion tensor imaging validates resting state temporal correlations. **NeuroImage**, v. 43, n. 3, p. 554–561, 2008.

SOHN, W. S. S. et al. Influence of ROI selection on resting functional connectivity: An individualized approach for resting fMRI analysis. **Frontiers in Neuroscience**, v. 9, n. JUL, p. 1–10, 2015.

SONG, J. et al. Age-related reorganizational changes in modularity and functional connectivity of human brain networks. **Brain connectivity**, v. 4, n. 9, p. 662–676, nov. 2014.

SOWELL, E. R. et al. Sex differences in cortical thickness mapped in 176 healthy individuals between 7 and 87 years of age. **Cerebral Cortex**, v. 17, n. 7, p. 1550–1560, 2007.

STORSVE, A. B. et al. Differential longitudinal changes in cortical thickness, surface area and volume across the adult life span: regions of accelerating and decelerating change. **The Journal of neuroscience : the official journal of the Society for Neuroscience**, v. 34, n. 25, p. 8488–98, 18 jun. 2014.

TAMNES, C. K. et al. Brain development and aging: overlapping and unique patterns of change. **NeuroImage**, v. 68, p. 63–74, mar. 2013.

TANGE, O. **GNU Parallel 20150322 ('Hellwig')**, 1 jan. 2015. Disponível em: <https://zenodo.org/record/16303>. Acesso em: 19 set. 2017

TERRY, R. D.; DETERESA, R.; HANSEN, L. A. Neocortical cell counts in normal human adult aging. **Annals of neurology**, v. 21, n. 6, p. 530–9, jun. 1987.

THAMBISETTY, M. et al. Longitudinal changes in cortical thickness associated with normal aging. **NeuroImage**, v. 52, n. 4, p. 1215–1223, out. 2010.

TING, C.-M. et al. Is First-Order Vector Autoregressive Model Optimal for fMRI Data? **Neural Computation**, v. 27, n. 9, p. 1857–1871, set. 2015.

TSANG, A. et al. White matter structural connectivity is not correlated to cortical resting-state functional connectivity over the healthy adult lifespan. **Frontiers in Aging Neuroscience**, v. 9, n. MAY, p. 1–13, 2017.

TSVETANOV, K. A. et al. Extrinsic and Intrinsic Brain Network Connectivity Maintains Cognition across the Lifespan Despite Accelerated Decay of Regional Brain Activation. **The Journal of neuroscience : the official journal of the Society for Neuroscience**, v. 36, n. 11, p. 3115–26, 16 mar. 2016.

VAN DEN HEUVEL, M. P.; HULSHOFF POL, H. E. Exploring the brain network: A review on resting-state fMRI functional connectivity. **European Neuropsychopharmacology**, v. 20, n. 8, p. 519–534, 2010.

VAN PETTEN, C. Relationship between hippocampal volume and memory ability in healthy individuals across the lifespan: Review and meta-analysis. **Neuropsychologia**, v. 42, n. 10, p. 1394–1413, 2004.

VIDAL-PIÑEIRO, D. et al. Accelerated longitudinal gray/white matter contrast decline in aging in lightly myelinated cortical regions. **Human Brain Mapping**, v. 37, n. 10, p. 3669–3684, 2016.

VIEIRA, B. H.; SALMON, C. E. G. **Influência da versão e plataforma sobre medidas da espessura cortical no software Freesurfer**Ribeirão Preto, São Paulo, Brazil, 2017.

WALHOVD, K. B. et al. Consistent neuroanatomical age-related volume differences

across multiple samples. **Neurobiology of Aging**, v. 32, n. 5, p. 916–932, 2011.

WANG, L. et al. Decoding Lifespan Changes of the Human Brain Using Resting-State Functional Connectivity MRI. **PLoS ONE**, v. 7, n. 8, 2012.

WANG, Y. et al. An Efficient and Reliable Statistical Method for Estimating Functional Connectivity in Large Scale Brain Networks Using Partial Correlation. **Frontiers in Neuroscience**, v. 10, n. MAR, 31 mar. 2016.

WESTLYE, L. T. et al. Increased sensitivity to effects of normal aging and Alzheimer's disease on cortical thickness by adjustment for local variability in gray/white contrast: A multi-sample MRI study. **NeuroImage**, v. 47, n. 4, p. 1545–1557, 2009.

WESTLYE, L. T. et al. Differentiating maturational and aging-related changes of the cerebral cortex by use of thickness and signal intensity. **NeuroImage**, v. 52, n. 1, p. 172–185, 2010.

WHITFIELD-GABRIELI, S.; NIETO-CASTANON, A. Conn: A Functional Connectivity Toolbox for Correlated and Anticorrelated Brain Networks. **Brain Connectivity**, v. 2, n. 3, p. 125–141, 2012.

WILKINSON, G. N.; ROGERS, C. E. Symbolic Description of Factorial Models for Analysis of Variance. **Applied Statistics**, v. 22, n. 3, p. 392, 1973.

WINKLER, A. M. et al. Cortical thickness or grey matter volume? The importance of selecting the phenotype for imaging genetics studies. **NeuroImage**, v. 53, n. 3, p. 1135–1146, nov. 2010.

ZHANG, H. Y. et al. Selective vulnerability related to aging in large-scale resting brain networks. **PLoS ONE**, v. 9, n. 10, p. 1–8, 2014.

ZHAO, L.; CHEN, Y.; SCHAFFNER, D. W. Comparison of logistic regression and linear regression in modeling percentage data. **Applied and environmental microbiology**, v. 67, n. 5, p. 2129–35, maio 2001.

ZHOU, D. et al. Cortical thickness asymmetry from childhood to older adulthood. **NeuroImage**, v. 83, p. 66–74, 2013.

ZIELINSKI, B. A. et al. Longitudinal changes in cortical thickness in autism and typical development. **Brain : a journal of neurology**, v. 137, n. Pt 6, p. 1799–812, jun. 2014.

ZILLES, K.; AMUNTS, K. Architecture of the Cerebral Cortex. In: **The Human Nervous System**. [s.l.] Elsevier, 2012. p. 836–895.